Science and Engineering Research Council
Rutherford Appleton Laboratory
CHILTON, DIDCOT, OXON, OX11 0QX

RAL-86-076

Meson Dynamics Beyond the Quark Model: A Study of Final State Interactions

K L Au, D Morgan and M R Pennington

September 1986

RAL-86-076
DTP-86-9

MESON DYNAMICS BEYOND THE QUARK MODEL: A STUDY OF FINAL STATE INTERACTIONS

by

K.L. Au[1], D. Morgan[2] and M.R. Pennington[1]
[1]Departments of Mathematical Sciences and Physics,
University of Durham, Durham, UK
[2]Rutherford Appleton Laboratory, Chilton, Didcot, Oxon, UK

Abstract:

A scalar glueball is predicted in the 1 GeV mass region. The present analysis is concerned with experimental evidence for such a state. It has been proposed that glueballs should be preferentially produced in supposedly glue rich processes like ψ decay and double pomeron enchange. However, any meson of such a mass and quantum numbers has very restricted decay channels available - essentially only $\pi\pi$ and, if the mass allows, $K\bar{K}$. In this case, any production process is very tightly correlated to elastic reactions, $\pi\pi \to \pi\pi$ and $\pi\pi \to K\bar{K}$, by unitarity. Novel processes cannot then reveal effects that could not be seen in these elastic reactions. Nevertheless, they can valuably supplement this standard information where it lacks precision. Recent high statistics results on central dimeson production at the ISR enable us to perform an extensive new coupled channel analysis of $I = 0$ S-wave $\pi\pi$ and $K\bar{K}$ final states. This unambiguously reveals three resonances in the 1 GeV region - $S_1(991)$, $S_2(988)$ and $\varepsilon(900)$ - where the naive quark model expects just two. We discuss in detail these new features, how they may be confirmed experimentally and give their present interpretation. The $S_1(991)$ is a plausible candidate for the scalar glueball. We examine other production reactions (heavy flavour decays and $\gamma\gamma$ reactions) leading to the same final states, and discuss how with future precision these can probe fine details.

Section 1 : Introduction

A key clue to the dynamics of fundamental interactions is the resulting spectrum of states. This is particularly so for the strong interaction, which being by far the most complex and least understood, has the most complicated spectrum. The realisation that the hundreds of strongly interacting states discovered in the 40's, 50's and 60's could be grouped in patterns was the crucial step in recognising that these were made of more fundamental building blocks we know as quarks[1]. Though we now know the theory of the interaction that binds these quarks to make hadrons, namely QCD, we unfortunately do not yet know how to calculate the details of hadron spectroscopy, except when simplifying approximations allow lattice computations[2], for example. Nevertheless, we believe that QCD should contain not only the regular $(q\bar{q})$ mesons and (qqq) baryons of the naive quark model, but also glueballs[3], hybrids[4] and various multi-quark configurations[5,6]. In common with all statements about the bound states of QCD, this is not proven, but the arguments are persuasive and suggest that the new states should occur in the range already accessible to experiment (say < 2 GeV). All models concur in predicting that the lightest glueball should be the scalar, 0^{++}, and the search for candidates is the principal motivation for this paper.

In the naive quark model, the relation between hadrons and their parton configurations is simple and clear cut. However, in QCD, the bound state wave-functions are inevitably much more complicated. Yet we know from experiment that the naive quark model components are rather dominant. The OZI rule and the whole symmetry pattern of hadron spectra and decays speaks to this. The success of the OZI rule suggests that the way to uncover glueballs is to select reactions which, on the parton level, proceed via gluonic intermediate states - for instance, the decay $\psi \to \gamma +$ hadrons. This channel has succeeded in revealing new states and, despite some interpretational caveats, the two new states, the $\iota(1440)$, 0^{-+}[7], and $\theta(1690)$[8], 2^{++}, would head any list of glueball candidates at the present time[9,10]. In this role, the θ has the special virtue of being a 'spare' state, pointing to new or extra physics.

The existence of plausible candidates for both the lowest mass 0^{-+} and 2^{++} glueballs intensifies the interest in seeking what should be the lightest

glueball of all - the scalar 0^{++}. A special mechanism, purportedly rich in glue (as amplified in Sects. 2 and 4), suitable for its production is double pomeron exchange[11], on which a series of experiments has been performed at the CERN ISR[12,13,14]. The highest statistics experiment by the AFS collaboration specifically studied centrally produced dimesons in what is known as the "ISR gluonium search experiment"[13], resulting in a $\pi\pi$ mass spectrum quite different from that of $\pi\pi$ scattering itself. However, we should not forget the key role played by unitarity whereby final state interactions shape and colour the actual spectra we observe. The fact that strong interaction processes must conserve probability severely limits the scope for new effects[15]. As we shall discuss, any extra low mass state should already have been seen in $\pi\pi$ scattering without any need for a special production mechanism. Nevertheless, so tight is the relationship required by unitarity between channels with essentially just $\pi\pi$ and $K\bar{K}$ final states, that any new experimental information can add greatly to our understanding of the I=0 J=0 sector. Though the "ISR gluonium search experiment" can of itself provide no new excitations, it can shed valuable light on states already there. For this it is ideally suited, because unlike classic processes like $\pi^-p \to \pi^-\pi^+n$, the S-wave $\pi\pi$ final state in $pp \to pp\pi\pi$ is not swamped by a dominant I=1 (ρ) signal. Thus the AFS data is a major addition, supplementing experimental information on meson-meson scattering. This allows us to perform a new coupled channel analysis of essentially all $\pi\pi$, $K\bar{K}$ information and obtain more detailed conclusions than previously possible[16].

The extent of this analysis we believe justifies the detail in which we discuss this work. In Sect. 2, we review the interplay of production mechanisms and final state interactions, which forms the basis for the extraction of meson scattering information. In Sect. 3 we outline the specific formalism we shall use to implement multi-channel unitarity, detail the parametrizations we consider and select the data we shall superimpose on these. In Sect. 4 we show how our formalism embraces the double pomeron exchange processes involved in central dimeson production. We consider the general mass dependence of the AFS data and then turn to the specific S-wave channel. In Sect. 5 we describe our combined fit of $\pi\pi$ and $K\bar{K}$ final state data, discuss the quality of the fits and their consistency with effects like S-D interference we have not specifically fitted. In Sect. 6 we show how these same amplitudes allow us to describe satisfactorily heavy flavour decays and the $\gamma\gamma$ process with $\pi\pi$ and $K\bar{K}$ final states and determine the corresponding couplings.

We then turn to examine the resonance content of our amplitudes. In Sect. 7 we enumerate the S-matrix poles that our I=0 J=0 amplitudes reveal - poles that are not imposed a priori. We shall see that around 1 GeV there are more poles in each of our solutions, regardless of their parametrization, than are required by the naive quark model. These are the firm results of our analysis.

Usually in meson spectroscopy, there is an almost self-evident link between poles of the S-matrix, the corresponding resonances and their parton interpretation. This is not the case for the I = 0 scalar sector, where the close proximity of a strongly coupled threshold complicates even the link between the poles of the multi-sheeted S-matrix and resonant states. This is reminiscent of the A(1405) problem in baryon spectroscopy[17]. In Sect. 8 we attack this problem by discussing what is a resonance and suggest a prescription for linking poles to resonances and then go on to speculate on the parton interpretation of our assignments. The outcome in the vicinity of $K\bar{K}$ threshold is a trio of resonances - $S_1(991)$, $S_2(988)$ and $\varepsilon(900)$ - in place of the usual two[18]. The S_1 has attributes compatible with a predominantly glueball composition. In section 9 we discuss the definitive results of our analysis, the questions it raises on the nature of resonances, the predictions it makes and what future experiments on these and related channels may reveal.

Section 2 : Production mechanisms and final state interactions

The OZI rule suggests that the way to look for glueballs is to consider processes with an initial state rich in glue. We then look at the meson final state of such reactions, for example the $\pi\pi$ mass spectrum. From this we learn about a process we like to regard as "glue" $\to \pi\pi$. It is natural then to compare and contrast this with the $\pi\pi$ mass spectrum from a reaction initiated by quarks. Let us recall how we learn about meson states in such channels as this will introduce many ideas relevant to gluonium searches.

In contrast to our very detailed access to baryons, essentially the only states of zero baryon number we can form in the laboratory are those found in e^+e^- annihilation. Consequently, our knowledge of the spectroscopy of mesons comes about almost entirely from production processes. There in πN or NN scattering, we analyse some sub-channel of the final state. For

example, we learn about the ρ from studying the ππ final state in $\pi^-p \to \pi^-\pi^+n$. Such processes are often thought of in a factorised way, wherein we regard the ρ as being first produced by the particular mechanism involved and then decaying in a universal fashion. This is the basis of the isobar picture.

In general, the production process is complex, depending on a multitude of kinematic variables and sub-reactions[19]. Consequently, the 2 or multi-body final state may have a quite different appearance in differing kinematic situations and, in particular, a "resonance" may appear to have a variable shape. Thus unless we have a detailed understanding of the production mechanism and the properties it must satisfy we may not know whether a short-lived state appearing in one channel is the same or different from that in some other. It is therefore essential to have an accurate description of production to be able to distinguish new from old effects. Thus in the investigation of final state interactions we report here, it will be necessary to outline for each reaction what the production mechanism is and how we are to describe it. To recognise a needle in the proverbial haystack, we have to have a detailed description of the haystack.

In general, production mechanisms cannot be accurately modelled. We therefore seek situations where these mechanisms simplify: at high energies and small momentum transfers, for example. There processes become dominated by exchanges in the t-channel, which carry well-defined quantum numbers and for which the Regge model provides an excellent phenomenological description. Thus the high energy production of the ρ in $\pi^-p \to \pi^-\pi^+n$ may be factorised in the t-channel to give information about $\pi"\pi" \to \rho \to \pi\pi$, where the "initial" state π is off-shell with a negative mass-squared. As recognised long ago by Chew and Low[20], and independently by Goebel[21], the pion has such a tiny mass that its pole at $t=0.02$ $(GeV)^2$ is appreciably felt in the scattering region of $t<0$. In reactions like $\pi^-p \to \pi^-\pi^+n$ or $\pi^-p \to K^-K^+n$, which are controlled by the exchange of pion quantum numbers in the t-channel, we can therefore factor off the nucleon vertex and extrapolate the residual meson vertex to the pion pole. We thus obtain information on physical $\pi\pi \to \pi\pi$, $\to K\bar{K}$ scattering. For the channels in question these have hitherto been the only purely mesonic processes, for which there has been sufficient experimental information to allow the extraction of amplitudes, thus our only source of information on what in

the naive parton description we may regard as quark interactions initiated by mesons.

By special 'glue-rich' mechanisms it is suggested we can similarly glean information on what we may think to be gluon interactions. Such a mechanism is believed to be double pomeron exchange[11]. Single pomeron exchange is what controls the pp total cross-section at high energies. This can be thought of, in parton terms, as the exchange of a colour singlet blob of glue between the colliding protons. The QCD interpretation of double pomeron exchange is that once in a while a colour singlet lump of glue may detach from each proton and fuse to give a system of pure glue. Such a process would be enhanced at certain masses if suitable glueball states exist. These being produced by two pomerons can only have I=0, even spin, even charge conjugation and natural parity, viz 0^{++}, 2^{++}, etc. Other types of glueball could not be excited by this mechanism.

Experiments on both "quark" and "glue" channels reveal that up to roughly 1.4-1.5 GeV in mass, 4π, 6π, etc, production are small enough (in a sense to be quantified later) to be neglected in comparison with the dominant ππ and $K\bar{K}$ channels. What is more, below ~ 1 GeV, ππ scattering is purely elastic and unitarity is a particularly powerful constraint[15]. When the $K\bar{K}$ channel opens up, it is known to couple strongly, so that a coupled channel analysis is essential and with detailed experimental information on both channels, this becomes feasible. In Sect. 3 we set out a formalism that will allow us to take into account the constraint of two channel unitarity so important for such an analysis. With this apparatus, we will be able to investigate simultaneously the way the I=0 S-wave appears in the seemingly quark initiated $\pi\pi \to \pi\pi$ $(K\bar{K})$ channels (Sect. 3) as well as the supposedly glue-rich reactions $pp \to pp\pi\pi(K\bar{K})$ of Sect. 4, and $\psi' \to \psi\pi\pi$, $\psi \to \phi\pi\pi$ of Sect. 6.

Section 3 : Multi-channel unitarity and final state interactions

3.1 Coupled channel unitarity

As already mentioned, we are interested in relations between processes leading to some common set of hadronic final states. Unitarity plays a crucial role in relating these. Let us first define the multichannel

hadronic amplitudes $\mathcal{T}_{ij}$, which are the appropriate $\mathcal{T}$-matrix elements, where i denotes the initial state and j the final one. In the particular example that will actually concern us,

$$\mathcal{T}_{11} = \mathcal{T}(\pi\pi \to \pi\pi)$$

$$\mathcal{T}_{12} = \mathcal{T}(\pi\pi \to K\bar{K}) \qquad (3.1)$$

$$\mathcal{T}_{22} = \mathcal{T}(K\bar{K} \to K\bar{K})$$

all for the I=0 S-wave. Each of these amplitudes will be functions of M, the c.m. energy and we use $s=M^2$. Normalising in the usual way, with the density of final states, ρ_j, equal to $2k_j/M$ with k_j the final state c.m. 3-momentum, unitarity takes the familiar form:

$$\mathrm{Im}\,\mathcal{T}_{ij} = \sum_k \rho_k \mathcal{T}^*_{ik} \mathcal{T}_{kj} \qquad (3.2)$$

We now want to know how to relate these amplitudes to those of other processes with the same final state. We shall use the term 'production processes' to denote any mechanism, like $\gamma\gamma \to$ hadrons or "$I\!P\,I\!P$"$\to$hadrons, where the incoming particles do not participate as intermediate states in unitarity sums for the final state channels; as far as unitarity is concerned, the incoming particles are non-strongly interacting. This concept embraces not only genuinely incoming mechanisms like "$I\!P\,I\!P$", but components within an isobar description, where to a good approximation certain of the final particles function as spectators (e.g. $\psi' \to \psi +$ hadrons, $\psi \to \phi\,\pi\pi$).

For each production process (c) and each available final hadronic channel (i), we need the production amplitude $\mathcal{F}_i^{(c)}$ in order to express the corresponding production cross-section $\sigma_i^{(c)}$ in terms of the initial flux, $f^{(c)}$, assumed known, and ρ_i, the appropriate density of final states:

$$\sigma_i^{(c)} = f^{(c)}\,\rho_i\,|\mathcal{F}_i^{(c)}|^2 \qquad (3.3)$$

The resulting spectrum is controlled by the dependence of $\mathcal{F}_i^{(c)}$ on the channel c.m. energy, M. Unitarity specifies the form of the imaginary part of $\mathcal{F}_i^{(c)}$ in the standard way as a sum over all available intermediate states:

$$\mathrm{Im}\,\mathcal{F}_i^{(c)} = \sum_j \rho_j \mathcal{F}_j^{(c)*} \mathcal{T}_{ji} = \sum_j \rho_j \mathcal{F}_j^{(c)} \mathcal{T}^*_{ji} \qquad (3.4)$$

Note that eq (3.4) in contrast to eq (3.2) is a linear constraint, this being a consequence of the assumed non-strongly interacting character of the incoming particles. Where just one final state is available, eqs (3.2,3.4) require that (modulo π's) the phase of the hadronic and all production processes should be the same - the familiar Watson's final state interaction theorem[22]. We are concerned with its multi-channel generalization[23].

To this end, we can immediately write down an expression for $\mathcal{F}_i^{(c)}$, which embodies the above constraints,

$$\mathcal{F}_i^{(c)} = \sum_j \tilde{\alpha}_j^{(c)} \mathcal{T}_{ji} \qquad (3.5)$$

with the $\tilde{\alpha}_j^{(c)}$ real. Such a form obviously satisfies eq (3.4) given eq (3.2). We can further delimit the $\tilde{\alpha}$'s by appeal to analyticity. All the right hand cut structure of $\mathcal{F}_i^{(c)}$ is explicitly included in the sum over $\mathcal{T}_{ji}$. This means that the $\tilde{\alpha}_j$'s can have no nearby singularities as functions of s and dictates that they should be smooth functions. In the case of interest with $\pi\pi$ final states, there is one further feature for which we must allow - the occurrence of Adler zeros near threshold.

That almost all S-wave amplitudes connecting to soft pions should have zeros close to threshold is a well-verified consequence of PCAC with the exceptions conforming to the expected pattern of Born terms allowed by through-going external particles (as in πN scattering)[24]. The actual position of the zero is process-dependent; in particular, the zero for the elastic amplitude $\mathcal{T}_{11}$ is shifted, or in some cases removed, when one turns to the associated production process. We can cater for this in the above formalism by dividing through by the zero of the elastic channel at $s=s_o$. Thus defining

$$T_{11} \equiv \frac{\mathcal{T}_{11}}{s-s_o} \qquad (3.6)$$

we can allow for zeros in the production process in question by requiring them to enter in the $\tilde{\alpha}^{(c)}$'s. For simplicity of discussion, we set the related zeros in $\mathcal{T}_{12}$ and $\mathcal{T}_{22}$ at the same position, since the data are only sensitive to the zero of $\mathcal{T}_{11}$. Thus

$$T_{ij} \equiv \frac{\mathfrak{I}_{ij}}{s-s_o} \tag{3.7}$$

enabling us to write

$$\mathfrak{I}_i^{(c)} = \sum_j \alpha_j^{(c)} T_{ji} \tag{3.8}$$

with the tilde over the α's removed to signify that they are coefficients of the 'reduced' T's. The $\alpha_j^{(c)}$ may be viewed as intrinsic couplings which control the propensity of process (c) to initiate production in channel j, the final outcome being determined by the final state interactions supplied by the T_{ji} factors[25].

It is interesting to compare the resulting expression for $\mathfrak{I}_i^{(c)}$ with that resulting from a one-channel analysis[15], where an application of unitarity and analyticity yields the form

$$\mathfrak{I}_1^{(c)} = P^{(c)}\, \Omega^{(c)} \tag{3.9}$$

Here $P^{(c)}$ is, in general, slowly varying, incorporating any zero factors, and $\Omega^{(c)}$, the Omnès function[26], is given by

$$\Omega^{(c)} = \exp\left[\frac{s}{\pi} \int_{4m_\pi^2}^{\infty} ds' \quad \frac{\phi^{(c)}(s')}{s'(s'-s)} \right] \tag{3.10}$$

with $\phi^{(c)}$ the phase of $\mathfrak{I}_1^{(c)}$. The corresponding expression for the reduced elastic amplitude T_{11} takes the form

$$T_{11} = n\, \Omega^{(el)} \tag{3.11}$$

where $\Omega^{(el)}$ is the analogue of eq (3.10) with the appropriate phase $\phi^{(el)}$ substituted for $\phi^{(c)}$. Below the second threshold ($s=4m_K^2$), all the phases in question are equal by Watson's theorem. This has the consequence, for the actual phases that pertain in practice, that the Ω's are effectively universal below the vicinity of the $K\bar{K}$ threshold. As previously discussed, this virtually eliminates any possibility of new processes uncovering new effects in the single channel region[15]. However, very close to $K\bar{K}$ threshold the signal may be individual to that reaction.

To see how this translates into the two-channel formalism, we need only compare the rival formulae for $\mathfrak{I}_1^{(c)}$:

$$\begin{aligned} \mathfrak{I}_1^{(c)} &= P^{(c)}\, \Omega^{(c)} \\ &= \alpha_1^{(c)} T_{11} + \alpha_2^{(c)} T_{21} \\ &= (\alpha_1^{(c)} + \alpha_2^{(c)} \frac{T_{21}}{T_{11}})\, n\, \Omega^{(el)} \end{aligned} \tag{3.12}$$

The quantity to compare with $P^{(c)}$ is $\tilde{P}^{(c)}$ defined by

$$\tilde{P}^{(c)} = (\alpha_1^{(c)} T_{11} + \alpha_2^{(c)} T_{21})/\Omega^{(el)} \tag{3.13}$$

which is real over the region of interest, since $\arg(T_{21}) = \arg(T_{11}) = \arg(\mathfrak{I}_1^{(c)}) = \phi^{(el)}$ by Watson's theorem. For the practical analysis to be described in Sect. 5, the resulting $\tilde{P}^{(c)}$ compares well with the corresponding $P^{(c)}$ (see Fig. 5.9), indicating the near universality of the Ω's below $K\bar{K}$ threshold.

A simple reaction which illustrates this intimate relationship between processes with the same final state imposed by unitarity and analyticity is $e^+e^- \to \pi^+\pi^-$. Here the production mechanism is explicitly controlled by one virtual photon to a high degree of accuracy and consequently the quantum numbers of the ππ final state are forced to be those of the photon and have isospin one. Through eqs (3.2-5, 3.9-11), the ρ signal in the elastic process is closely related to that in e^+e^-, the Omnès function being almost identical. The small difference in line shape of the ρ in these two channels is a result of the difference between n (recall eq (3.11)) and $P^{(ee)}$ expected from their differing left hand cut structures - $P^{(ee)}$ in particular, having no cut, is just a simple polynomial. This relationship has been extensively investigated in studies of the pion's electromagnetic form-factor[27].

As we shall see the situation in the I=0 J=0 channel with strongly overlapping resonances and a nearby threshold greatly complicates this simplicity. Indeed, the I=0 S-wave constitutes the most significant non-trivial mesonic example of coupled channel unitarity amenable to detailed analysis. It is to this we now turn.

3.2 Parametrizations of the K- and M-matrices

In the following sections, we shall be reporting the results of fits to both production and scattering information on the I=0 $\pi\pi$ and $K\bar{K}$ S-waves. To relate these in the way required by unitarity, we will need expressions for the $\underset{\sim}{J}_{ij}$, which will be an integral part of our treatment of the production processes. We therefore begin by writing down the standard formulation of the $\underset{\sim}{J}$-matrix in terms of the K-matrix and its inverse the M-matrix. It is in terms of these that we parametrize the fit to the scattering data on $\pi\pi \to \pi\pi$ and $K\bar{K}$ and express the amplitudes for " $I\!P\,I\!P$" $\to \pi\pi$ and $K\bar{K}$, and other processes. In matrix form, the necessary equations are:

$$\underset{\sim}{J} = \underset{\sim}{K}\,[\,\underset{\sim}{1} - i\underset{\sim}{\rho}\,\underset{\sim}{K}]^{-1} \tag{3.14}$$

$$= [\underset{\sim}{M} - i\underset{\sim}{\rho}]^{-1} \tag{3.15}$$

Here, $\underset{\sim}{\rho}$ is the diagonal matrix with diagonal elements ρ_1, ρ_2, $\underset{\sim}{K}$ is a real symmetric matrix and $\underset{\sim}{M}$ its inverse. The associated $\underset{\sim}{S}$-matrix is defined by

$$\underset{\sim}{S} = \underset{\sim}{1} + 2i\underset{\sim}{\rho}^{\frac{1}{2}}\,\underset{\sim}{J}\,\underset{\sim}{\rho}^{\frac{1}{2}} \tag{3.16}$$

$$= [\,\underset{\sim}{1} + i\underset{\sim}{\rho}^{\frac{1}{2}}\,\underset{\sim}{K}\,\underset{\sim}{\rho}^{\frac{1}{2}}][\,\underset{\sim}{1} - i\underset{\sim}{\rho}^{\frac{1}{2}}\,\underset{\sim}{K}\,\underset{\sim}{\rho}^{\frac{1}{2}}]^{-1} \tag{3.17}$$

In the fits reported in Sect. 5, we take $\underset{\sim}{K}$, which is now 2x2, of the form[28] with $s=M^2$

$$K_{ij} = \frac{(s-s_o)}{4m_K^2}\sum_p \frac{f_i^p f_j^p}{(s_p-s)(s_p-s_o)} + \sum_{n=0} c_{ij}^n \left[\frac{s}{4m_K^2}-1\right]^n \tag{3.18}$$

$$\equiv (s-s_o)\hat{K}_{ij}$$

Our 'reduced' T-matrix elements (cf eqs (3.6-8)) are then given by

$$\underset{\sim}{T} = \hat{\underset{\sim}{K}}\,[\,\underset{\sim}{1} - i\underset{\sim}{\rho}\,\underset{\sim}{K}]^{-1} \tag{3.19}$$

Note, importantly, the single appearance of $\hat{\underset{\sim}{K}}$ in this formula. Alternatively, we parametrize the $\underset{\sim}{M}$-matrix, eq (3.15), as

$$M_{ij} = \frac{a_{ij}}{s-s_o} + \sum_p \frac{f_i'^p f_j'^p}{s_p' - s} + \sum_{n=0} c_{ij}'^n \left[\frac{s}{4m_K^2}-1\right]^n \tag{3.20}$$

In eqs (3.18,20), $s=s_o$ represents the Adler zero of the T-matrix, eqs (3,6,7). The number of poles and order of polynominal in eqs (3.18,20) required to fit the data will be detailed in Sect. 5. Finally, for the α_i's we take the simple power expression

$$\alpha_i = \sum_{n=0} \alpha_i^n \left[\frac{s}{4m_K^2}\right]^n \tag{3.21}$$

(Note that we have now ceased to label the initiating reaction and use the superfix label to identify terms in this Taylor expansion). The number of terms we take will depend upon the range of energies over which we are fitting data. For example for the $\psi' \to \psi\pi\pi$ decay, where phase space is limited to $279 < M < 589$ MeV, a linear form is adequate, while for the " $I\!P\,I\!P$" reaction, since we fit S-wave information up to 1700 MeV, it is necessary to use quadratic forms.

In order to determine the parameters in our K- and M-matrix expressions, we need to fit data on the classic hadronic phase-shift data on J_{11} and J_{12}. We shall see later that in fact a combined fit to the " $I\!P\,I\!P$" production results is even more constraining, since we can profit from the additional statistical weight and the distinct and efficient partial wave separation these new data allow. As is customary, the $K\bar{K}$ channel is assumed to dominate the inelasticity from $\pi\pi$, rendering a two channel analysis a good approximation. We will comment in detail later when and where this assumption breaks down and the likely effect of this.

3.3 Data selection

Given this framework, one is looking for information on just 3 parameters at each energy, δ_{11}, η_{11} and ϕ_{12}. These fix J_{11} and J_{12}, through the usual relations

$$J_{11} = [\eta_{11}\, e^{2i\delta_{11}} - 1]/2i\rho_1 \tag{3.22}$$

$$J_{12} = [1-\eta_{11}^2]^{\frac{1}{2}}\, e^{i\phi_{12}}/2(\rho_1\rho_2)^{\frac{1}{2}} \tag{3.23}$$

The quantities η_{11} and δ_{11} have been determined in numerous analyses of dipion production experiments. Of these, we select as input to the present fit, the classic energy independent analysis by the CERN-Munich group of their high statistics experiment on $\pi^-p \to \pi^-\pi^+n$ at 17 GeV/c[29,30]. These results are strongly supported by earlier experiments, in particular by the LBL $\pi^+\pi^-$ experiment of Protopopescu et al[31]. Above $K\bar{K}$ threshold, we supplement this $\pi^-\pi^+$ information with the phase shifts derived by Cason et al from an analysis of their 8 GeV/c experiment on $\pi^+p \to \Delta^{++}\pi^0\pi^0$[32]. However, below 1 GeV, the S-wave solutions of Cason et al are controversial being in total disagreement with the $\pi^-\pi^+$ results of LBL and CERN-Munich. We therefore exclude their results at lower $\pi\pi$ masses. Above 1 GeV, when many waves become important particularly in $\pi^-\pi^+$ scattering, a multitude of partial wave solutions is possible. These are constrained by fixed t-dispersion relations to essentially two solutions[33]. Of the $\pi^+\pi^-$ solutions found in the energy independent analysis of Martin and Pennington[33], the $\pi^0\pi^0$ results of Cason et al[32] and the polarized target data of the ACCMOR collaboration[34] favour the so-called β' solution. We therefore input this solution together with the phase shift solutions of Ochs[30] and of Cason et al[32]. The reason for including as independent data sets the results of both the Ochs and the Martin and Pennington analyses of the same $\pi\pi$ data is that these analyses have differing constraints and the resulting S-wave, being the lowest wave in data dominated by higher waves up to spin 3, is poorly determined, and has sizeable error ellipses (shown on representative data points in Fig. 5.4). Our aim is to pick out a smooth track through this error corridor.

Under the two-channel assumptions, additional and perhaps more reliable information on η_{11} eqs (3.22,23), comes from the analogous $K\bar{K}$ production experiments with incoming pion beams. There have been a number of experiments both on K^+K^- and $K^0_sK^0_s$ production[35,36,37]. Besides fixing the magnitude of $\mathfrak{I}_{12}$, these also provide information on its phase, ϕ_{12}, relative to one of the other participating waves, in practice the D-wave. On the magnitude, $|\mathfrak{I}_{12}|$, the various experiments concur fairly well; however, there is a significant disagreement as to the phase behaviour of $\phi_{SD} \equiv |\phi_{12}-\phi_D|$ below 1150 MeV. According to the K^+K^- experiment of Ref. 35, ϕ_{SD} is flat over this energy domain whilst the other $K\bar{K}$ experiments find a steep rise (Fig. 5.6); at the lowest energy, the discrepancy is some 70^0[38]. Since 'a priori' we do not know which, if either, is correct, we input the results of

the amplitude analyses of two representative high statistics experiments:

(1) by Cohen et al[35] of their $\pi^-p \to K^-K^+n$ and $\pi^+n \to K^+K^-p$ 6 GeV/c data, and
(2) by Etkin et al[37] of their $\pi^-p \to K^0_sK^0_sn$ 23 GeV/c data.

These appear to span the range of experimental possibilities.

In order to extract ϕ_{12} from the published information on ϕ_{SD}, we need to know the behaviour of the D-wave phase in $\pi\pi \to K\bar{K}$. Below roughly 1.4 GeV, this is dominated by the f-resonance and accordingly assumed to be given by

$$\tan \phi_D = \frac{\sum_i m_f \Gamma_f^i \beta_2^i(s)\, \theta(s-s_i)}{m_f^2 - s} \qquad (3.24)$$

where i runs over all contributing channels $\pi\pi$, $\eta\eta$, $K\bar{K}$, ... each with threshold at $s=s_i$. We input the barrier factor β_2, suggested by duality[39] from the nearest crossed-channel singularity, to be

$$\beta_2^i(s) = \left[\frac{s-s_i}{m_f^2-s_i}\right]^{\frac{1}{2}} \quad \frac{P_2(1+2m_\rho^2/(m_f^2-s_i))}{P_2(1+2m_\rho^2/(s-s_i))}$$

where we take the standard PDG values for the f-resonance mass and width, and their uncertainties[18].

Such a form for ϕ_D we believe more plausible than that modelled by Etkin et al[37] below 1.2 GeV and this is the form we take to extract ϕ_{12}, appropriately folding in the uncertainties in ϕ_D given by those on m_f and Γ_f^i, which are typically 1^0-4^0. Since the D-wave phase given by eq (3.24) accords well with D-wave modelled by Cohen et al[35] below 1.4 GeV, where it is f-dominated, we take their plotted values of ϕ_{12} directly as input. The resulting phases are shown in Fig. 5.6, while the magnitude of $|\mathfrak{I}_{12}|$ is plotted in Fig. 5.5.

A priori we have no reason to favour one experiment over the other (and in fact the analysis by Görlich et al[40] of their polarized target results disagrees with all of them). It is however worth noting that other experiments on $K\bar{K}$ production from Wetzel et al, Costa et al and Polychronakos et al[36], while all agreeing on the magnitude of the cross-section, tend to support the phase of Etkin et al, Fig. 5.6. On the other hand, Cohen et al would justifiably argue that their analysis is the only

one amenable to the necessary I = 0,1 separation. In face of this, we shall henceforth assume that the results of Cohen et al and of Etkin et al span the range of current knowledge of ϕ_{12}. Their sizeable disagreement means that our input on the $\pi\pi \to K\bar{K}$ channel is far from homogeneous and we will describe in Sect. 5 the effect this has. Lastly, the uncertainties in ϕ_{12} within each experiment are very similar, reflecting their comparable statistics. Only the second data point of Etkin et al with a quoted $\pm 6^0$ on ϕ_{SD} is acutely out of line and its error has been increased to $\pm 20^0$ in our global fit to all these data, see Fig. 5.6.

A guide to where our two channel saturation of unitarity breaks down is afforded by comparing the S-wave inelastic cross-section, viz $(1-\eta_{11}^2)/4$, as determined from the analyses of the CERN-Munich $\pi\pi$ scattering data[29] and the better defined $K\bar{K}$ contribution to this given by the actual $\pi\pi \to K\bar{K}$ cross-section on which essentially all experiments agree[35,36,37]. We see in Fig. 5.5 this comparison suggests the importance of other final states above 1.4 GeV. There already exists experimental evidence of a by no means negligible $\eta\eta$ S-wave signal in the f-region[41] and 4π production is beginning to take off[42]. Rather than attempt to fit obviously inconsistent data, in which the better determined $K\bar{K}$ cross-section would dominate this aspect of the fit, when clearly the total inelastic cross-section is more likely to be that of the CERN-Munich results of Fig. 5.5 if other channels were included, we have determined solutions in which the $\pi\pi \to K\bar{K}$ data above 1.4 GeV are switched in and out. The results we describe in Sect. 5 will for the most part be those with it out and we will discuss later the rather small effect that neglecting other inelastic channels has on our results.

Section 4: The AFS reaction

4.1 Double pomeron mechanism

The AFS experiment[13] was designed to study central dimeson production in pp→pp(MM). The triggering is such that though this experiment was performed at the CERN ISR, where the square of the c.m. energy, s_{tot}, is almost 4000 GeV^2, most of this momentum continues along the direction of the two beams. The protons scatter at tiny angles and only a small amount of momentum is transferred from each: $-0.015 > t > -0.045$ (GeV/c)^2. Importantly, this is a far smaller range than any other experiment[12,14]. Moreover, the two mesons

produced are well separated in rapidity from the on-going protons, so that the mechanism for their production is naturally factorised from the scattering of the protons. The Regge model provides a phenomenologically well-tested description for this[43]. The satisfactory factorisation of the dimeson production from the forward going protons means that this reaction can be regarded as $(p\bar{p})(p\bar{p}) \to \pi\pi$ and the formalism of Sect. 3.1 is applicable to its analysis.

The quantum numbers of the "reggeons" coupling to the protons (Fig. 4.1) are those appropriate to pp elastic scattering. At such high energies, these exchanges are dominated by vacuum quantum numbers carried by the "pomeron". Though the motivation for this experiment, as discussed in the introduction, is predicated on the specific idea that the pomeron is a colour singlet configuration of glue so that the central production of mesons is generated by the fusing of glue rather than quarks[11], knowledge of the exact nature of the production mechanism is inessential for our analysis which only needs an accurate phenomenological description.

The pomeron, having vacuum quantum numbers, fixes the quantum numbers of the dimeson final state to have I=0 and even spin. Contamination from lower lying Regge exchanges like the ρ shows up in the dimeson angular distribution having odd angular momentum components in addition to a ρ peak in the $\pi\pi$ mass spectrum. This signal allows such extraneous effects from non-vacuum quantum numbers to be removed, as discussed extensively in Refs. 13 and 44. With such a tiny range of t in this particular experiment, such contamination from non-pomeron exchanges is believed to be under control and readily separated.

The Mueller-Regge approach gives us a description for the contribution for the $pp \to pp(MM)$ process. With s_{tot} the total c.m. energy squared, M the mass of the meson pair, t_1 and t_2 the square of the momentum transferred at each pp vertex (fig 4.1) and y the rapidity, such a Regge analysis allows us to factorise off the pp vertices and pomeron propagators to give what we may regard as a pomeron-pomeron cross-section (much like the γγ process studied in $e^+e^- \to e^+e^-X$ - see Sect. 6.2) defined by

$$\frac{d^4\sigma}{dt_1 dt_2 dy dM^2/s_{tot}} = \alpha'^2\, \beta_{pp\,I\!P}(t_1)^2\, \beta_{pp\,I\!P}(t_2)^2\, |\xi_{I\!P}(t_1)|^2 \xi_{I\!P}(t_2)|^2$$

$$\left[\frac{\alpha(s_{tot})}{\alpha(M^2)}\right]^{\alpha_{I\!P}(t_1)+\alpha_{I\!P}(t_2)} \frac{M^2}{s_{tot}}\, \sigma_{I\!P\,I\!P}(M) \qquad (4.1)$$

where $\xi_{I\!P}(t)$ is the 'signature' factor for the reggeon, normalized so that $Im\xi=1$, and α' is the Regge slope of 0.9 GeV^{-2} introduced to make all the couplings β dimensionless. With such a normalization the pomeron contribution to the pp total cross-section is then

$$\sigma_{pp}^{tot} = \alpha'\, \beta_{pp\,I\!P}(0)^2 \qquad (4.2)$$

The explicit M^2/s_{tot} in eq (4.1) is a flux factor, which is to be distinguished from the $\alpha(s_{tot})/\alpha(M^2)$ factor. Though when $s_{tot} >> M^2 >> 1$ GeV^2, this also becomes s_{tot}/M^2. In general $\alpha(M^2) = 1/2 + \alpha' M^2$ is expected from the f-dominance of the pomeron; such a form provides an extrapolation to low dimeson masses of this Regge behaviour[45]. As s_{tot} is so enormous, $\alpha(s_{tot})$ can be replaced by $\alpha' s_{tot}$, leading to the expression

$$\frac{\alpha(s_{tot})}{\alpha(M^2)} = \frac{\alpha' s_{tot}}{\frac{1}{2} + \alpha' M^2} = \frac{s_{tot}}{M_\rho^2 + M^2} \qquad (4.3)$$

In the AFS experiment, t_1 and t_2 cover such a tiny range near the forward direction that we can take $t_1=t_2=0.03$ $GeV^2=t$ and $\alpha_{I\!P}(t)=1$. Then we simply have

$$\sigma_{I\!P\,I\!P}(M) = \frac{1}{2\alpha'^2\, \beta_{pp\,I\!P}(t)^4} \frac{(m_\rho^2+M^2)^2}{M^3} \frac{d^4\sigma}{dt_1 dt_2 dy dM} \qquad (4.4)$$

4.2 Overall mass dependence of the cross-section

Though this is inessential to our spectroscopic analysis of these data, it is interesting to see if we can understand the mass dependence of this cross-section over the whole region studied. Expressing the cross-section in terms of the $I\!P\,I\!P$ amplitude $\mathfrak{F}(M^2,z)$, where z is the cosine of the scattering angle of the mesons in the pomeron-pomeron c.m. for dipion production, this amplitude can be crudely modelled by one pion exchange.

That the $I\!P\,I\!P \to MM$ process has such a one meson exchange Born term means that the Adler condition requires no vanishing of such amplitudes close to threshold[24], in contrast to $\pi\pi$ scattering itself. This will be important later on. This $I\!P\,I\!P$ reaction is in many ways similar to the $\gamma\gamma$ process[46]. Though both have one meson exchange Born terms (whether reggeised or not is almost irrelevant), their phenomenology requires this contribution to have low partial wave components that are strongly absorbed. Exactly how is not well understood[46]. Nevertheless, we can use such a model to illustrate the overall trend of the dipion mass spectrum. To confront the data we have to fold in the experimental angular acceptance function. From Cecil's thesis[44] we learn that this is

$$A(M,z) = \sum_{L\ even} (2L+1)\, H_L(M)\, P_L(z) \qquad (4.5)$$

with z the cosine of the scattering angle in the dimeson rest frame and where the coefficients $H_L(M)$ are given by Cecil for $L \leq 8$ up to 2.5 GeV - the acceptance function is roughly like $(1-z^2)^2$. With a free overall normalisation, we see from Fig. 4.2, where (M^4) times the experimental cross-section is plotted, such a model can crudely describe the fall of the data. Of course, this amplitude has no explicit M^2-channel dynamics. From old ideas on the duality, we may expect pion exchange to average this in some sense, which it approximately does. However, such duality was never a well-defined concept for pomeron processes[47], as discussed again in Sect. 4.4, so perhaps we should not expect any better agreement. We would expect such an approximation to model the trend of the earlier data of Waldi et al[12], if we knew the relative acceptance and included the effects of the larger range in t_1, t_2 in eq (4.1).

4.3 S-wave dimeson production

Let us now turn to our main purpose which is to analyse S-wave dimeson production. Decomposing the $I\!P\,I\!P$ cross-section into components for which the dimeson final state has definite spin J, the contribution a partial wave $\mathfrak{F}^J(M)$ makes is

$$\sigma^J_{I\!P\,I\!P}(M) = 16\pi \frac{\sqrt{M^2-4\mu^2}}{M^3} (2J+1)\, |\mathfrak{F}^J(M)|^2 \qquad (4.6)$$

where μ is the mass of each of the final state mesons, π or K as appropriate. Detailed analysis of the dimeson angular distribution shows

that the cross-section is overwhelmingly S-wave to well beyond 1 GeV. The AFS collaboration have separated out this S-wave component up to 2.3 GeV and it is this we shall study in both the $\pi\pi$ and $K\bar{K}$ channels. From the tables of Ref. 13, we can deduce these S-wave cross-sections in 50 MeV bins by folding in the appropriate acceptance function, or more readily we can read off the full-corrected S-wave cross-section from Cecil's thesis[44] Fig. 7.11 (our Fig. 5.7) in 25 MeV bins. The corresponding S-wave amplitudes are then given by combining eqs (4.4, 6) to give

$$|\mathfrak{J}^{J=0}(M)|^2 = N \frac{(m_\rho^2+M^2)^2}{\sqrt{M^2-4\mu^2}} \frac{d^4\sigma^{J=0}}{dt_1 dt_2 dy dM} \qquad (4.7)$$

where

$$N = \left[32\pi\ \alpha'^2\ \beta_{pp\,I\!P}(t)^4\right]^{-1}$$

The circumstance that the $\pi\pi$ and $K\bar{K}$ channels both couple strongly must be allowed for in the formalism. From Sect. 3.1 we have for $I\!P\,I\!P \to \pi^+\pi^-$

$$\mathfrak{J}_1^{I\!P\,I\!P} = \sqrt{\frac{2}{3}}\left[\alpha_1^{I\!P\,I\!P}\ T_{11} + \alpha_2^{I\!P\,I\!P}\ T_{21}\right] \qquad (4.8)$$

where the $\sqrt{2/3}$ is the appropriate isospin Clebsch-Gordan coefficient, and for $I\!P\,I\!P \to K^+K^-$

$$\mathfrak{J}_2^{P\ P} = \frac{1}{\sqrt{2}}\left[\alpha_1^{I\!P\,I\!P}\ T_{12} + \alpha_2^{I\!P\,I\!P}\ T_{22}\right] \qquad (4.9)$$

where again $1/\sqrt{2}$ is an isospin factor. The functions α_1 and α_2 contain the left hand cut singularities of the $I\!P\,I\!P$ amplitude which differ from those of $\pi\pi$ scattering being in principle complicated by additional singularities of the six point function $pp \to pp\pi\pi$ as studied by Halliday[48]. Nevertheless, with such a small range in t_i, the major difference along the right hand cut is, as we have already remarked, the fact that the Adler condition requires no near threshold zero in the $I\!P\,I\!P$ channel, in contrast to most other pion processes we consider. So though we parametrize α_1, α_2 by simple polynomials in M^2 suitable to describe their smooth behaviour along the right hand cut, they are not expected to vanish close to threshold. The reader sceptical of the details of the Regge analysis from Eqs. (4.1, 4, 7) need not despair, since our treatment and hence our conclusions, do not necessitate these forms being exact. Any imperfections in these flux

factors for $I\!P\,I\!P$ scattering will naturally be smooth functions of dimeson mass and consequently absorbable in the α_i's. It is only the interpretation of these as 'intrinsic couplings' that is affected. Nevertheless the fact that $\tilde{P}$ of Eq. (3.13) turns out to be almost constant, Sect. 5.2, indicates that these Regge forms are borne out by experiment.

In principle, knowing $\mathfrak{J}_{11}$, $\mathfrak{J}_{12}$ and $\mathfrak{J}_{22}$ from fitting the $\pi\pi \to \pi\pi$ and $\to K\bar{K}$ channels, the ISR data just determine α_1, α_2. However, the AFS results provide significant extra information on the hadronic $\mathfrak{J}_{ij}$ in the 1 GeV region to add to the traditional meson scattering processes, largely because the $\pi\pi$ S-wave is small there and the angular distribution in $\pi\pi \to \pi\pi$ scattering controlled by S-P interference effects. In contrast, the $I\!P\,I\!P$ reaction is overwhelmingly S-wave even at 1 GeV and a more accurate signal is obtained. Thus the AFS data acts as a severe constraint on the determination of even $\mathfrak{J}_{11}$ and $\mathfrak{J}_{12}$, particularly through the crucial $K\bar{K}$ threshold region. In Sect. 5 we describe fits to the data selected in Sect. 3.3, together with the AFS S-wave dimeson results[13,44].

4.4 Note on the D-wave cross-section

Using notions of duality one can also estimate the expected cross-section for f-resonance production in this double pomeron process. Assuming the triple Regge coupling of the f to two pomerons determined in $pp \to pX$ with the f-exchange having zero mass extrapolates on shell in the same way as the f coupling to $\pi\pi$ does, one predicts from the triple Regge analysis of Inami and Roberts[49] that the f-signal in the reaction $pp \to pp\pi\pi$ in the kinematic regime of the AFS experiment should be at least 5μb GeV^{-4} for $d^4\sigma/dt_1 dt_2 dy\, dM$ integrated over the f-width[50]. The partial wave analysis[13,44] gives the 'observed' cross-section to be merely (0.5 ± 0.3) μb GeV^{-4}. This discrepancy, discussed in more detail in Ref. 50, could be ascribed either to a failure of simplistic duality ideas for pomeron couplings or an incorrect modelling of the relative D-wave acceptance in this experiment or both. Even if the experimental D-wave acceptance is at fault, this has little bearing on the predominantly S-wave cross-section we use, since such correction factors will inevitably be smooth functions of dimeson mass and so, as discussed in Sect. 4.3, absorbable in the coupling functions $\alpha_i(s)$. It is for this reason that the previous simpler analysis[15] using earlier data with no acceptance corrections or partial wave separation at all is

quite consistent with the present treatment Sect. 5.2.

Nevertheless, the fact that the f-signal is so small in the AFS results, while clearly seen in other ISR experiments with larger t_1, t_2 ranges (Fig. 4.1) may indicate that the fIPIP coupling has a more complicated t-dependence than we have naively assumed. Only by comparing the relative t-dependence of the S and D-waves at both large and small momentum transfers will we understand this dramatic difference between the 3% D-wave in the AFS experiment in the f-region and 47% in that with the SFM.

Section 5: Solutions required by experiment

5.1 The Fit

In section 3 we introduced a formalism to implement two channel unitarity. This is readily expressed in terms of either the K-matrix, or its inverse the M-matrix, eqs (3.14, 15). Their real matrix elements we parametrize by sums of poles plus simple polynomials in s, the square of the dimeson mass, eqs (3.18, 20). These forms determine the $\mathcal{J}$-matrix elements $\mathcal{J}_{ij}$, eqs (3.14, 15) and, through the channel dependent functions α_i, the amplitudes for each production process, eq (3.8). In this section we describe the outcome of an extensive global fit of these forms to the I=0 S-wave data on $\pi\pi \to \pi\pi$, $\pi\pi \to K\bar{K}$ selected in sect 3.3 and the cross-section for $\pi\pi$, $K\bar{K}$ production in the AFS experiment discussed in Sect. 4.

In general, we have not concerned ourselves with the fact that the experimental results are binned. In fitting, we have treated each datum as though it represented the value of the experiment at the bin's mean energy value. This is appropriate for smoothly varying amplitudes. However, in the case of the AFS results in the neighbourhood of 1 GeV, for both $\pi\pi$ and $K\bar{K}$ channels[13], we have actually averaged the parametrizations over the bin widths, using Simpson's rule, when comparing with these data. This correctly allows for any rapid variation in the $\mathcal{J}$-, and consequently $\mathcal{F}$-, matrix elements in this region. We have found many equally good fits to all the 258 data in the mass range from $\pi\pi$ threshold up to 1.7 GeV. These are characterised by their type of parametrization and denoted accordingly by K_1, K_3 and M-fits.

In terms of the K-matrix of eqs (3.14,18), we find the most economical fits (in terms of the number of parameters) to have at least one pole of the K-matrix. (Such a pole does not necessarily impose poles in the $\mathcal{J}$-matrix, if the polynomial "background" is sufficiently complicated). We find this pole always lies close to $K\bar{K}$ threshold and the parameters of a typical one pole solution (K_1) are shown in Table 5.1. The quality of the fit to all the data is shown in the table and in Figs. 5.1-8. Apart from the revised error on one datum discussed in sect 3.3, no attempt has been made to weight particular sets of data in their contribution to χ^2 by anything other than the errors quoted in the relevant analysis of each data set. The $\chi^2/d.f$ is then roughly 1.3. As seen from Figs. 5.1-8 the major contribution to χ^2 comes from the conflicting data sets on ϕ_{12}, Fig. 5.6. Leaving out either of these, i.e. exercising a prejudice as to which is correct, decreases the $\chi^2/d.f.$ in our otherwise global fit. This exercise favours Etkin et al[37] over Cohen et al[35] with a $\chi^2/df.$ of only 1.09 compared with 1.23. The parameters of the solution, K_1 (Etkin), fitting the $\pi\pi \to K\bar{K}$ results of just Etkin et al are listed in Table 5.1 too. However, we find our amplitudes change so little between such alternatives that for the most part we quote those of the compromise global fit[51], Figs. 5.1-8. We will comment later on this stability. Apart from the troublesome $\pi\pi \to K\bar{K}$ results, the data are very well fitted as illustrated in Figs. 5.1-8, even, for example, the 3 data sets on the $\pi\pi$ phase, δ_{11}, above 1 GeV from CERN-Munich as analysed by Ochs[30] and by Martin and Pennington[33] and from the $\pi^0\pi^0$ results of Cason et al[32]. Though these are not exactly consistent, the fit has found a very satisfactory smooth track through these data, see Figs. 5.2, 4.

As already remarked in Sects. 1 and 4, the input of the AFS double pomeron results is a severe constraint on the solution, not just on the couplings α_i, for which quadratic forms have been used (eqs 3.8, 21), but on the strong interaction amplitudes $\mathcal{J}_{11}$ and $\mathcal{J}_{12}$. The AFS data tightly restrict how the amplitudes develop through the $K\bar{K}$ threshold region. This is reflected in the much more striking and stringent conclusions we will be able to deduce from this analysis than was previously possible using just elastic hadronic reactions. Notice in Fig. 5.7, the shoulder at $M \sim 0.9$ GeV before the steep fall. This is an important feature of both the AFS data[13] and all our fits as will be discussed in Sect. 7. Such a structure is also seen in the $\gamma\gamma$ data discussed in Sect. 6.2.

It is important to note that the rapid variations in $\mathcal{J}$-matrix elements required by experiment in the crucial $K\bar{K}$ threshold region, Figs. 5.1-8, are not wholly generated by the nearby K-matrix pole. Rather they are due to the interplay between this pole and the "background" polynomial. Because of the structures required near $K\bar{K}$ threshold, we have not been able to find solutions without a K-matrix pole with less than 40 parameters, though with more parameters we believe this may be possible. We have on the other hand been able to find further solutions with additional poles in the K-matrix and a consequently simpler polynomial background, cf eq (3.18). The parameters of a typical three pole solution, K_3, are tabulated in Table 5.1. The introduction of more poles turns out not to change the global description of the data and the fits are almost indistinguishable from K_1 of Figs. 5.1-8. One of the poles is always near that in K_1, ie near $K\bar{K}$ threshold, while the other two are dispersed, so that compared with solution K_1 the effect of these extra poles in K_3 is just to reparametrize the smooth background - one pole occurs below $\pi\pi$ threshold reparametrizing left hand cut effects and the other above the region we fit reparametrizing the high energy continuum. The quality of the fits is remarkably similar, as are the detailed features of these different amplitudes, as we shall describe in Sect. 7.

In an attempt to obtain distinct solutions, we have tried to fit the data with an M-matrix parametrization, eq (3.20). Since the M-matrix is the inverse of the K-matrix, non-factorising poles of one are zeros of the other. From PCAC we expect the amplitudes $\mathcal{J}_{11}$ and $\mathcal{J}_{12}$ to have low energy Adler zeros eqs (3.7,18). We therefore require the M-matrix to have a pole at $s=s_o$, cf eqs (3.20,18). Once again we find an economical description of these multifarious data sets requires another (factorising) pole in the M-matrix. This pole is closely related to that near 1 GeV in the K-matrix fits, as will be discussed again in Sect. 7. That such a pole should occur is no surprise. A factorising pole in the K-matrix generates a simple pole in det $\underset{\sim}{K}$ (no double pole). Such a pole automatically generates a nearby zero. This is because in the neighbourhood of the pole, the pole term takes on all values from $-\infty$ to $+\infty$. A zero then automatically occurs, provided the background is non-zero: how near it is to the pole depends on the relative strength of the pole's couplings and the "background" polynomial. Such a zero in the det $\underset{\sim}{K}$ requires a pole in its inverse, viz det $\underset{\sim}{M}$. The parameters of the typical M-fit are also listed in Table 5.1. Again the

quality of the fit is excellent and the resulting physical amplitude almost identical to solutions K_1 and K_3 - see Sect. 7. The small differences between these amplitudes is highlighted by looking at the Argand plot of the $\pi\pi \to \pi\pi$ S-wave, $\rho_1\mathcal{J}_{11}$. In Fig. 5.3 the solutions K_1, K_1(Etkin), K_3 and M are compared. They are essentially identical except for the energy range of 960 to 1100 MeV, and then only K_1 (Etkin) differs above 1040 MeV. In this region of $K\bar{K}$ threshold, the amplitudes are varying most rapidly and so differences become exaggerated. Focussing on K^+K^- threshold where each solution leaves the circle and remembering that unitarity requires $\phi_{11} = \phi_{12}$ up to this energy, we see how changes in this point can bring a sizeable difference in ϕ_{12} with only a small change in the corresponding amplitudes and their consequent pole structure (see Sect.7.1). From Fig. 5.3, the phase ϕ_{11} $[\phi_{11} = \delta_{11} + \tan^{-1}((1-\eta)/(1+\eta)\tan\delta_{11})]$ is seen to fall quickly above K^+K^- threshold by almost 90^0 before rising again. It seems rather natural that ϕ_{11} and ϕ_{12} having been equal up to K^+K^- threshold should tend to keep together in the 8 MeV up to $K^0\bar{K}^0$ threshold. It is a feature of all our solutions that ϕ_{12} does indeed fall initially just as implied by the $\pi\pi \to K\bar{K}$ results of Etkin et al[37].

Our fitting procedure is predicated on the assumption that the $\pi\pi$ and $K\bar{K}$ channels exhaust the content of unitarity in the energy range for which we fit, namely up to 1.7 GeV. We know, of course, that this is a far too strong an assumption even above 1.2 GeV. Results on the $n\bar{n}$ final state[41] suggest that this may contribute 2% to the inelastic cross-section even in the f region - see Fig. 5.5. Such an additional channel would in fact have only a small effect on our amplitudes. More serious is the appreciable onset of 4π channels near ρ-ρ threshold[42] as mentioned in Sect. 3.3. In Fig. 5.5 we compare results on the inelastic $\pi\pi$ cross-section as determined from the elastic channel by CERN-Munich[29] with the $K\bar{K}$ contribution according to Cohen et al[35] and Etkin et al[37], for example. As discussed already in Sect. 3.3, the fit K_1, of Table 5.1, follows the larger inelastic cross-section implied by the CERN-Munich results. We also report a variant, K_1', on this solution in which the inelastic cross-section is required to resemble more the above $K\bar{K}$ contribution. The truth presumably lies somewhere between the two. In obtaining this solution no phase input on ϕ_{12} has been imposed above 1.4 GeV, just its magnitude. This is because the strict imposition of the $K\bar{K}$ phase (as determined by Cohen et al, for example) is surely over-restrictive in the presence of other appreciable

open channels. Nevertheless, by introducing more parameters a satisfactory fit to the phase information on ϕ_{12} (from Cohen et al) can be obtained giving a solution with a similar pole content to K_1'. As expected, the differences between K_1 and K_1' only occur above 1.4 GeV and then largely in their couplings to $K\bar{K}$. In Sect. 7 we will exhibit these differences which are again small.

5.2 Consistency checks

Here we perform two consistency checks on our solutions and how they fit the AFS double pomeron results. The first is to consider how this much more sophisticated and complete treatment is related to our earlier single channel Omnès analysis using 40% of the AFS statistics with their preliminary treatment of their acceptance. As detailed in Sect. 3.1, this can be done by comparing the two channel function $\tilde{P}$ of eq (3.13) with the single channel P, eqs (3.9, 12), which in Ref. 15 we took to be a constant. The $\tilde{P}$ from our fits is plotted in Fig. 5.9 and is seen to remain remarkably flat, emphasising the universality of the Omnès function below $K\bar{K}$ threshold and indicating no dramatic difference in the way the $\pi\pi$ final state couples to $\bar{p}p$ than to $\pi\pi$ itself. This is to be contrasted with our discussion of the $\gamma\gamma$ process in Sect. 6.2.

In fitting the AFS data we have only considered the S-wave cross-section, eq (4.7), with no reference to its phase. However, there does exist phase information on this channel as analysed by Cecil[44]. Our second check is therefore to compare the prediction for the S-D wave interference predicted by our solutions with that given by experiment. With the D-wave phase assumed dominated by just the f -contribution and so given again by eq (3.24) and its normalisation chosen to reproduce the reported height of the D-wave cross-section (one further parameter), we obtain the prediction shown in Fig. 5.10 in excellent agreement with AFS's experimental interference[13]. Deviations at higher $\pi\pi$ masses are to be expected as the D-wave phase is no longer f-dominated. The ability of our solutions to predict results not fitted make this a very satisfactory test of our amplitudes.

Section 6: Other sources of dimeson final states

6.1: Heavy flavour decays

The dipion mass spectrum observed in the decay of $\psi' \to \psi\pi\pi$ is seen to peak at high $\pi\pi$ masses ($\sim$ 600 MeV). This is often spoken of as reflecting some low mass epsilon-like structure in the I=0 S-wave $\pi\pi$ system. This is to forget that $\pi\pi$ and $K\bar{K}$ decays of the states of hidden charm and hidden beauty are subject to exactly the same constraints as all other hadronic decays by virtue of their common final states. The amplitudes for these S-wave decays are also given by the formulae of Sects. 3.1, 2.

Let us first consider the decays $\psi' \to \psi\pi\pi$ and $T' \to T\pi\pi$ (generically $V' \to V\pi\pi$). The phase space for the $\pi\pi$ final state is limited by the V' - V mass differences of less than 600 MeV. The experimental spectrum for the decay A → B(MM) can be expressed in terms of the appropriate S-wave amplitude $\mathfrak{F}(M)$ by

$$\frac{d\Gamma}{dM} = \frac{\pi^2}{2M_A^3}\left\{\left[(M_A+M_B)^2-M^2\right]\left[(M_A-M_B)^2-M^2\right]\left[M^2-4\mu^2\right]\right\}^{\frac{1}{2}} \left|\mathfrak{F}(M)\right|^2 \qquad (6.1)$$

where M is the dimeson mass and once again μ is the mass of the individual mesons in this pair. The amplitude $\mathfrak{F}$ will be given by an equation of the form (3.8). The functions α_1 and α_2 are expected to contain an Adler zero, as PCAC requires such a zero close to threshold for these ψ' and T' decays, there being no Born term. Otherwise we expect these functions α_1 and α_2 to be simple as these channels have a suppressed left hand cut, since the OZI rule "forbids" $\psi\pi$ and $T\pi$ intermediate states, Fig. 6.1. We therefore parametrize them by a linear function of M^2. The position of the on-shell zero is to be determined by the data. It turns out that the experimental results are well-described by such forms which incorporate the crucial twin ingredients of PCAC and final state interactions required by unitarity[52]. Others[53] have fitted these, and earlier data on the same channels[54-59], with just the constraint of PCAC and a single channel analysis, ie in our language setting T_{11} in eq (3.8) to be a constant and α_2 to zero. In the small mass region explored in these decays, it happens to be true that T_{11} is slowly varying. However, the advantages of this fuller treatment are:

(i) no such fortuitous accidents are needed; nevertheless, a peaking at

larger $\pi\pi$ masses is generated by the low mass suppression provided by the Adler zero rather than a localised ε enhancement;
(ii) by performing a coupled channel analysis we can determine the relative couplings to $\pi\pi$ and $K\bar{K}$.

In Table 6.1 we give the position of the zero, s_o, and the ratio of α_1 to α_2 for the fit to each data set shown in Figs. 6.2,3. Note from Fig. 6.3 that the quality of the fits to the T' data, whether of the ARGUS group at DORIS[56] with over 5000 acceptance-corrected events or the CESR groups[57,58] with over 4000 such events, is excellent. In contrast, the ψ' data, Fig. (6.2), with merely a thousand acceptance corrected events from each of Mark II[54] and Crystal Ball[55] are considerably poorer. This suggests that the statistical errors on the Crystal Ball $\pi^0\pi^0$ results in particular, which are all that are shown in Ref. 55, are far from the total uncertainties on these data.

The one surprise among these decays is when we turn to T" → T$\pi\pi$, which with a larger mass difference allows $\pi\pi$ masses up to 900 MeV. Even though the statistics are poor with only fifty or so events from both CLEO[60] and CUSB[61], Fig. 6.4, we see the data are consistent with unadorned phase space. In our terminology, α_1 and α_2 appear constant and show no sign of vanishing near threshold. Why the Adler zero does not occur in this channel is a mystery. No Born term in the T" → T$\pi\pi$ channel is known, but these data do suggest some unexpected dynamics, which more data would hopefully illuminate.

A particularly fortunate situation would arise if one of these narrow states below heavy flavour threshold would allow $\pi\pi$ masses beyond $K\bar{K}$ threshold. This, together with explicit information on the $K\bar{K}$ channel, would allow another look into the S* region, which at present only the AFS data explores fully. Several such channels are possible but all have complications. First, there is $\psi \to \phi(MM)$, where the ϕ is isolated by its $K\bar{K}$ decay mode. This channel allows dimeson masses up to 2 GeV, again has suppressed left hand cut effects (we know of no $\psi\pi$ or ψK states in keeping with the OZI rule, Fig. 6.5) and can have quite different couplings to $\pi\pi$ and $K\bar{K}$ from any of the channels previously discussed. Here, the "S*" shows as a peak near $K\bar{K}$ threshold, Figs. 6.6,7. This is a sign that the $K\bar{K}$ couplings are dominant, as the presumed $s\bar{s}$ structure of the ϕ would imply, Fig. 6.5(b). The only published data from Mark II at SPEAR[62] are far too

poor to be very precise. However, a dramatic improvement is expected in the near future with results from Mark III at PEP and DM2 at DCI on both the $\phi\pi\pi$ and $\phi K\bar{K}$ channels. Preliminary results have been presented at the 1986 Rencontre de Moriond[63,64] to which we apply our analysis. Knowing $\mathcal{J}_{11}$ and $\mathcal{J}_{21}$, these data can be fitted to determine the coupling functions α_1 and α_2. These each contain the Adler zero for this channel, but with the present uncertainties we merely put s_o, eqs (3.18,20), equal to its $\pi\pi$ position, Table 5.1. As an indication of what can be achieved, we have fitted quadratic forms for the α_i's simultaneously to the published Mark II[62] and preliminary Mark III data[63]. The parameters are listed in Table 6.1 and the fits shown in Figs. 6.6-8. Though the fits are shown as continuous curves they are in fact averaged over the same bins as the data shown, just as for the AFS results (Sect. 5.1). This is essential only in the $K\bar{K}$ threshold region, where our amplitudes have local structure (see Sect. 7.1) resulting in the shoulder and fall in the $|P|P \to \pi\pi$ spectrum (Fig. 5.7), while giving a peak in the present $\psi \to \phi\pi\pi$ distributions (Figs. 6.6-8). Data with sufficient statistics to allow finer binning may usefully check our amplitudes in the 1 GeV region. Indeed, we eagerly await the final Mark III and DM2[64] results, which, once acceptance corrected, the dimeson mass accurately calibrated and the S-wave separated, could be added to the data sets of Sect. 3.3 to constrain the determination of our basic hadronic amplitudes $\mathcal{J}_{ij}$ of Sect. 5.1.

Another reaction with far higher statistics, for which data have been available for a number of years is $\psi \to \omega\pi\pi$[66]. This channel exposes a large $\pi\pi$ mass region and is known to have a sizeable D-wave signal as the f-resonance is clearly seen. However, analysis of this decay is complicated by crossed channel effects[67]. The $\pi\pi$ spectrum, even if it were angular separated, could not be discussed without regard to strong reflections from the $\omega\pi$ channel which, again because of final state interaction effects, has a sizeable B-signal. To arrive at any conclusions from this channel, a full Dalitz plot analysis is necessary together with a complete treatment of the $\omega\pi$ as well as coupled $\pi\pi$ channel.

6.2: Two photon channel

In describing the pomeron-pomeron mechanism in Sect. 4, we have drawn an analogy, at least theoretically, to the two photon process accessible in

$e^+e^- \to e^+e^-(MM)$. Unfortunately only relatively poor statistics results exist for this in principle cleaner channel[46]. Data have been published on dipion production from PLUTO at Petra[68] and from DM1 at DCI[69], Fig. 6.9, the shape of which has been recently corroborated by preliminary results from DM2 at DCI[70]. In the absence of angular separation, we naively assume that all the data below 1 GeV is S-wave. Then having determined $\mathfrak{T}_{11}$ and $\mathfrak{T}_{21}$ in Sect. 5, we can fit these $\gamma\gamma$ data using the analogue of the $I\!P\,I\!P$ scattering formula eq (4.6):

$$\sigma_{\gamma\gamma}^{J=0}(M) = \frac{\sqrt{M^2-4\mu^2}}{M^3} \left| \mathfrak{T}^{J=0}(M) \right|^2 \qquad (6.2)$$

and so determine α_1, α_2 for the $\gamma\gamma$ process. Just as for the $I\!P\,I\!P$ reaction, these are not expected to have an Adler zero, as there is here too a non-zero pion exchange Born contribution. The results of a fit to the PLUTO[68] and DM1[69] data are shown in Fig. 6.9, with the corresponding parameters listed in Table 6.1. We would predict that the DM2[70] data when finalised should have the same form as this.

To compare the $\gamma\gamma$ and $I\!P\,I\!P$ couplings, we plot the relevant function $\tilde{P}$ of eq (3.13) in Fig. 6.10 to be contrasted with Fig. 5.9. We see that while the effective coupling to the $I\!P\,I\!P$ channel shows no mass dependence compared with $\pi\pi$ itself, the $\gamma\gamma$ couplings increase towards 1 GeV. If the data above 1 GeV were angularly separated, and the $K\bar{K}$ channel also explored, we could use our analysis to determine the $\gamma\gamma$ couplings of the scalar states in our amplitudes - states we reveal in Sects. 7, 8. A crude extrapolation of the S-wave couplings of Fig. 6.10 up to 1.4 GeV (unconstrained by any data in that region!) does suggest however that there is a large S-wave signal under the f and emphasises the importance of a partial wave separation before results on the size of the f signal can be believed. Moreover, after this analysis was completed, new results from the TPC $\gamma\gamma$ collaboration have been published[71], which do not agree with the PLUTO data of Fig. 6.9 (and hence 6.10) and so no firm conclusions can be drawn until this discrepancy is resolved. Nevertheless, the formalism outlined in Sect. 3 should apply as previously discussed for instance by Lyth[72] and by Mennessier[73].

Section 7 : Poles of the S-matrix

7.1 : Where the poles are

In the following sections, we resume our main theme addressing the question: What I=0 scalar dynamics is entailed by our combined fit? The ensuing discussion may appear tortuous : that is inevitable given the complexity of the phenomena. When people discuss the pseudoscalars or tensors, there is no question that the $\iota(1440)$ or $\theta(1690)$ are resonances or what the other 0^{-+} and 2^{++} states are; speculative interpretation starts from that point. For the scalars, especially in the I=0 sector, it is a major and subtle enterprise to establish what the resonances are, still more to assign meaningful parameters. The difficulty stems from all the classic complications of the resonance concept occurring simultaneously: resonances are variously broad and overlapping with substantial coupling to strongly opening channels. That is why we have to proceed in rather slow careful stages.

In the present section, we list and discuss the pole content of our solutions pointing out how our rather elaborate pole scenario is tied to the phenomena it explains and to general requirements on possible structures of the S-matrix. The ensuing list of poles and residues is the objective outcome of our analysis. As we shall show in this section, in all our solutions, we always find seven poles of the S-matrix below 1.7 GeV. In Sect. 8, we attribute these to four resonances, two broad objects $\varepsilon(900)$ and $\varepsilon'(1430)$[74] and two narrow resonances $S_1(991)$ and $S_2(988)$, which together reproduce the S^* phenomenon. Couplings to $\pi\pi$ and $K\bar{K}$ reveal the $\varepsilon(900)$ and $\varepsilon'(1430)$ to be consistent with a $(u\bar{u} + d\bar{d})$ composition; likewise the $S_2(988)$ shows an $(s\bar{s})$ composition and the $S_1(991)$ behaves like an SU(3) singlet, compatible with a glueball make-up.

Having sketched our destination, we now proceed to detail and justify this pole content of our solutions. This entails specifying not only positions and residues, but also on which sheet of the energy plane poles are located, Fig. 7.1. This latter is only an issue when dynamical activity coincides with the opening of a new threshold - precisely, the present case. Normally, all but one of the unphysical sheets of the energy plane is remote and resonances are unambiguously identified with poles on the adjacent

sheet, e.g. for ρ(770) sheet II and for f(1270) sheet III. A new threshold temporarily multiplies possibilities, since three unphysical sheets adjoin the physical region and can be the seat of physically significant resonance poles. The resulting structure is conveniently displayed in a k_2 plane (Fig. 7.2a), which explicitly distinguishes the two alternatives $k_2 = \pm \sqrt{\frac{1}{4} E^2 - m_K^2}$ corresponding to a given complex energy E.

Resonance poles usually have images on related sheets, for example, the physical f-pole has a counterpart on Sheet II and that of the ρ on Sheet III. In the k_2-plane, these images occur at approximately the mirror positions $k_2^{II} = - k_2^{III}$, as follows directly from the Breit-Wigner description of these resonances. Normally, this phenomenon of pairing is of no physical importance. It is only where resonances occur close to the corresponding threshold that both members of such a duo get the chance to affect the physics. As we shall see, the present solutions illustrate this possibility in quite a complex fashion.

Before elaborating on this, we need to amplify the statement that resonance poles usually have images and to explain how exceptions come about. The general idea is as follows: let $\underset{\sim}{T}^{II}$ denote the scattering matrix on Sheet II and $\underset{\sim}{T}^{III}$ its counterpart on Sheet III. The analytic continuation from one to the other is specified by the relation[75]

$$[\underset{\sim}{T}^{III}]^{-1} = [\underset{\sim}{T}^{II}]^{-1} + 2i\underset{\sim}{\rho}_2 \qquad (7.1)$$

and resonances are associated with zeros of det $(\underset{\sim}{T}^{-1})$. Normally, the variation with energy that produces such zeros is already present in the corresponding inverse K-matrix elements (cf eq (3.15)). A resonance pole in T^{II} then readily induces an image pole in T^{III} and vice versa; this is what usually occurs. However, it can happen that the K-matrix elements are essentially constant. Then it is the phase space factors, in particular the rapidly varying ρ_2, which feeds the resonant variation. In this case, the image pole does not occur (or has "moved off to infinity") and one has the situation referred to as a virtual bound state. The pole configuration that our solutions generate combine both possibilities. Despite appearances this corresponds to quite a simple structure of the K-matrix.

As already described in Sect. 5, we have performed fits using both K-matrix

and M-matrix forms. The former yielded solutions for 1 explicit K-matrix pole, denoted K_1, a variant K_1', and a solution for 3 poles, labelled K_3; corresponding to the latter we obtained a single fit which we term M. The pole pattern that emerges from each of these types of solution is remarkably stable. The details are displayed in Tables 7.1,2, and Figs. 7.2,3. Each solution is seen to have seven 'nearby' poles, denoted A-G. Though S-matrix poles are not demanded by the forms with which we fit, they are the most important outcome of our solutions. Table 7.1 gives their positions for our representative solutions K_1, K_1', K_3 and M, while Fig. 7.2a, b displays these in the k_2 and energy planes respectively, the latter illustrating how sheet II and sheet III poles form pairs, viz D-E and G-F. In Fig. 7.3 are plotted the complex residues of these poles, defined by:

$$\gamma_i \gamma_j = \lim_{s \to s_R} (s_R - s)\, T_{ij} \qquad (7.2)$$

In fact, to make the plot intelligible we show γ_1 and $\tilde{\gamma}_2 = - \gamma_2$. The average value of these couplings for each of our seven poles are tabulated in Table 7.2. Such residues are a prime clue as to the parton content on the associated resonances as discussed in Sect. 8.3.

We must remark that the foregoing are not the only structures in our amplitudes. Forms which fit data along a limited region of the real axis in the energy plane inevitably also have distant poles which are mere artefacts of the parametrization and consequently are unstable. Such poles occur for all our solutions on the physical sheet I. Though such poles violate causality, they always occur at least 500 MeV into the complex plane and so have no effect on the nearby structures reliably determined by the data.

To gain a mental picture of the complex pole scheme that has emerged, it is helpful to flip between the plot in terms of the k_2-plane (Fig. 7.2a) and that in the energy plane (Fig. 7.2b). Read together, these display a short range system comprising the triplet A, B, C governing the $K\bar{K}$ threshold region, and long range structure dominated by the pole pairs D-E and G-F. It is the former that constitutes the principal novelty of our solutions. The poles revealed by many previous analyses (using subsets of the data we consider) are illustrated in Fig. 7.4[76]. As will be seen[76], analyses of the S* have quite a long history[77] with one pole[78,79] and two pole scenarios[29,30,80,81] having early exemplars. For discussions in a similar

spirit to the present one (although leading to quite different conclusions owing to different input) see especially Refs. 81, 82 and 83. (The last of these focusses very much on the $K\bar{K}$ data of Ref. 35 and only uses $\pi\pi$ information over the very restricted mass range 0.91 to 1.05 GeV). The PDG average[18] (in our terms for the position of pole A) is dominated by the result of fitting the low statistics data on $\psi \to \phi\pi^+\pi^-$ of Ref. 62. This we believe to be quite unjustified as evidenced by the ease with which we fit the same data (Fig. 6.2) using our own $\mathcal{T}$-matrix solutions with their appreciably different pole positions (see Fig. 7.4(b) and caption thereof). These various analyses[76] have commonly reported just one pole (similar to A), or sometimes two, to describe the S* effect whilst we find three. Wherein lies the difference? More generally, what is the role of all our poles in achieving the reported fits? For the present we focus on the pole positions deferring interpretation of the associated residues (Table 7.2 and Fig. 7.3) until Sect. 8.

As a step to answering the above questions, we examine what types of energy variation alternative pole configurations can achieve. Suppose just one pole controlled the $K\bar{K}$ threshold region, say at a position $k_2=k_A$. There will in general be a background phase, δ_b. Allowing for this, a minimal representation for the $\pi\pi$ S-matrix element $\mathcal{S}_{11}$ is simply:

$$\mathcal{S}_{11} = \left(\frac{k_2 + k_A^*}{k_2 - k_A}\right) e^{2i\delta_b} \qquad (7.3)$$

This illustrates the rule that a pole at $k_2=k_A$ automatically entails an associated zero of $\mathcal{S}_{11}$ at the mirror point $k_2=-k_A^*$. This is a general result and follows from analytically continuing unitarity to the pole. The pole A of our fit (on sheet II) produces the familiar sharp rise of the $\pi\pi$ phase shift just below $K\bar{K}$ threshold seen in Fig. 5.1. This is the classic signal for the S^* resonance and, for that reason, some version of A has featured in all analyses of the past 13 years[76] (cf Fig. 7.4). The associated zero of $\mathcal{S}_{11}$ required by unitarity of itself produces a deep dip in the inelasticity, η_{11}, just above threshold, Fig. 5.2. Such a feature is qualitatively in agreement with experiment. It is for achieving quantitative agreement that other poles come into play[84].

It has long been argued[29,30,80,81,19] that a one-pole description of the S^*-effect gives too blunt a signal in $\sigma(\pi\pi \to K\bar{K})$ (or, equivalently in the behaviour of η_{11}) as compared to the data. The qualitative effect is easily understood, either in terms of the poles and zeros picture sketched above,

or by remarking that having just a sheet II pole with no corresponding sheet III image is, in a sense, to have half a resonance. Away from the resonance, the corresponding amplitude falls like $|E - E_{res}|^{-\frac{1}{2}}$, rather than as $|E-E_{res}|^{-1}$. Already for fitting the CERN-Munich $\pi\pi$ phase-shift data[29] (part of the input to the present fit), two-pole ansatzes yield much better fits to the S^* region than do one pole formulae, such as arise from the complex scattering length description. The contrast is very clearly exposed in Ref.81 (see especially their Fig. 2) wherein a two-pole description is seen to be far superior for following the long range trends of both δ_{11} and η_{11}. How does our solution with 3 poles fare in comparison ? It turns out that the phase shift prediction hardly differs, but the inelasticity profile has a less pronounced and broader minimum (Fig. 5.2), consonant with the actual $\pi\pi \to K\bar{K}$ cross-section information used in the present fit and the assumption that the $K\bar{K}$ channel saturates inelasticity. The way our fit has responded to this requirement is to move pole C upwards towards the real axis (Fig. 7.4) as compared to Ref.81's version of this feature. Finally, all this readily provides an excellent fit to the $I\!P I\!P \to \pi\pi$ production spectrum including the shoulder just below 1 GeV.

The primary role of the pole B in a χ^2 sense is to enable the locations for A and C, required by the data, to co-exist within the general constraints of unitarity. As we shall report in Sect. 7.2, removal of pole B dramatically worsens the fits. There are, of course, potentially, much more direct signals for B. The expected sharp peak in $\sigma(I\!P I\!P \to K\bar{K})$ just above threshold is to an extent borne out by the data (Fig. 5.8). With a pole so close to threshold very striking differences should appear between spectra for K^+K^- and $K_S^0K_S^0$. The latter channel should also register a very sharp peak (uncontaminated by a $\phi(1020)$ signal) in $K^-p \to A(\Sigma)K_S^0K_S^0$. Another consequence of B should be a very sharp downward blip in $\phi_{12} = \arg \mathcal{T}_{12}$ just above threshold and indeed there are hints of such behaviour in the observations (Fig. 5.6). We have previously[16] suggested that this feature of the input plays a significant role in selecting the 3-pole option. We now know this not to be the case (see Sect. 7.2 following).

Our long range pole pairs D-E and G-F are certainly the absolute minimum of complexity needed to describe the presently available data. An important goal for future experiments is to establish whether it is also sufficient. Already, additional structure has been claimed, for example by Etkin et al[85]

on the basis of $\pi\pi \to K\bar{K}$ information, and also from an amplitude analysis of $\eta\eta$ production[41]. Nevertheless, the scheme for the long range poles, revealed by our solutions, is attractive from the point of view of economy. As always, it will be difficult to tie down detailed pole parameters closely; indeed their very existence is deduced from long range phase movements (cf discussion of the analogous but much less complicated $\kappa(1350)$ effect in $K\pi$ scattering[86]). Nevertheless, the pairing D-E successfully unites the source of the slow rise of δ_{11} from $\pi\pi$ threshold (the old $\varepsilon(900)$ effect) principally given by D with the description of phase movements above 1 GeV via E. In Sect. 8, we shall base our resonance assignments on the foregoing pattern of short range and long distance poles.

7.2: the role of pole B

The principal new feature of our analysis is that we find 3 poles, A, B, C in the region of $K\bar{K}$ threshold rather than the one or two of previous treatments, which only considered subsets of the data we have used. Remember that our parametrizations do not 'a priori' have any particular number of poles of the S-matrix, yet all our solutions have this same A, B, C structure.

When resonances are narrow and non-overlapping and a single channel predominates, it is relatively easy to investigate the effect of adding in or taking out particular resonances. In the present situation with strongly coupled channels, this is non-trivial to implement because of the over-riding need to ensure that unitarity remains satisfied. Nevertheless, we present here a way to discuss why our analysis finds 3 poles in the neighbourhood of $K\bar{K}$ threshold whilst previous treatments did not.

To allow the number of $\mathcal{S}$-matrix poles to be fixed "a priori", consider the Jost function (or determinant[87]), which up to some real function $d(k_2^2)$, is the denominator of the $\mathcal{S}$-matrix, so that

$$\phi(k_2) = d(k_2^2)\,[1 - i\rho_1 K_{11} - i\rho_2 K_{22} - \rho_1\rho_2 \det K] \qquad (7.4)$$

The zeros of ϕ, which correspond to poles of $\underset{\sim}{\mathcal{S}}$ or $\underset{\sim}{\mathcal{J}}$ and thus to resonances, are its sole source of variation apart from distant effects from the $\pi\pi$ threshold and from left hand cuts. The function $\phi(k_2)$ thus provides a

highly suitable vehicle for exploring possible pole scenarios for the $K\bar{K}$ threshold region. Indeed, it enables one to parametrize amplitudes explicitly in terms of poles by representing the Jost function by a simple product of zeros (one for each pole) and an entire function. Thus, we write for example

$$\phi(k_2) = \left[1 - \frac{k_2}{k_{2A}}\right]\left[1 - \frac{k_2}{k_{2B}}\right]\left[1 - \frac{k_2}{k_{2C}}\right] \exp\left[\sum_{n=0} \gamma_n k_2^n\right] \qquad (7.5)$$

where the γ_n are complex numbers and $k_2 = k_{2j}$ (j = A, B, C,) are the three poles A, B and C. Comparing eqs (7.4,5) above $\pi\pi$ threshold, we can read off K_{11}, K_{22} and $\det \underset{\sim}{K}$ and consequently relate the $\underset{\sim}{\mathcal{J}}$-matrix elements to the parameters of eq (7.5). Unitarity, of course, requires K_{12} real, i.e. $\eta_{11} \leq 1$. Unfortunately, here this condition is not automatic requiring $K_{11} K_{22} \geq \det \underset{\sim}{K}$ which, though trivially fulfilled by a $\underset{\sim}{K}$ or $\underset{\sim}{M}$ -matrix parametrization, is easily lost writing $\phi(k_2)$ as a product of zeros. This condition must thus be checked at every stage. Practice shows this constraint greatly restricts the acceptable region of the γ_n parameter space.

The arbitrary function $d(k_2^2)$ cancels out in physical quantities, viz the $\mathcal{J}_{ij}$, as does any arbitrary real function in eq (7.5). Thus we can set $\mathrm{Re}\,\gamma_{2n} = 0$ for all n. Such a form as eq (7.5) with only 3 poles (and not the 7 of Fig. 7.2) can only be expected to represent experiment in a limited region of the k_2 plane. Specifically, from Fig. 7.2a, we see that we can expect the poles D-G to provide just a smooth background for $|k_2| \leq 0.24$, say, i.e. $0.87 \leq E \leq 1.10$ GeV. Our aim is first to show that a fit of all the data in this limited energy regime with a 3 zero form like eq (7.5) is possible and then to compare this with a similar fit using a two zero form (i.e. to remove the B pole). Because of the condensed ranges of the parameters that allow unitarity to be fulfilled, we must choose the starting parameters with care. In the case of the 3 pole scenario, these are readily found by first fitting the form eq (7.5), to any of the amplitudes we already found with 3 poles. We then refit the experimental data within a $|k_2| < 0.24$ GeV radius of $K\bar{K}$ threshold. The result for all the classic $\pi\pi$, $K\bar{K}$ and AFS double pomeron data are listed in Table 7.3. In this narrow energy range, the discrepant results on ϕ_{12}, Fig. 5.6, play a dominant role. Hence, the compromise fit has a χ^2/d.f. of 2.2, while selecting Etkin et al[37] very satisfactorily reduces this to 1.1 for the 3-pole fit. The 17

parameters, of Table 7.3, are the complex numbers k_{2A}, k_{2B}, k_{2C}, $\gamma_n (n = 0,3)$ and the real functions $\alpha_1^{IP\,IP}$, $\alpha_2^{IP\,IP}$. The success of such a fit illustrates that a parametrization in which poles of the S-matrix simply enter as a product of zeros in the Jost function is viable.

Our next step is to compare such a fit with one with only two poles. To obtain good starting parameters without the B pole, we choose a form with the positions of A and C as found by Fujii and Fukugita[81] fitted just to the CERN-Munich $\pi\pi$ data[29]. A perfectly adequate fit can be retained not only when the $\pi\pi$ results of Cason et al[32] are added, but when we include one of the $\pi\pi \to K\bar{K}$ data sets. This shows that a two pole scenario is equally possible for all the classic dimeson channels. It is when the AFS results on $\pi\pi$ and $K\bar{K}$ channels[13] are introduced that the 2-pole form fails dramatically even in this limited energy regime. With many random starts, the best χ^2's we have achieved are listed in Table 7.3. All are considerably worse than the corresponding 3-pole solutions. The fits are no longer able to reconcile the AFS data with any of the results on $\pi\pi \to K\bar{K}$. Even to achieve these limited successes, the poles A, C both move very close to the axis from the Fujii-Fukugita positions[81] (Figs. 7.2b, 7.4) to compensate for the lack of the B pole.

This analysis unambiguously favours our solutions with 3 poles in the neighbourhood of $K\bar{K}$ threshold. The confidence level for this is some 30%, while that for just 2 poles, when the AFS information is included, is less than 0.01%!

Section 8 : Resonance assignments and interpretation

8.1 Introduction

Converting the pole structure reported in the previous section to a resonance spectrum presents some unusual methodological problems. As already emphasized, most resonance poles have replicas on associated sheets. Usually, this fact though true is academic; not so here. A striking illustration is provided by our pole pair (D-E) (of Fig. 7.2) each member of which plays a key role in the appropriate energy domain - pole D below $K\bar{K}$ threshold, pole E above. The total resonance phenomenon (for example, the

overall phase movement required by Levinson's theorem (see Sect. 9.1 below)) stems from both poles. We require this fact to be reflected in the quantitative characterization of the associated resonance. The resonance parameters assigned have somehow to blend the characteristics of the two partners. Proposing a recipe for this is the main task of the following subsection. We of course apply the method to all our poles. For the pair (G-F) the exercise is perhaps unnecessary since G is very remote, however we persist with it for uniformity of treatment. In contrast, when we address the triplet (A,B,C) we rely crucially on our method to select which two poles shall be partnered and which the odd man out: this delivers (A-C) as another standard paired-up resonance leaving B, unpaired, as a $K\bar{K}$ virtual bound state. Although this seems the most natural and rational division, the conclusion as to the number of dynamical agencies present is independent of such assignments. No matter how the poles are paired we have extra dynamics.

8.2 Prescription for quantitative resonance assignments

Consider the task we are presented with. We start off with the pole parameters listed in Table 7.2 and the residue information illustrated in Fig. 7.3; more generally, with the solutions from which they arise. We wish to organize the poles into resonances and to extract masses and reduced widths (or equivalently relative coupling constants). For the second stage of extracting parameters, we want our procedure to follow closely the standard recipe one would adopt for a single resonance far from any threshold. Such a system should be describable by a factorizing Breit-Wigner form in general with background phases:

$$T_{ij}^{BW} = \frac{g_i g_j}{s_R - s - i\rho_1 g_1^2 - i\rho_2 g_2^2} \; e^{i(\delta_i^b + \delta_j^b)} \qquad (8.1)$$

This will have complex residues at the pole owing principally to the background phases; however one conventionally uses the corresponding moduli, $|\gamma_I|$, as effective coupling constants. For the resonance position or mass one normally takes the real part of the complex pole position

$$m_R = \mathrm{Re}(E_R) \qquad (8.2)$$

where $E_R^2 = s_R$. Our goal is to devise a prescription for the present more

complicated situation that adheres as closely as possible to the above simple recipe whilst allowing for the 'pairing' phenomenon.

Let us now focus on this aspect. We have already argued in Sect. 7 that the respective pole pairs (D,E) and (G,F) should be associated simply from their nearness in the energy plane. We now ask: can this pairing be systematized to yield a plausible prescription for assigning resonance parameters; then, can we extend the resulting recipe to rationalize the triplet of poles (A,B,C) governing the S^* region? This will lead us to the idea of 'λ-tracking' now to be described. To see how sheet II and sheet III poles might be associated, recall how poles of $\underset{\sim}{\mathcal{T}}$ arise within the unitarity formalism previously presented (3.14,15). For example, in terms of $\underset{\sim}{K}^{-1} \equiv \underset{\sim}{M}$, the elements of the corresponding $\underset{\sim}{\mathcal{T}}$-matrix may be conveniently written in the form

$$\mathcal{T}_{ij} = U_{ij}/\Delta \tag{8.3}$$

with

$$\Delta \equiv \det M - i\rho_1 M_{22} - i\rho_2 M_{11} - \rho_1\rho_2 \tag{8.4}$$

and

$$U_{11} = M_{22} - i\rho_2 \;\; ; \;\; U_{12} = -M_{12} \;\; ; \;\; U_{22} = M_{11} - i\rho_1 \tag{8.5}$$

The poles of $\underset{\sim}{\mathcal{T}}$ correspond to zeros of Δ; the relevant sheet structure arises from the factors of $\rho_2(\equiv 2k_2/E)$ in (8.4) and (8.5). The fact that there exist pole pairs (X-Y) with X on sheet II and Y on sheet III means that switching ρ_2 to $-\rho_2$ in (8.5) only slightly disturbs the zeros of Δ. To explore and exploit this association, replace ρ_2 everywhere in the above formula by $\lambda\rho_2$ and study how the zeros move as λ varies <u>continuously</u> from + 1 to - 1. We shall pair those poles joined by the shortest track in the energy plane as λ is varied. This, for example, naturally connects poles D and E of Fig. 7.2(b). A priori any route in the complex λ plane with these end points might prove advantageous; confining ourselves to real values, we still have the option to proceed via zero or via infinity[88]. For the case in point, it turns out to be the latter alternative that provides the desired linkage. This is illustrated in Fig 8.1 which shows the 'λ-trajectories' for solution K_1 (full lines correspond to $-1<|\lambda|<1$, dashed lines to $-i<\lambda<i$). The 'via-infinity' routing not only upholds the natural

pairing of D and E and of G and F but unambiguously selects A as companion for C leaving B untwinned. The latter can be viewed as originating from a zero of $M_{22}-i\rho_2$ slightly shifted by intra-channel coupling; its trajectory consequently disappears into the $K\bar{K}$ threshold singularity (Fig. 8.1). The method therefore classes B as a $K\bar{K}$ virtual bound state. There is an element of convention in this categorization of the (A,B,C) triplet; we earlier proposed a classification in which B and C were paired and A unattached[16]. The present arrangement has the double advantage of maintaining the same procedure as for (D-E) and (G-F) and of keeping the resonance description close to the pole phenomena that it is supposed to describe. The discussion in Sect. 8.3 of what parton content should be ascribed to our spectrum is based on the above resonance assignments selected by our λ-tracking procedure.

Before proceeding to that discussion, we need to extract masses and widths corresponding to the associated pole pairs. The above λ-connection suggests an obvious way to proceed based on the $\lambda = \infty$ point where the extrapolations from X and Y coalesce. Inspection of formulae (8.3) and (8.4) (with $\rho_2 \to \lambda\rho_2$) shows the $\lambda \to \infty$ limit of the trajectory to correspond to a zero of $M_{11} - i\rho_1$. This we <u>define</u> to be the resonance location corresponding to the pole pair in question:

$$(X,Y) \to (M_{11} - i\rho_1) = 0\Big|_{s=s_{XY}} \tag{8.6}$$

The corresponding residues $\bar{\gamma}_1$ and $\bar{\gamma}_2$ can likewise be defined in terms of the $\lambda \to \infty$ limit - for $\bar{\gamma}_1$ straightforwardly and for $\bar{\gamma}_2$ with an extra factor of λ inserted. The need for this latter factor in $\gamma_2(\lambda)$ to avoid a zero limit is obvious from (8.4) and (8.5) (with $\rho_2 \to \lambda\rho_2$) from which the actual limiting values can also be read off:

$$\bar{\gamma}_1^2 = \lim_{s\to s_{XY}} -(s-s_{XY})/(M_{11} - i\rho_1) \tag{8.7}$$

$$\bar{\gamma}_2^2/\bar{\gamma}_1^2 = -(M_{12}^2/\rho_2^2)\Big|_{s=s_{XY}} \tag{8.8}$$

The extrapolation of residues is illustrated in Fig. 8.2 again for the solution K_1. As will be noted, the emergent resonance parameters differ little from a simple average of the corresponding values for the constituent poles. Application of these procedures yields the resonance parameters

listed in the first three blocks of Table 8.1, the values attributed to B being just those for the corresponding $\mathcal{J}$-matrix pole.

Table 8.1 presents the input to our resonance characterization in some detail to give an impression of variability from solution to solution. In the main, this is not very great except for the D-pole parameters according to solution M. These appear anomalous and have accordingly been omitted from the final averages along with the corresponding E-pole values. The case for extra dynamics in the I=0 scalar channel rests squarely on the number of $\mathcal{J}$-matrix poles given in Tables 7.1 and 7.2. The subsequent re-packaging outlined above is secondary. Our aim is to provide a rational principle for associating poles on sheets II and III. Thereby we find our 7 $\mathcal{J}$-matrix poles transmute into 4 resonances. By use of a particular (as we would claim, rational) convention, we are able to extract their specific parameters (Table 8.1), which for convenience we summarize in Table 8.2.

Section 8.3: Parton composition of our states

Granted the above description, what can we say about interpretation: how far does our spectrum cohere with standard quark model systematics and what evidence does it provide for the intrusion of new types of dynamics?

Conventional quark model classification looks to find meson families arranged in ideally mixed nonets, generically $[S(I=0), V(I=1), K(I=\frac{1}{2}), S'(I=0)]$[89] with a standard pattern of masses and decay couplings given by the presumed quark content and the OZI rule. This is the benchmark against which we have to discern novelties and aberrations. Reality is a little more complicated and various mechanisms are invoked to explain departures from this idealized pattern (cf discussion in section 9.1 below). Specializing to the I=0 sector we should find at a minimum the two standard ground-state ($q\bar{q}$) compounds, ideally mixed if no special mechanism operates. Additions can come either from radial excitations or from non-standard configurations such as glueballs, hybrids and multiquark compounds[3-6]. According to the observed systematics, radial recurrences should only occur at the top end of our range if at all. Among non-standard configurations, the most natural incursion would be from a ground-state scalar glueball, $\varepsilon_g(0^{++})$. According to models, this should occur at a lower mass than its pseudo-scalar counterpart, $\eta_g(0^{-+})$. If $\iota(1440)$ is identified with η_g, ε_g

should occur well within our range. In the absence of mixing it should be a pure SU(3) singlet. The other non-standard configurations, like hybrids, etc, all entail the existence of I≠0 companions (extra δ's and κ's). Existing information on the relevant decay channels (which could certainly stand improvement) does not provide any clear signals for such additions; we shall therefore provisionally ignore these other possibilities. Another possible type of intrusion we have to keep in mind is from what we shall term 'molecular' or 'bootstrap' resonances such as can occur in multihadron systems from explicit hadron exchanges (again see discussion in Sect. 9.1 below).

Spectroscopic assignments normally invoke both mass-splittings and decay branching ratios. For the present case where very broad states are involved rendering precise mass values ambiguous, the only standard diagnostic we have available is the pattern of branching ratios and that only as between $\pi\pi$ and $K\bar{K}$. In the final column of Table 8.2, we list the $|g_\pi/g_K|$ ratios that we have empirically determined.

We now compare these empirical ratios with theoretical expectations such as sketched above. Although we would in general expect mixing among the different components, we begin by looking at the outcome of simple idealized SU(3) configurations (Table 8.3); as we shall see, there is at present no need to go beyond this simple framework.

On this basis, $S_2(988)$ is a natural candidate for the regular ($s\bar{s}$) ground state. Direct confirmation that $S_2(988)$ is built of strange constituents could be sought in precision data on radiative ϕ decay: $\phi \to \gamma S_2$. This process should provide γ rays of some 30 MeV with a spread of only a few MeV from the ϕ width. This should yield a clear signal readily distinguishable from the continuum.

With S_2 thus allotted to the quark model's lowest ($s\bar{s}$) state, $\varepsilon(900)$ looks well placed to be its non-strange counterpart. Such a dual identification is not quite trouble free if one demands simple conformity to naive quark model patterns. There should be a mass-splitting of several hundred MeV (cf $M_\phi^2 - M_\omega^2 \simeq .43\ \mathrm{GeV}^2$) and the total reduced widths ($g_\pi^2 + g_K^2$) should be commensurate. Perhaps additional mechanisms operate to shift the ($s\bar{s}$) level down in mass and weaken its coupling; we return to this in Sect. 9.1 below.

One feature of Table 8.3 one might naively hope to exploit is its prediction not only of the magnitude but also of the sign of g_π/g_K. Unfortunately, background phases can wipe out the consequent distinction between for instance ϵ_{ns} and ϵ_8 (cf. Table 8.3). The observed coupling ratios (Fig. 7.3) mildly uphold the ϵ_{ns} assignment for $\varepsilon(900)$ and are otherwise inconclusive.

Already we have candidates for the two standard quark model levels. What role should we assign to our remaining states? Looking first at $S_1(991)$, the decay ratios (Tables 8.2, 8.3) show it to be compatible with an SU(3) singlet identification. It is thus a prime candidate within our spectrum for the I=0 scalar glueball. Such a significant assignment obviously merits extensive checking and probing. Since the spectrum that we report is such an interlocking package, what is mostly needed is additional and more refined data of the kind we have already discussed in Sects. 3 and 4. This could be usefully supplemented by new high precision experiments on dimeson production reactions like $K^-p \to K\bar{K}\Lambda$. One might also seek specific evidence that S_1 not only exists but is veritably a glueball. According to the general parton picture of such reactions, $\gamma\gamma$ excitations of S_1 should be suppressed, though final state interactions could counter this tendency as occurs for $\gamma\gamma \to \pi^0\pi^0$ in the f region.

The final component of our solutions is the $\varepsilon'(1430)$[74] of Table 8.3. Its parameters could well undergo revision since it occurs at the upper end of our energy range where unconsidered channels start to play an appreciable role (note also that there have been claims for additional structure[85,41] cf Sect. 7). The numbers listed in Table 8.2 point to a predominantly ϵ_{ns} SU(3) composition for the $\varepsilon'(1430)$. As to its actual parton constitution, perhaps it is the ϵ_{ns} member (again following the notation of Table 8.3) of the first $(q\bar{q})$ radial excitation. Etkin et al's S(1730)[37] could be the corresponding ϵ_s if it is confirmed.

The outcome of the above discussion may be summarized as follows: The resonance content of the I=0 S-wave below 1.5 GeV primarily couples to $\pi\pi$ and $K\bar{K}$. It comprises

(a) A narrow resonance $S_1(991)$ very close to $K\bar{K}$ threshold

$$E_R \simeq 0.991 - 0.021i \quad (g_\pi \simeq 0.22,\ g_K \simeq 0.28)$$

which manifests itself via sheet II and sheet III poles A and C (details in Tables 7.1, 7.2).

(b) A $K\bar{K}$ bound state $S_2(988)$ yielding pole B ($g_\pi \simeq 0, g_K \simeq 0.35$)

(c) An $\varepsilon(900)$

$$E_R \simeq 0.91 - 0.35i \qquad (g_\pi \simeq 0.52,\ g_K \simeq 0.27)$$

which corresponds to sheet II and sheet III poles D and E (cf Tables 7.1, 7.2)

(d) An $\varepsilon'(1430)$

$$E_R \simeq 1.43 - 0.20i \qquad (g_\pi \simeq 0.6,\ g_K \cong 0.16)$$

corresponding to poles F and G. (cf Tables 7.1, 7.2)

The way our spectral assignments for the I=0 scalars would fit into the overall pattern for the lower meson families is displayed in Table 8.4.

Section 9: Discussion

In Sect. 9.2 we summarise our results, consider their implications and describe how they may be confirmed. First, we assemble some general remarks about different types of resonance and how to distinguish them.

Section 9.1: What is a resonance and how can we deduce its structure?

The foregoing analysis raises a number of general questions: How in a complicated situation do we tell what resonances are present? Are they

always to be assigned to simple constituent model[90] levels? What parameters ought to be attributed to them and do these need reprocessing before direct comparison with constituent model states? Concerning these latter, is the conventional picture adequate both as to its treatment of mixing and of confinement? In one way and another, we are concerned with mechanisms that obscure the direct intuitive link between resonant phenomena perceived at the hadron level and spectroscopic simplicities in the parton substructure.

Complications can enter at both ends of this chain. The actual phenomena can be complex and hard to classify, whilst the simplicities of the ideal constituent model can be corrupted by mixing and special couplings like that of the axial anomaly to the pseudo-scalars. Finally, the link between the two levels of explanation can be distorted by various effects to do with unitarity, like thresholds, and quark model boundary conditions. Ideally, one would like to pass directly between the phenomena and realistic calculations of bound state wave functions. Instead, one has to 'go the long way round' with all risks of distortion this brings. The general issues raised go far beyond the scope of this paper, however a few salient points deserve mention. This will serve not only to amplify the preceeding discussion but also to advertise some alternative methods of interpretation that have been proposed.

Given a resonant situation, where $\underset{\sim}{J}(E)$ has a pole or poles, an obvious aim is to furnish a rational quantitative description on which subsequent taxonomy can work. One wants to say what resonances are present, to 'type' them in all meaningful respects and to assign suitable and convenient parameters - masses, coupling constants and the like. The paradigm cases are the very sharp resonances like the J/ψ where the concept merges into that of a decaying particle; however, the various resonant phenomena that we encounter in particle physics force us to extend this framework. Wherever possible we adhere to the unstable particle analogy; hence the drive to characterize resonances by masses and coupling constants as if we were dealing with decay governed by an effective Lagrangian. It is this spirit of viewing 'decay' as a perturbation that informs the characterization of resonances by parameters of associated K-matrix poles; also related prescriptions for 'taking out' final state interactions[91].

Efforts to apply these notions usually encounter complications and ambiguities. Scalar decay channels, both the I=0 sector of present concern

and its I≠0 companions, abundantly illustrate this: resonances are variously wide, overlapping and coupled to strongly opening channels. The greatly enlarged scope for complexity this brings is amply borne out by the detailed phenomenology of the preceding sections. We have seen how adjacent to a strongly opening threshold the issue of replica poles can assume real importance; our scenario requires three such pairs and one singlet with the character of a virtual bound state. We described a method for marrying pole-partners and showed how for the present solutions it turns out that resonance pairs are most naturally associated to zeros of $M_{11}-i\rho_1$. There is no overall tie-up to poles of the K-matrix; something more general is needed to provide an embracing scheme of resonance identification. This leads on to the question, by no means confined to the present case, of how overlapping resonances should be thought of as combining. A priori one might conceive either an addition of K-matrix (or M-matrix) poles or a multiplication of S-matrix elements (addition of phase shifts). The character of our solutions and the interpretation we have offered tend strongly to the latter, multiplicative, alternative. If one converts the above $M_{11}-i\rho_1$ denominator, which as we have seen 'drives' most of our resonances, to a central phase shift, $\bar{\delta}$, by the formula

$$M_{11} = \rho_1 \cot \bar{\delta} \qquad (9.1)$$

then the resulting $\bar{\delta}$ (Fig 9.1) appears as the sum of individual resonance phase contributions. Such multiplicative combination demotes the significance of K-matrix or M-matrix poles as direct pointers to the underlying resonance physics. This should be borne in mind whenever one encounters overlapping resonance situations[92].

All our solutions do nonetheless possess a K-matrix pole near $K\bar{K}$ threshold which acts in conjunction with a large and distinctive background. These conspire to achieve a nearby zero of det $(\underset{\sim}{K})$ enabling the resulting structure to be approximated by the form

$$K_{ij}^{th} = \frac{g_i g_j (s-s_o)}{(s_1-s)(s_1-s_o)} - h_i h_j \equiv \frac{g_i g_j}{(s_1-s)} + L_{ij} \qquad (9.2)$$

with an identical structure automatically prevailing for the inverse matrix M_{ij}^{th}. Such a form automatically yields 3 poles in the associated $\underset{\sim}{J}$-matrix. From this point of view, our three poles (A,B,C) are inextricably

connected[93] and arise from the conjunction of the K-matrix and M-matrix poles exhibited in (9.2). Quantitatively, it is the large background contribution L_{22} in (9.2) which is the prime causative factor in producing the $K\bar{K}$ bound state B ($S_2(988)$). Even if one removes the K-pole, leaving just the L_{ij} contributions to (9.2), $\underset{\sim}{T}$ still has a pole like B.

Resonances that arise from constant K-matrix elements with the energy variation supplied by phase space are often assumed to be of a different dynamical character from those corresponding to strongly varying K-matrix (or M-matrix) elements. The distinction appealed to is between those resonances that arise from overt exchange forces in the hadron channels studied and those whose dynamical source lies at the constituent level and which couple to the observed hadrons through decay. It is natural to call the former category molecular[94] or bootstrap resonances; the latter will be termed normal substructure resonances - normal resonances for short. They correspond to CDD poles in a dispersion relation analysis (see below). According to the quark model, most hadron levels should be normal resonances; the conventional classification relies on this. From time to time the suspicion arises that this or that specimen is a 'molecular' intruder[95]. The distinction is often elusive since the relevant phenomena can and often do co-exist - (recall the near success of the bootstrap programme of the 1960's).

A transparent way to exhibit how the above type ambiguity arises is to write down the appropriate inverse partial wave dispersion relation: In shorthand form,

$$T^{-1} = \int \frac{\mathrm{Im}T_L^{-1}}{s'-s} + \int \frac{\rho\theta}{s'-s} + \sum_i \frac{R_i}{s_i-s} \qquad (9.3)$$

The first term on the right arises from exchange or bootstrap effects, the second from thresholds (such as feature in the unitarized quark model[91] - see below); the third contribution contains the CDD poles[96,97] that carry the 'normal' signal. Besides illustrating the above type ambiguity, this equation shows how various latent complications can interfere with the pristine, Breit-Wigner, picture; the principle distortions come from threshold effects and left hand cut exchanges. Such embellishments have maximum scope for broad S-wave states making it no surprise that the corresponding amplitudes are somewhat complicated. The so-called

'unitarized quark model'[91] graphically illustrates the scope for non-trivial threshold effects (albeit within a highly specific and somewhat ad hoc framework of assumptions).

How, short of solving the complete theory, are we to tell normal and molecular resonances apart? A number of indicators have been proposed at various times. There is the notion underlying Levinson's theorem[98] according to which long-range phase-shift movements afford a kind of topological classification for alternative dynamics. For a bootstrap resonance, the phase should slowly decrease after the resonant rise; for a normal resonance not so. It would commonly be assumed that the clear existence of a corresponding K-matrix pole such as occurs for a Breit-Wigner resonance, indicates normality. A signal for the contrary situation could perhaps be the absence of a K-pole counterpart. In practice, this may be difficult to establish.

These are the sorts of consideration that have commonly been adduced in trying to clarify ambiguous situations. A familiar example is that of the $\Lambda(1405)$ pole in $\bar{K}N$ and $\pi\Sigma$ scattering[17]: does it correspond to a coupled channel K-matrix pole or does the resonance only arise from inter-channel coupling? This still unresolved question is not obviously crucial for the ultimate validity of the quark model description but has to be settled before resonance parameters can be extracted for symmetry comparisons. Very similar questions figured in the discussion of the present solutions. In particular, we have been concerned whether resonances have associated poles on each of the accessible sheets[99]. The absence of such companion poles tends to argue for a 'molecular' rather than a 'normal' assignment, but is not decisive since these mechanisms are not mutually exclusive but on the contrary are frequently conjoined.

In this connection, there has been an interesting suggestion from Weinstein and Isgur[100] that a bootstrap effect would operate in the I=0 and I=1 $K\bar{K}$ systems. (Thus far, the phenomenological interest has been mainly with the I=1 part of this package[101,102] which has been invoked to explain anomalous features of $\iota(1440)$ decay to $\delta\pi$). Such effects do not however per se ensure a molecular character for the resonances involved. In terms of eq (9.3), where there is already a 'normal' resonance driving term, the effect of additional overt forces (left hand cut contributions) is merely to shift the ensuing resonance from it original position (c.f. discussion by Dalitz et al in Ref. 17). This could possibly account for the relatively low mass of our

($s\bar{s}$) candidate $S_2(988)$; perhaps also for its small coupling.

Most of the foregoing discussion has focussed on complications at the hadron level. One further suggestion deserving mention is Jaffe and Low's concept of the P-matrix[104]. Although motivated at the parton level (the underlying idea is that constituent model states sometimes have unphysical boundary conditions) this again involves a transmutation of the physical scattering amplitudes at the hadron level so as to derive quantities directly comparable with constituent model states. However, the poles of the P-matrix for the presently reported solutions do not appear to clarify the dynamics.

9.2 Summary and conclusions

By considering a number of reactions leading to $\pi\pi$ and $K\bar{K}$ final states, we have effected a new amplitude analysis of I=0 scalar dimeson production from threshold to beyond 1.6 GeV. The resonance spectrum that emerges comprises two broad objects $\varepsilon(900)$ and $\varepsilon'(1430)$ similar to those found in previous analyses and <u>two</u> narrow resonances $S_1(991)$ and $S_2(988)$ corresponding to the S^* phenomenon. Attributing the S^* effect to two resonances rather than, as previously, to a single object is the principal novelty of our amplitude. As we have stressed, it offers a potential solution to an outstanding problem of spectroscopy – the identity of the hypothesized scalar glueball. For this, the $S_1(991)$ forms a very plausible candidate. Of course (as discussed in Sect. 8.3), further experimental evidence is needed to confirm this assignment. If the $S_1(991)$ does prove to be the lowest mass glueball, not only will this vindicate the prediction of bag modellers[105], gluon condensate calculators[106] and lattice computers of the pure gauge sector[107], but will serve as a calibration fixing the crucial missing parameter needed to normalise their whole glueball spectrum. In addition the $S_2(988)$ is well suited to fill the role of conventional ($s\bar{s}$) ground state.

Whence came this convenient complication of the S^* structure? This was a question that we addressed in some detail (Sect. 7.2) concluding that, among the present input, it is predominantly the new DPE data on $I\!P\,I\!P \to \pi\pi$ and its interplay with traditional $\pi\pi$ processes that require the additional pole. As we discussed, much more direct signatures of the extra resonance would show in various reactions producing $K\bar{K}$ final states if only the precision were sufficient. Even with existing data, $\pi\pi \to K\bar{K}$ information is an

important ingredient to our fit and, as mentioned, very significant discrepancies remain among the published results, notably regarding the relative phase of the $\pi\pi \to K\bar{K}$ amplitude below 1200 MeV. Our overall solution, which fits the highly structured $I\!P\,I\!P \to \pi\pi$ information so well, disfavours the flat phase alternative for $\mathcal{J}(\pi\pi \to K\bar{K})$. Experiment must be the final arbiter. However, the large effort needed to repeat the existing experiments is unlikely to be forthcoming quickly. In the short term, resources would probably be better directed to studying new reactions like $K^-p \to \Lambda(\Sigma)K^0_S\,K^0_S$ or in accumulating better statistics on $I\!P\,I\!P \to K\bar{K}$.

The AFS experiment has certainly demonstrated the power of the DPE approach to meson spectroscopy. (Note the interesting D-wave structure reported in Ref. 14). Although that particular programme terminated with the ISR, it is much to be hoped that the work will continue elsewhere at the SPS and/or Tevatron colliders, keeping the strong features, requirement of very low t for the through going beam particles (Fig. 4.1) and good resolution, whilst remedying limitations of angular acceptance and sensitivity to different particle types. An unanticipated benefit of the DPE approach to meson production is its emphasis on low partial waves in contrast to traditional OPE reactions like $\pi N \to \pi\pi N$ in which the higher waves dominate. A prime motivation for the AFS experiment was the presumed tendency of the DPE mechanism to favour glueball production. Supposing $S_1(991)$ to be a glueball, the $I\!P\,I\!P$ couplings that we find (Table 7.2 end column), provide no support for this notion. This may be a problem for OZI systematists but does not detract from DPE as an exploratory tool.

Other 'production reactions' (in our terminology this includes various heavy flavour decays) are beginning to provide useful information on scalar final states. As yet, the data are restricted both statistically and in the mass range explored and partial wave separation is usually lacking. It was not therefore appropriate to proceed as we did with the AFS results and let the production data help select the strong interaction amplitudes. Instead, we merely sought to demonstrate consistency, only allowing the characteristic reaction couplings ($\alpha^{(c)}$ of eq. (3.8) above) to vary. The systematics of these is itself an interesting subject for study. Among reactions discussed are, $\gamma\gamma \to \pi\pi$, $\psi' \to \psi\pi\pi$, $\Upsilon'(\Upsilon'') \to \Upsilon\pi\pi$ and $J/\psi \to \phi\pi\pi$. Information on this latter process and its companion decay $J/\psi \to \phi K\bar{K}$ will shortly be greatly enhanced. It may then be appropriate to emulate the treatment of the AFS data.

For the higher mass range that we explore, information is needed on other coupled channels like 4π and $\eta\eta$. The latter has been quite extensively explored in a recent experiment at CERN[41]. According to the accompaning (somewhat restricted) amplitude analysis, the partial wave structure is very different from that reported here, in particular the S-wave cross-section peaks at 1200 and 1600 MeV with a sharp dip in-between. The difference of this spectrum from that found for $\pi\pi$ and $K\bar{K}$ final states, although formally possible, seems unlikely and merits further investigation.

A characteristic feature of the resonance pole structure that we have reported is its complexity - 7 poles for 4 resonances - and this has led us into various procedural issues of resonance identification. To those who might find such complexity innately implausible we would say: 'where more likely than for an S-wave resonant system straddling a strongly coupled threshold?' Fine points of interpretation are in any case secondary; it is the pole structure which is the objective fact to be confirmed or rejected. Concerning general possibilities for S-wave resonant structures we clearly need more case-law and it would be very helpful to have some related phenomena, notably $\delta(980) \to \eta\pi$, $K\bar{K}$, better studied. Certainly, complete and detailed elucidation of the $I = 0$ scalar system is going to be a lengthy process. Nevertheless, our extensive analysis does reveal definite evidence for dynamics beyond the naive quark model with three states in the 1 GeV region. This richness may prove a key signature of non-perturbative QCD.

Acknowledgements

It is a pleasure to thank the AFS collaboration, in particular Michael Albrow, Anthony and Janet Carter and Peter Cecil for helpful discussions on their data. We thank Barry Wicklund and Ron Longacre for correspondence on the data of Refs. 35 and 37 and Serban Protopopescu for his observations. A preliminary account of this work was presented (by DM) at the 1986 Rencontre de Moriond and led to stimulating comments notably from Wolfgang Ochs. Here too we heard of the new results in prospect on $J/\psi \to \phi\pi\pi(K\bar{K})$. MRP is grateful to Roger Phillips and the RAL theory group for travel support.

References

1. M. Gell-Mann, Phys. Lett. 8, 214 (1964); G. Zweig, CERN preprint 8419/TH-412 (1964); R.H. Dalitz, Proc. Oxford Conf. on Elementary Particles 1965, Eds. R.G. Moorhouse et al., Rutherford laboratory 1966) p. 157; F.E. Close, 'An Introduction to quarks and partons', Academic Press (London), 1979.
2. M. Teper, Proc. Int. Europhysics Conf. on High Energy Physics, Brighton, UK, 1983, eds. J. Guy and C. Costain, p4; Inv. talk at "Workshop on non-perturbative methods". Montpellier, France, July 1985, Southampton preprint SHEP 85/86-10.
B. Berg, Proc. XVI GIFT Int. Seminar on "New perspectives in quantum field theory", Jaca, Spain, June 1985, eds. J. Abad and M. Asorey.
3. H. Fritzsch and P. Minkowski, Nuov. Cim. 30A, 393 (1975); P.G.O. Freund and Y. Nambu, Phys. Rev. Lett. 34, 1645 (1975); R. Jaffe and K. Johnson, Phys. Lett. 60B, 201 (1976); J. Kogut, D. Sinclair and L. Susskind, Nucl. Phys. B114, 199 (1976); D. Robson, Nucl. Phys. B130, 328 (1977); J. Bjorken, SLAC Summer Institute on Particle Physics, SLAC-PUB-2372 (1979).
4. F.E. Close, 'Experimental meson spectroscopy-1983', AIP Conf. Proc. No. 113, ed. S.J. Lindenbaum, p 117; M.S. Chanowitz, Proc. XIVth Intern. Conf. on multi-particle dynamics at high energies (Lake Tahoe, 1983), eds J.F. Gunion and P.M. Yager (World Scientific, Singapore) p 716.
5. R.L. Jaffe, Phys. Rev. D15, 267 (1977).
6. For general reviews of glueballs, hybrids etc. see : T. Barnes, Invited talk Bonn ESLA meeting (Bad Honnef, October 1984), Rutherford preprint RAL-85-005 (1985); J.F. Donoghue, 'Hadron Spectroscopy - 1985', AIP Conf. Proc. No. 132, ed. S. Oneda (1985) p 460.
7. D. Scharre et al, Phys. Lett. 97B, 329 (1980); J.D. Richman, Proc. of XXth Rencontre de Moriond, ed. J. Tran Thanh Van, Editions Frontieres (1985) p 471. For a review see: D. Hitlin, Proc. 1983 Intern. Symp. on lepton and photon interactions at high energies, eds. D.G. Cassel and D.L. Kreinick (Cornell, Ithaca) p 746.
8. C. Edwards et al, Phys. Rev. Lett. 40, 458 (1982); see also D. Hitlin Ref. 7.
9. For reviews see : S. Meshkov, Proc. XVIIIth Rencontre de Moriond, ed. J. Tran Thanh Van, 1983, p 427; S.U. Chung, Proc. 12th Int. Winter Meeting on Fundamental Physics, Santander, Spain, ed. M. Aguilar-Benitez, April 1984, p 295; J.F. Donoghue, Proc. 1984 Yukon Advanced

Study Institute on the quark structure of matter, eds. N. Isgur, G. Karl and P.J. O'Donnell (World Scientific, Singapore) p 145; S. Cooper, Proc. Int. Europhysics Conf. on High Energy Physics, Bari, Italy, 1985, eds. L. Nitti and G. Preparata, p 947 and Berkeley Conference 1986. See also P.M. Fishbane and S. Meshkov, Comm. on Nucl. and Particle Physics, XIII, 325 (1984).

10. A more rational notation for mesons has recently been proposed and implemented in the latest PDG Tables (Ref. 18). The changes impinge considerably on the states of present concern. Since this paper has to present a number of unfamiliar spectroscopic concepts we have adhered to the old notations to prevent readers having to grapple with two types of novelty at once. To re-orient to the new terminology the reader should substitute

$S(975) \rightarrow f_0(975)$ $\quad\quad$ $\iota(1440) \rightarrow \eta(1440)$

$\delta(980) \rightarrow a_0(980)$ $\quad\quad$ $\theta(1690) \rightarrow f_2(1720)$

$\varepsilon(1300) \rightarrow f_0(1300)$ $\quad\quad$ $f(1270) \rightarrow f_2(1270)$

Our proposed $I = 0$ scalar spectrum then comprises:

$f_0(991)$, $f'_0(988)$, $f_0(900)$, $f_0(1430)$.

11. F.E. Low, Phys. Rev. D12, 163 (1975); S. Nussinov, Phys. Rev. Lett. 34, 1286 (1975) and Phys. Rev. D14, 246 (1976); D.M. Chew and G.F. Chew, Phys. Lett. 53B, 191 (1974); D. Robson (Ref. 3).
12. R. Waldi, K.R Schubert and K. Winter, Z. Phys. C18, 301 (1983).
13. T. Åkesson et al., Nucl. Phys. B264, 154 (1986).
14. A. Breakstone et al., Z. Phys. C27, 205 (1985).
15. D. Morgan and M.R. Pennington, Phys. Lett. 137B, 411 (1984).
16. Some key results of the present analysis were reported in : K.L. Au, D. Morgan and M.R. Pennington, Phys. Lett. 167B, 229 (1986).
17. R.H. Dalitz et al., Proc. Intern. Conf. on hypernuclear and kaon physics (MPI, Heidelberg, 1982) Report MPIH-1982-V20, ed. B. Povh, p 201.
18. Particle Data Group (PDG), Review of Particle Properties April 1986 ed, M. Aguilar-Benitez et al., Phys. Lett., 170B, 1 (1986).
19. For a general discussion see : B.R. Martin, D. Morgan and G. Shaw, 'Pion-pion interactions in particle physics', Academic Press (1976).
20. G.F. Chew and F.E. Low, Phys. Rev. 113, 1640 (1959).

21. C.J. Goebel, Phys. Rev. Lett. 1, 337 (1958).
22. K.M. Watson, Phys. Rev. 88, 1163 (1952).
23. For a related discussion see - I.J.R. Aitchison, Nucl. Phys. A189, 417 (1972).
24. S.L. Adler, Phys. Rev. 137, B1022 (1965) and 139, B1638 (1965); S.L. Adler and R.F. Dashen, 'Current Algebras and Applications to Particle Physics' Benjamin, NY (1968).
25. In the applications to follow, we need to apply eq (3.8) below some of the thresholds, specifically below $K\bar{K}$ threshold for the two channel ($\pi\pi$ and $K\bar{K}$) case that we actually consider. The necessary analytic continuations are straightforwardly (and standardly) accomplished by substituting $i\rho_2$ by $-|\rho_2|$ in the explicit formulae for T_{11} and T_{12} (cf eq (3.19)).
26. R. Omnès, Nuov. Cim. 8, 316 (1958); see also G. Barton, 'Introduction to Dispersion Techniques in Field Theory', (Benjamin, New York 1965).
27. For a recent example see - L.M. Barkov et al., Nucl. Phys. B256, 365 (1985).
28. One can allow independent Adler zeros in K_{11}, K_{12}, K_{22}, but this has very little effect on our fits.
29. G. Grayer et al., Nucl. Phys. B75, 189 (1974).
30. W. Ochs, Univ. of Munich thesis (1974).
31. S. Protopopescu et al., Phys. Rev. D7, 1280 (1973).
32. N.M. Cason et al., Phys. Rev. D28, 1586 (1983).
33. A.D. Martin and M.R. Pennington, Ann. Phys. (NY) 114, 1 (1978).
34. H. Becker et al., Nucl. Phys. B151, 46 (1979).
35. D. Cohen et al., Phys. Rev. D22, 2595 (1980).
36. W. Wetzel et al., Nucl. Phys. B115, 208 (1976); V.A. Polychronakos et al., Phys. Rev. D19, 1317 (1979); G. Costa et al., Nucl. Phys. B175, 402 (1980).
37. A. Etkin et al., Phys. Rev. D28, 1786 (1982).
38. See Ref. 37 Figs 8,9 for a useful compilation but beware of energy shifts.
39. M.R. Pennington and C. Schmid (unpublished) referenced in M.R. Pennington and S. Protopopescu, Phys. Rev. D7, 1429 (1973).

40. L. Görlich et al., Nucl. Phys. B174, 16 (1980).
41. D. Alde et al., Nucl. Phys. B269, 485 (1986).
42. M. Alston-Garnjost et al., Phys. Lett. 36B, 152 (1971); W.Y. Lee, Proc. 1975 Int. Symp. on Lepton and Photon Interactions at High Energies, Stanford, ed. W.T. Kirk, p 213 .
43. D.M. Chew and G.F. Chew, (Ref. 11); B.R. Desai, B.C. Shen and M. Jacob, Nucl. Phys. B142, 258 (1978), for general reviews see S.N. Ganguli and D.P. Roy, Phys. Rep. 67, 201 (1980) and G. Alberi and G. Goggi, Phys. Rep. 74, 1 (1981).
44. P.C. Cecil (thesis, Cavendish Lab, Cambridge, 1984) - Rutherford Appleton preprint RAL-T-004 (1984).
45. Such an extrapolation is natural from B_6 phenomenology as discussed in M.R. Pennington, Nucl. Phys. B137, 77 (1978).
46. M. Poppe, DESY report 86-014 (Feb, 1986).
47. See for example - H. Harari, Proc. Roy. Soc. Lond. A318, 355 (1970).
48. I.G. Halliday, Nucl. Phys. B114, 157 (1976).
49. T. Inami and R.G. Roberts, Nucl. Phys. B93, 497 (1975).
50. M.R. Pennington,1984 (unpublished).
51. In Ref. 16, we quoted results for the favoured Etkin et al[37] phase, ϕ_{12}.
52. D. Morgan and M.R. Pennington, Phys. Rev. D12, 1283 (1975).
53. L.S. Brown and R.N. Cahn, Phys. Rev. Lett. 35, 1 (1975); T-M Yan Phys. Rev. D22, 1652 (1980); Y-P Kuang and T-M Yan, Phys. Rev. D24, 2874 (1981).
54. MK II Collab: T.M. Himel, SLAC Pub 223 (1979).
55. Crystal Ball Collab: M. Oreglia et al., Phys. Rev. Lett. 45, 959 (1980).
56. Argus Collab: H. Albrecht et al., Phys. Lett. 134B, 137 (1984).
57. CLEO Collab: D. Besson et al., Phys. Rev. D30, 1433 (1984).
58. CUSB Collab: V. Fonseca et al., Nucl. Phys. B242, 31 (1984).
59. Crystal Ball Collab: D. Gelphman et al., Phys. Rev. Lett. D32, 2893 (1985).
60. CLEO Collab: J. Green et al., Phys. Rev. Lett. 49, 617 (1982).
61. CUSB Collab: G. Mageras et al., Phys. Lett. 118B, 453 (1982).

62. G. Gidal et al., Phys. Lett. 107B, 153 (1981).
63. MK III preliminary results on $\psi' \to \phi\pi\pi$ etc. presented at XXIth Rencontre de Moriond, March 1986 by U. Mallik.
64. DM2 preliminary results on $\psi' \to \phi\pi\pi$ etc. presented at Moriond 1986 (cf Ref. 63) by A. Falvard.
65. The preliminary DM2 results presented at Moriond in 10 MeV bins appear to be shifted by some 10 MeV from those of our other $\pi\pi$, $K\bar{K}$ channels and so have not been included in these tentative fits. By the time the final results on these ψ decays are available, hopefully such problems will have been resolved.
66. F. Vannucci et al., Phys. Rev. D15, 1815 (1977).
67. M.R. Pennington, 1976 (unpublished).
68. Ch. Berger et al., Z. Phys. C26, 199 (1984).
69. A. Courau et al., Nucl. Phys. B271, 1 (1986).
70. Z. Ajaltouni et al. contribution to 1985 Kyoto Lepton-Photon symposium referenced by H. Kolanoski, Proc. 1985 Int. Symp. on Lepton and Photon Interactions at High Energies, eds. M. Kanuma, K. Takahashi, p 90.
71. H. Aihara et al, Phys. Rev. Lett. 57, 404 (1986).
72. D.H. Lyth, Nucl. Phys. B30, 195 (1971).
73. G. Mennessier, Z. Phys. C16, 241 (1983).
74. For earlier discussion of objects like our $\varepsilon'(1430)$ see especially B. Hyams et al., Nucl. Phys. B64, 134 (1974) and W. Ochs, Ref. 30; P. Estabrooks, Phys. Rev. D19, 2678 (1979); A.B. Wicklund et al., Phys. Rev. Lett. 45, 1469 (1980); A.C. Irving et al., Ref. 83; for further references see Ref. 18 (p 194).
75. Here ϱ_2 means $\begin{bmatrix} 0 & 0 \\ 0 & \rho_2 \end{bmatrix}$ with ρ_2 defined on sheet II; if it were defined on sheet III, a minus sign would be required.
76. References to the points displayed may be found in Ref. 18 p 184.
77. M. Alston-Garnjost et al., Ref. 42; S.M. Flatte et al., Phys. Lett. 38B, 232 (1972).
78. G. Grayer et al., '$\pi\pi$ scattering - 1973' AIP Conf. Proc. No 13, ed. P.K. Williams and V. Hagopian (1973) p 117.
79. S.M. Flatte et al., Ref. 77; cf. also S.M. Flatte, Phys. Lett. 63B, 224 (1976).

80. D. Morgan, Phys. Lett. 51B, 71 (1974).
81. Y. Fujii and M. Fukugita, Nucl. Phys. B85, 189 (1975).
82. A.D. Martin, E. Ozmutlu and E.J. Squires, Nucl. Phys. B121, 514 (1977).
83. A.C. Irving, A.D. Martin and P.J. Done, Z. Phys. C10, 45 (1981).
84. We emphasize that all through this part of our discussion it is the number of T-matrix poles (required to describe the S^* region) that is in question. This is not to be confused with alternative K-pole forms that we have experimented with for fitting.
85. A. Etkin et al., Phys. Rev. D25, 2446 (1982).
86. See Ref. 18 p 235.
87. M. Kato, Ann. Phys. (NY) 31, 130 (1965) - see also Ref. 81.
88. Note that for determining where a specified function has zeros these alternatives are completely on a par; we could re-parametrize just as naturally in terms of $1/\lambda$.
89. The symbols S, V, K, S' refer to the internal structure.
90. We coin this phrase to extend the concept of quark model states to include systems with constituent gluons. A perfect illustration is afforded by the low-lying states of the bag model.
91. N.A. Törnqvist, Phys. Rev. Lett. 49, 624 (1982).
92. A. Etkin et al., Phys. Lett. 165B, 217 (1985); S.J. Lindenbaum and R.S. Longacre, Phys. Lett. 165B, 202 (1985).
93. Quite an illuminating exercise is to perform an extrapolation of the phase-space factors like that previously described but with both ρ_1 and ρ_2 re-scaled, say by a factor λ_{12}. For $\lambda_{12} \to 0$, B and C link to the K-matrix pole, while, for $\lambda_{12} \to \infty$, C and A associate to the M-matrix pole.
94. The concept of a 'molecular' resonance has recently been popularized by the authors of Refs. (100) and (101).
95. The deuteron is in the same sense a molecular bound state so the phenomenon certainly does occur.
96. L. Castillejo, R.H. Dalitz and F.J. Dyson, Phys. Rev. 101, 453 (1956).
97. See Ref. 19 p 237 et seq - see also Ref. 87.

98. The original theorem (N. Levinson, Kgl. Danske Videnskab. Selskab Mat - fys. Medd. 25, No 9 (1949)) concerns a system described by a Schrödinger equation. In particle physics, the essential result is that, barring coincidences, $[\delta(E)]^{\infty}_{\text{threshold}} = \pi[n_c - n_B]$ with n_c the number of CDD poles and n_B the number of bound states (cf. Ref. 19).
99. In general, we would expect 'normal' resonances to possess image poles. Thus, if $\underset{\sim}{T} = [\underset{\sim}{M} - i\underset{\sim}{\rho}]^{-1}$ has a pole on sheet II, arising from variations of the $\underset{\sim}{M}$ elements, switching the sign say of ρ_2 should produce an image pole not much displaced in E.
100. J. Weinstein and N. Isgur, Phys. Rev. Lett. 48, 659 (1982) and Phys. Rev. D27, 588 (1983).
101. M. Frank et al., Phys. Rev. D32, 2971; T. Barnes, Phys. Lett. 165B, 434 (1985).
102. Further elucidation of the I=1 δ(980) system is a high priority for sorting out the scalars (cf. Cahn and Landshoff Ref. 103).
103. R.N. Cahn and P.V. Landshoff, Nucl. Phys. B266, 451 (1986).
104. R.L. Jaffe and F.E. Low, Phys. Rev. D19, 2105 (1979).
105. J.F. Donoghue, K. Johnson and B.A. Li, Phys. Lett. 99B, 416 (1981); C.E. Carlson, T.H. Hansson and C. Petersen, Phys. Rev. D27, 2167 (1983); M. Chanowitz and S. Sharpe, Nucl. Phys. B222, 211 (1983); See also - R.L. Jaffe, K. Johnson and Z. Rydak, Ann. Phys. (NY) 168, 344 (1986).
106. V.A. Novikov, M.A. Shifman, A.I. Vainshtein and V.I. Zakharov, Nucl. Phys. B191, 301 (1981).
107. Ph. de Forcrand, G. Schierholz, H. Schreider and M. Teper, Z. Phys. C31, 87 (1986); A. Patel et al., Harvard preprint, HUTP-86/A035 (1986); J. Hoek, Rutherford Appleton preprint, RAL-86-034 (1986) - cf. also Ref. 2.

Parameter	K_1	K_1(Etkin)	K_1'	K_3	M	
s_o	-0.0110	-0.0162	-0.0141	0.0220	-0.0074	
s_1	0.9247	0.9383	0.9226	0.0544	0.9828	
s_2				0.9547		
s_3				2.2815		
f_1^1	-0.2242	-0.1659	-0.2334	0.0870	0.1968	
f_2^1	0.5829	0.5852	0.5969	0.3800	-0.0154	
f_1^2				-0.1298		
f_2^2				0.6011	0.1131	a_{11}
f_1^3				-2.1130	0.0150	a_{12}
f_2^3				4.1900	-0.3216	a_{22}
c_{11}^0	0.7347	0.4247	0.7871	-0.9527	0.0337	
c_{11}^1	-0.5266	-0.5822	-0.5610	-0.6893	-0.3185	
c_{11}^2	2.6151	2.5478	1.6987	1.1313	-0.0942	
c_{11}^3	-1.7747	-1.7387	-2.0451	-2.1052	-0.5927	
c_{11}^4	0.8031	0.8308	0.6361		0.1957	
c_{12}^0	-3.2762	-3.1401	-3.3270	0.6619	-0.2826	
c_{12}^1	-0.6662	-0.1359	-0.4788	1.9239	0.0918	
c_{12}^2	0.8778	1.0286	1.1362	0.3866	0.1669	
c_{12}^3	-2.1190	-2.3029	-1.0623	1.5638	-0.2082	
c_{12}^4	0.2319	0.1944	0.6290		-0.1386	
c_{22}^0	-2.6785	-2.8447	-2.7914	-3.4567	0.3010	
c_{22}^1	7.9951	6.9164	7.5952	-1.8117	-0.5140	
c_{22}^2	5.5763	5.2846	4.5612	2.4379	0.1176	
c_{22}^3	-1.4956	-0.9646	-0.9356	-2.7982	0.5204	
c_{22}^4					-0.3977	
α_1^0	-0.4012	-0.5711	-0.4700	-0.2368	0.1393	
α_1^1	0.5468	0.7800	0.6593	0.3186	-0.02775	
α_1^2	0.2440	0.1622	0.2036	0.3131	0.3952	
α_2^0	3.273	3.310	3.542	3.328	3.241	
α_2^1	-3.483	-3.533	-3.824	-3.763	-3.432	
α_2^2	1.183	1.193	1.284	1.340	1.141	
N_{Data}	258	224	244	258	258	
N_{Parm}	24	24	24	28	24	
χ^2	303	219	307	305	303	
χ^2/df	1.29	1.09	1.40	1.31	1.29	

Table 5.1 Parameters of our fits. The four significant figures are to allow an accurate reproduction of the fit rather than an indication of their accuracy. All dimensional parameters in appropriate powers of GeV.

Process	Experiment	s_o/m_π^2	$\alpha_1(s)$	$\alpha_2(s)$	χ^2/data
$\psi' \to \psi\pi\pi$	Mark II	5.4	-0.176	1.0	28/23
	Crystal Ball				97/26
$T' \to T\pi\pi$	Argus	3.4	-0.176	1.0	9/13
	CLEO				7/11
	CUSB				10/14
	Crystal Ball				5/10
$T'' \to T\pi\pi$	CLEO	∞	-0.176	1.0	13/11
	CUSB		(fixed)		1/6
$\psi \to \phi\pi\pi$	Mark II				39/18
$\psi \to \phi K\bar{K}$	Mark II	-0.5	$\alpha_1^0 = 0.53$	$\alpha_2^0 = 0.08$	1/4
$\psi \to \phi\pi\pi$	Mark III	(fixed)	$\alpha_1^1 = -1.58$	$\alpha_2^1 = 3.64$	50/38
$\psi \to \phi K\bar{K}$	Mark III		$\alpha_1^2 = 1.23$	$\alpha_2^2 = -2.72$	1/5
$\gamma\gamma \to \pi\pi$	PLUTO	∞	$\alpha_1^0 = -0.44$	$\alpha_2^0 = 1.11$	12/17
			$\alpha_1^1 = -2.46$	$\alpha_2^1 = 7.99$	
	DM1		$\alpha_1^2 = 0$	$\alpha_2^2 = -8.10$	4/6

Table 6.1: Parameters of fits to heavy flavour decays and $\gamma\gamma \to \pi\pi$ with s_o the position of the process-dependent Adler zero and the coupling functions $\alpha_i(s)$ of eq (3.21) normalised so that $\alpha_2(4m_K^2) = 1$.

Solution						
Pole	Sheet	K_1	K_3	M	K_1'	average
A	II	1.002-0.026i	1.005-0.025i	0.997-0.025i	1.000-0.026i	1.001-0.026i
B	II	0.986	0.990	0.990	0.987	0.988
C	III	0.984-0.021i	0.988-0.018i	0.983-0.018i	0.984-0.021i	0.985-0.020i
D	II	0.88-0.40i	0.91-0.31i	(1.42-0.46i)	0.83-0.42i	0.87-0.38i
E	III	0.95-0.37i	0.96-0.30i	(0.99-0.50i)	0.90-0.39i	0.94-0.35i
F	III	1.48-0.26i	1.40-0.18i	1.37-0.26i	1.42-0.20i	1.42-0.23i
G	II	1.52-0.26i	1.40-0.17i	1.36-0.26i	1.40-0.18i	1.42-0.22i
χ^2/NDF		1.3	1.3	1.3	1.4	

Table 7.1: Pole positions, E_R(GeV), for various solutions described in the text.

Pole	E_R(GeV)	γ_1(GeV)	($\|\gamma_1\|$)	γ_2(GeV)	($\|\gamma_2\|$)	$\alpha_{IP\,IP}$
A	1.001-0.026i	0.02-0.26i	(0.27)	0.25+0.25i	(0.35)	0.9
B	0.988	0.011-006i	(0.01)	0.35-.01i	(0.35)	1.0
C	0.985-.020i	0.07+0.18i	(0.19)	0.09+0.18i	(0.20)	0.6
D	0.87-0.38i	0.44-0.21i	(0.49)	0.27-0.13i	(0.30)	0.7
E	0.94-0.35i	0.39-0.26i	(0.47)	0.21-0.14i	(0.25)	0.6
F	1.42-0.23i	0.43+0.36i	(0.56)	0.08-0.01i	(0.08)	0.9
(G)	1.42-0.22i	0.45+0.32i	(0.55)	0.10-0.03i	(0.10)	1.0

Table 7.2: Average pole positions, residues and IP IP couplings, $\alpha_{IP\,IP}$, for our specimen solutions ($\alpha_{IP\,IP} \equiv |\alpha_1\gamma_1 + \alpha_2\gamma_2|$)

No. of Poles	$\pi\pi \to K\bar{K}$ data set	χ^2	No. of data	No. of parameters	χ^2/df
3	1,2	66	47	17	2.2
2	1,2	96	47	20	3.6
3	1	37	39	17	1.7
2	1	70	39	20	3.7
3	2	22	37	17	1.1
2	2	49	37	20	2.9

Table 7.3: Quality of Jost function fits. The 1,2 for the $\pi\pi \to K\bar{K}$ data sets refer to Cohen et al[35] and Etkin et al[37] respectively.

sol^n	E_R E_R^X	E_R^Y	g_1 $\lvert\gamma_1\rvert^X$	$\lvert\gamma_1\rvert^Y$	g_2 $\lvert\gamma_2\rvert^X$	$\lvert\gamma_2\rvert^Y$
(X,Y)=(A,C)						
K_1	(1.002,-0.026)	(0.984,-0.021)	0.27	0.20	0.37	0.19
K_3	(1.005,-0.025)	(0.988,-0.018)	0.27	0.19	0.34	0.23
M	(0.997,-0.025)	(0.983,-0.018)	0.26	0.20	0.33	0.21
K_1'	(1.001,-0.026)	(0.984,-0.021)	0.27	0.19	0.35	0.20
$S_1(991)$	(0.991,-0.021)		0.22		0.28	
(X,Y)=(D,E)						
K_1	(0.88,-0.40)	(0.95,-0.37)	0.53	0.52	0.33	0.26
K_3	(0.91,-0.31)	(0.96,-0.30)	0.41	0.41	0.28	0.24
(M)	(1.42,-0.46)	(0.99,-0.50)	0.47	0.34	0.57	0.62
K_1'	(1.01,-0.40)	(0.95,-0.39)	0.43	0.41	0.32	0.33
$\epsilon(900)$	(0.91,-0.35)		0.52		0.27	
(X,Y)=(G,F)						
K_1	(1.52,-0.26)	(1.48,-0.26)	0.70	0.62	0.27	0.24
K_3	(1.40,-0.17)	(1.40,-0.18)	0.41	0.37	0.12	0.12
M	(1.36,-0.26)	(1.37,-0.26)	0.61	0.80	0.19	0.16
K_1'	(1.42,-0.22)	(1.42,-0.33)	0.55	0.57	0.10	0.08
$\epsilon'(1430)$	(1.43,-0.20)		0.58		0.16	
B						
K_1	0.987		0.02		0.39	
K_3	0.990		0.00		0.30	
M	0.990		0.02		0.31	
K_1'	0.987		0.02		0.38	
$S_2(988)$	0.988		0.02		0.35	

Table 8.1 - Derivation of resonance parameters (complex energies shown as (ReE, ImE); M-fit values not used in determining $\epsilon(900)$ parameters).

Resonance	Poles	E_R(GeV)	g_π(GeV)	g_K(GeV)	$\lvert g_\pi/g_K \rvert$
$S_1(991)$	A,C	0.991-0.021i	0.22	0.28	0.8
$S_2(988)$	B	0.988	0.02	0.35	0.06
$\epsilon(900)$	D,E	0.91-0.35i	0.52	0.27	1.9
$\epsilon'(1430)$	G,F	1.43-0.20i	0.58	0.16	3.6

Table 8.2: I = 0 S-wave resonances below 1.6 GeV from our fits.

Scalar designation	Simple constituent model[90] realization	Final Dimeson State - P_1P_2 $\pi\pi$	$K\bar{K}$	$\eta_8\eta_8$
ϵ_1	$(u\bar{u}+d\bar{d}+s\bar{s})/\sqrt{3}$ or gg	0.87	1	− 0.5
ϵ_8	$(u\bar{u}+d\bar{d}-2s\bar{s})/\sqrt{6}$	-1.73	1	− 1
ϵ_{ns}	$(u\bar{u}+d\bar{d})/\sqrt{2}$	1.73	1	− 0.33
ϵ_s	$s\bar{s}$	0	1	− 0.67

Table 8.3: Relative branching amplitudes for $S \to P_1P_2$ in SU(3) according to various idealized composition possibilities.

J^{PC}	I=1	I=0	I=½	I=0	Candidate for glue dominated states	Candidates for radial recurrences
(ideal scheme)	$V(m_o)$	$S(m_o)$	$K(m_o+\Delta)$	$S'(m_o+2\Delta)$	-	-
0^{-+}	$\pi(138)$	$\eta(550)$	$K(496)$	$\eta'(958)$	$\iota(1440)$	$\pi(1300), K(1400)$ $\eta(1275)$
1^{--}	$\rho(770)$	$\omega(783)$	$K^*(892)$	$\phi(1020)$		$\rho(1590), \phi(1680)$
2^{++}	$A_2(1320)$	$f(1270)$	$K(1425)$	$f'(1525)$	$\theta(1720)$	$f(1810)$
1^{++}	$A_1(1275)$ or (1056)	$D(1285)$	$Q_A(1270)$ $Q_B(1406)$	$E(1420)$		
1^{+-}	$B(1235)$	$H(1190)$				
0^{++}	$\delta(983)$	$\epsilon(900)$	$\kappa(1350)$	$S_2(988)$	$S_1(991)$	$\epsilon'(1430), S(1730)$

Table 8.4 Provisional placement of our I = 0 scalars in the low-lying meson spectrum.

Figure Captions

Fig 4.1 The double Pomeron exchange graph controlling central dimeson production in pp → pp(MM).

Fig 4.2 The general trend of the double Pomeron exchange cross-section for dipion production may be attributed to pion exchange. Normalised to the AFS data[13] and folding in their acceptance, this "duality average" is plotted together with the AFS results on $M^4 d^4\sigma/dt_1\, dt_2\, dy\, dM$ as a function of dipion mass M. For ease of plotting, the factor M^4 has been included as this conveniently reduces the scale of the M-dependence.

Fig 5.1 The I = 0 S-wave phase shift, δ^0_o, for ππ scattering (denoted δ_{11} in the text) from the CERN-Munich group[29]. The hatched band represents the continuation down to threshold provided by the Roy equations[33]. The curve shows a fit typical of all our solutions.

Fig 5.2 The ππ I = 0 S-wave phase-shift, δ^0_o, and inelasticity η^0_o (denoted by δ_{11}, η_{11} in the text) above $K\bar{K}$ threshold showing the CERN-Munich results as analysed by Ochs[30] and the preferred B solution of Cason et al[32]. Again the curves show a typical fit given by our solutions.

Fig 5.3 The ππ I = 0 S-wave amplitude $\rho_1 \mathcal{T}_{11}$ shown in an Argand plot comparing the solutions K_1(●), K_1(Etkin) (▼), K_3(Δ) and M(□). The last three are only shown where they differ from solution K_1.

Fig 5.4 The ππ I = 0 S-wave amplitude $\rho_1 \mathcal{T}_{11}$ shown in an Argand plot with solution K_1 compared with the CERN-Munich results from the energy-independent analysis of Martin and Pennington[33] from 1.15 to 1.69 GeV in 20 MeV bins. Error ellipses have been drawn at representative energies.

Fig 5.5 The cross-section for inelastic I = 0 S-wave ππ scattering. This cross-section is proportional to $\frac{1}{4}(1-\eta_{11}^2)$, where η_{11} is the ππ inelasticity, and it is this that is plotted from the analyses of the CERN-Munich ππ results by Ochs[30] (●) and by Martin and Pennington[33] (Δ). The I = 0 S-wave ππ → $K\bar{K}$ contribution to this inelastic cross-section is plotted from the results of Cohen et al[35] (x) and Etkin et al[37] (0). Some of the data points have been displaced for easier presentation. The full curve corresponds to solution K_1 and the dotted one to K_1' as described in the text.

Fig 5.6 The phase of I = 0 S-wave ππ → $K\bar{K}$ scattering from Cohen et al[35] (0), Etkin et al[37] (●), and from Wetzel et al (▲), Polychronakos et al (▼) and Costa et al (Δ)[36]. Experiment determines the phase of this S-wave relative to the D-wave. Modelling that by resonance dominated forms gives the S-wave phase, ϕ_{12}, shown.

Fig 5.7 Mass spectrum of centrally produced S-wave ππ events in pp → ppππ from the AFS Collaboration[13] are shown above 1 GeV. These data have been corrected for acceptance[44]. The curves show a typical fit given by solution K_1.

Fig 5.8 Mass spectrum of centrally produced S-wave ππ and $K\bar{K}$ events in pp → pp(MM) from the AFS Collaboration[13] are shown above 1 GeV. These data have been corrected for acceptance[44]. The curves show a typical fit given by solution K_1.

Fig 5.9 A plot of the effective two-channel coefficient function of the Omnès representation, eqs (3.13), for the production process pp → ppππ as a function of dipion mass, M for a representative solution, K_1. The flatness indicates the near equality of the Omnès function for this process and ππ scattering itself, eqs (3.12, 13).

Fig 5.10 The AFS results on S-D wave interference in pp → ppππ[13] are compared to the prediction from our analysis with our solutions determining the S-wave and the D-wave assumed dominated by the f-resonance below 1.4 GeV. (At higher ππ masses, this simple model of the D-wave becomes inadequate).

Fig 6.1 Parton diagram of the decay $V' \to V\pi\pi$, with V made of heavy quarks v, so that v = c, b means V = ψ or T, emphasising the gluonic nature of the intermediate state expected in this picture.

Fig 6.2 The $\pi\pi$ mass spectrum for the decay $\psi' \to \psi\pi^+\pi^-$ as a function of M^2 for (a) $\pi^+\pi^-$ from Mark II[54], (b) $\pi^0\pi^0$ from Crystal Ball[55]. The curves show the results of a combined fit typically given by our S-wave solutions.

Fig 6.3 The $\pi\pi$ mass spectrum for the decay $T' \to T\pi\pi$ as a function of M for:
(a) $\pi^+\pi^-$ from Argus[56]
(b) $\pi^+\pi^-$ from CLEO[57]
(c) $\pi^+\pi^-$ from CUSB[58]
(d) $\pi^0\pi^0$ from Crystal Ball[59].
The curves show the results of a combined fit typically given by our S-wave solutions.

Fig 6.4 The $\pi\pi$ mass spectrum for $T'' \to T\pi^+\pi^-$ as a function of M from
(a) CLEO[60]
(b) CUSB[61]
The curves show the data are essentially consistent with phase space with no low mass Adler suppression.

Fig 6.5 Parton line diagrams of the processes
(a) $\psi \to \phi\pi\pi$, (b) $\psi \to \phi K\bar{K}$.

Fig 6.6 The $\pi\pi$ and $K\bar{K}$ mass spectra for the decays $\psi \to \phi(MM)$ from Mark II[62]. Our solutions typically give the curves shown which in fact represent the average over each bin width, assuming pure S-wave.

Fig 6.7 The preliminary $\pi\pi$ and $K\bar{K}$ mass spectra for the decays $\psi \to \phi(MM)$ from Mark III presented by Mallik[63]. Our solutions are exemplified by the curves shown; these represent the average over each bin width, assuming pure S-wave.

Fig 6.8 As for Fig 6.7 with the $\pi\pi$ data above 600 MeV in 30 MeV bins.

Fig 6.9 The $\pi\pi$ mass spectrum for the process $\gamma\gamma \to \pi^+\pi^-$ from
(a) the PLUTO Collaboration[68],
(b) DM1[69]
Note that in plot (b) the purely leptonic contribution to the detected final state has been folded in to allow comparison with the DM1 results[69]. Assuming the $\pi\pi$ data is S-wave dominated, our solutions readily accord with these spectra as shown by the curves.

Fig 6.10 Effective two channel coefficient function for an Omnès representation of the process $\gamma\gamma \to \pi\pi$. The data are from PLUTO[68] and the curve corresponds to the fit shown in Fig 6.8. This is to be contrasted with the flat function of Fig 5.9 for $I\!P\,I\!P \to \pi\pi$ indicating that the S-wave states have from 0.3 to 1 GeV an increasing coupling to $\gamma\gamma$ with increasing mass compared to $\pi\pi$ and $I\!P\,I\!P$. However, these conclusions are not definitive without partial wave separation, information on the $K\bar{K}$ channel and a resolution of the experimental inconsistency between different $\gamma\gamma$ data sets.

Fig 7.1 Sheet structure of the energy plane.

Fig 7.2 Positions of the 7 poles A-G for representative solutions (cf Table 7.1):
(a) plotted in k_2 plane (corresponding real energies shown in brackets)
(b) Plotted in E plane with insert showing $K\bar{K}$ threshold region enlarged: X for sheet II, ● for sheet III. The curved patches indicate spread among solutions.

Fig 7.3 Complex residues γ_1 and $\tilde{\gamma}_2(\equiv -\gamma_2)$ (cf Eq (7.2)) corresponding to poles of Fig 7.2. Dots correspond to individual solutions (Table 7.1), full lines to vector averages of these and dashed vectors to associated $I\!P\,I\!P$ couplings $\alpha_{I\!P\,I\!P} \equiv \alpha_1\gamma_1 + \alpha_2\gamma_2$.

Fig 7.4 Present pole pattern compared to previous findings as listed in Ref. 18: (a) overview (b) detail for the $K\bar{K}$ threshold region. Notations: our average pole locations (Table 7.2): ● (Sheet II), X (Sheet III); in (a) points labelled 'h' and 'e' are from Refs. 30 and 85 respectively; in (b) the cross with error bars depict PDG average (Ref. 18), 'g' the value inferred from Ref. 62, 'f' the outcome of the one-pole fit of Ref. 81 and O(x) that from the associated two-pole fit[81].

Fig 8.1 'λ-trajectories' for solution K_1 (see discussion following Eq (8.5)). Full lines denote 'via-infinity' extrapolations $-1 \leq 1/\lambda \leq 1$ and dashed lines the corresponding 'via-zero' connections $-1 \leq \lambda \leq 1$.

Fig 8.2 Residue extrapolations corresponding to pole trajectories of Fig. 8.1. Capital letters label $\bar{Y}_1$ curves and small letters $\bar{Y}_2$ curves, cf Eqs (8.7, 8.8).

Fig 9.1 'Central' phase shift $\bar{\delta}$ of eq (9.1) for solution K_1 (full line) decomposed into sum of $S_1(991)$ resonance contribution $\bar{\delta}_1$ (dashed line) and residual phase variation $\bar{\delta}_2(\equiv \bar{\delta}-\delta_1)$ (dot-dashed line).

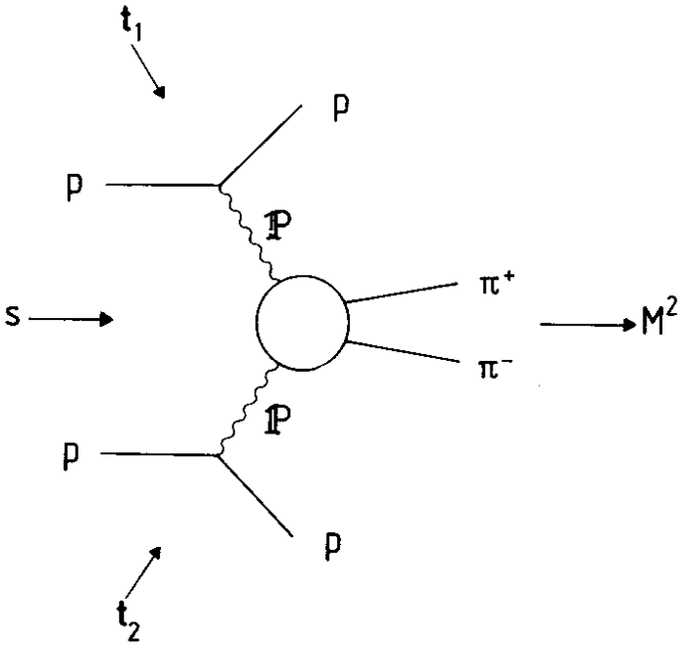

FIG. 4.1

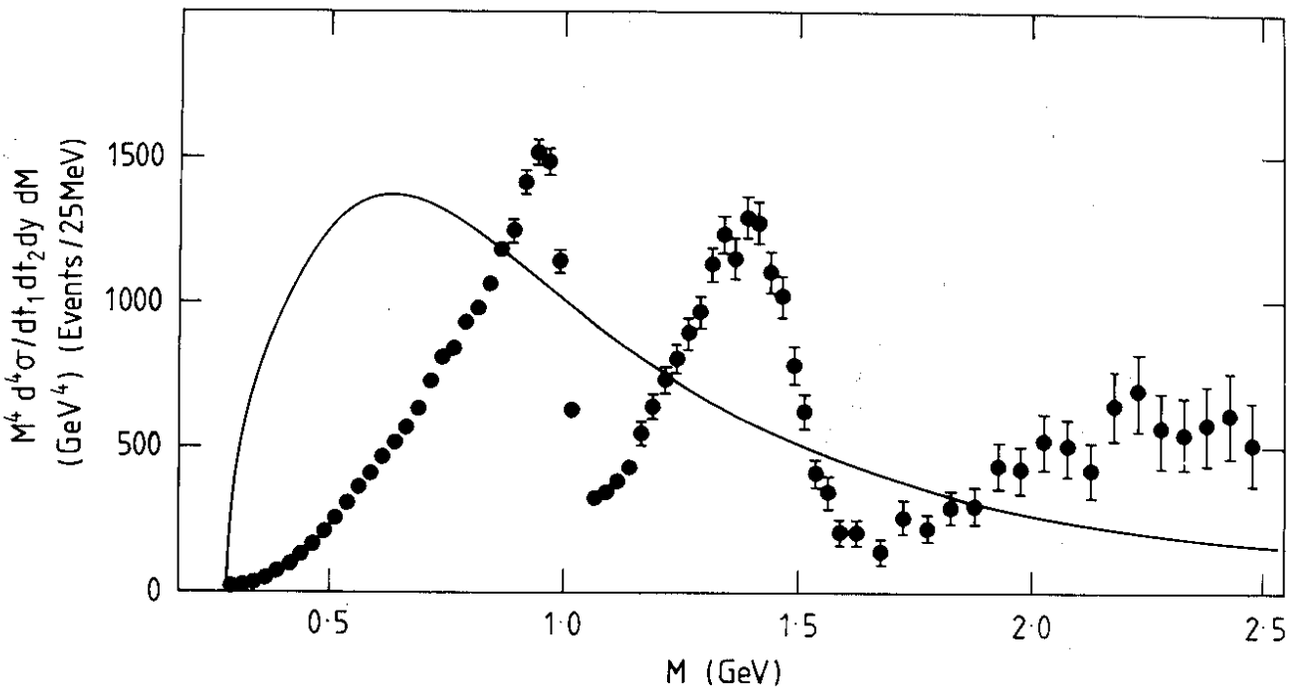
$M^4\, d^4\sigma/dt_1 dt_2 dy\, dM$
(GeV^4) (Events/25MeV)
1500
1000
500
0
0·5
1·0
1·5
2·0
2·5
M (GeV)

FIG. 4.2

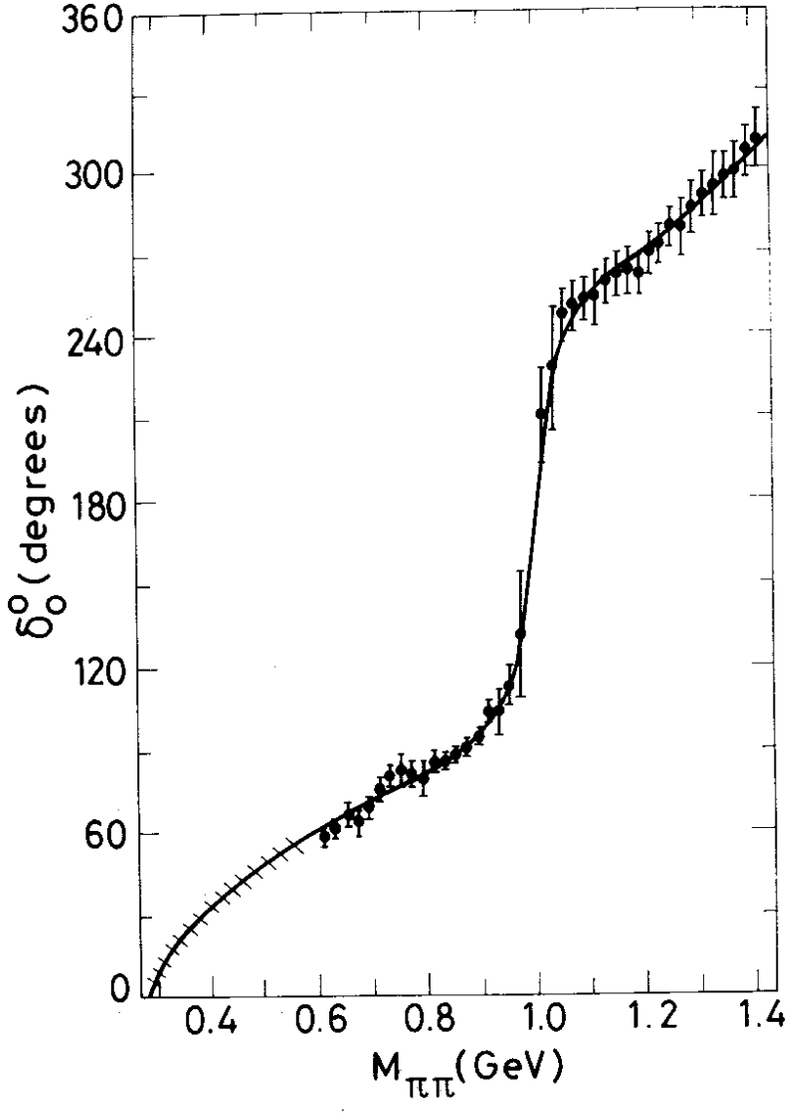
360
300
240
180
120
60
0
δ_0^0 (degrees)
0.4
0.6
0.8
1.0
1.2
1.4
$M_{\pi\pi}$(GeV)

FIG. 5.1

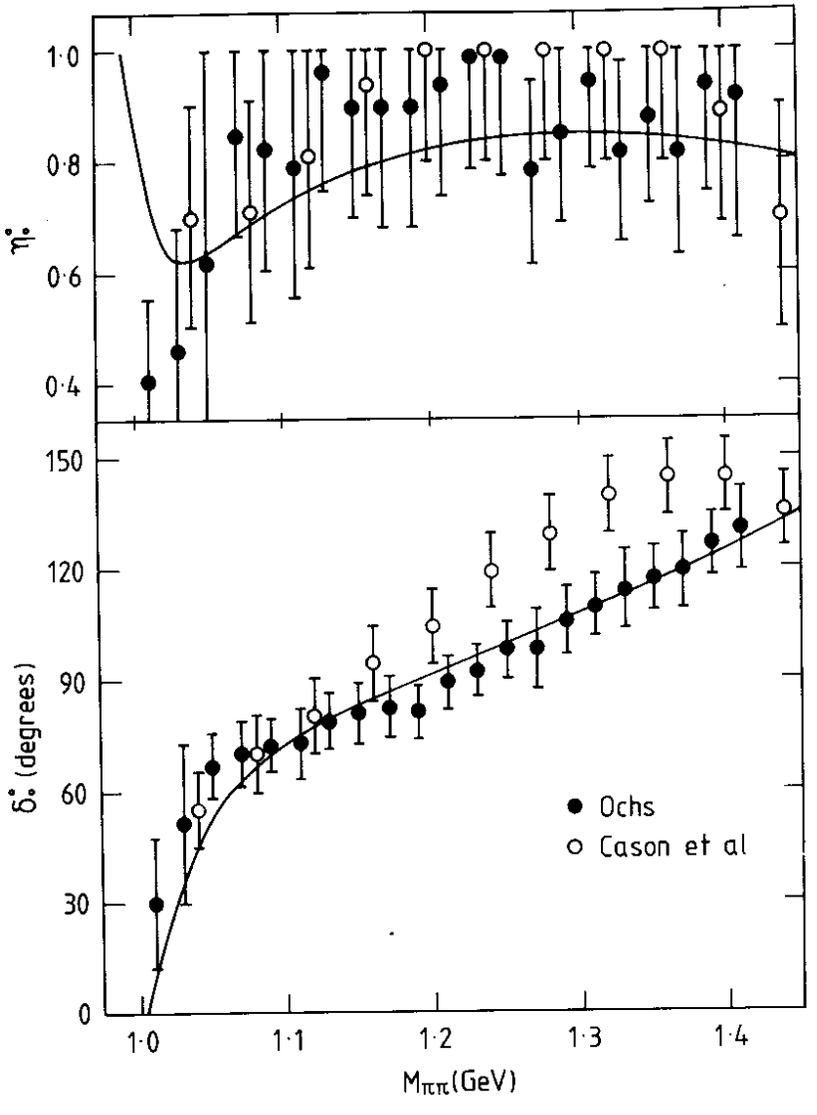
1·0
0·8
0·6
0·4
η^0
150
120
90
60
30
0
δ^0 (degrees)
Ochs
Cason et al
1·0
1·1
1·2
1·3
1·4
$M_{\pi\pi}$(GeV)

FIG. 5.2

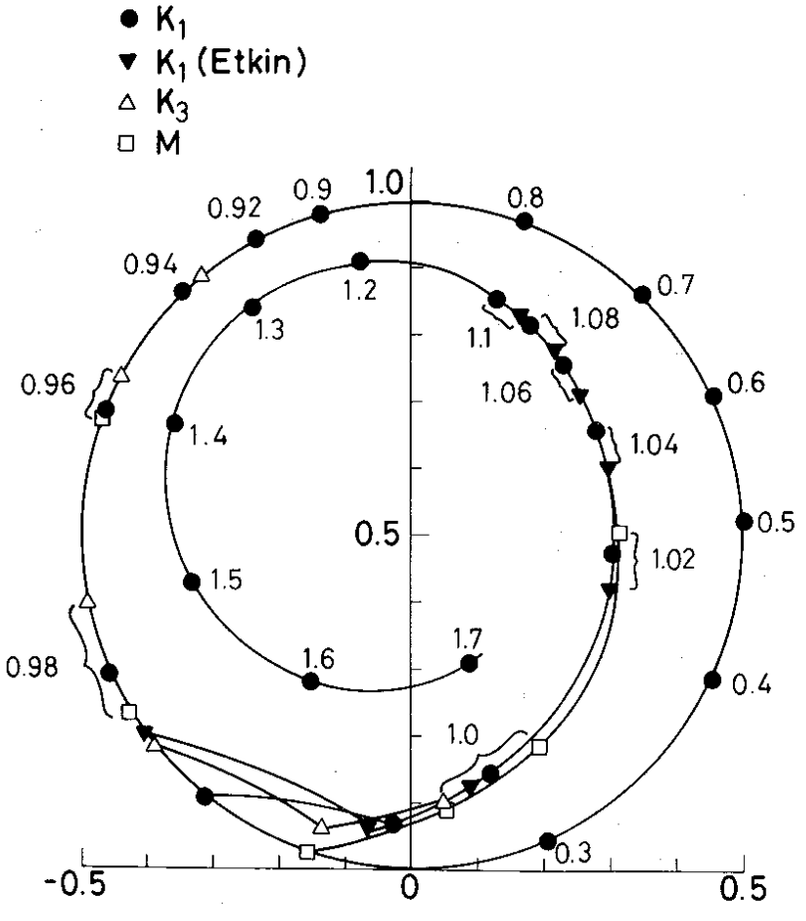
● K_1
▼ K_1 (Etkin)
△ K_3
□ M
1.0
0.9
0.92
0.8
0.94
0.7
0.96
0.6
0.98
0.5
0.4
0.3
1.2
1.3
1.1
1.08
1.06
1.4
1.04
0.5
1.02
1.5
1.7
1.6
1.0
-0.5
0
0.5

FIG. 5.3

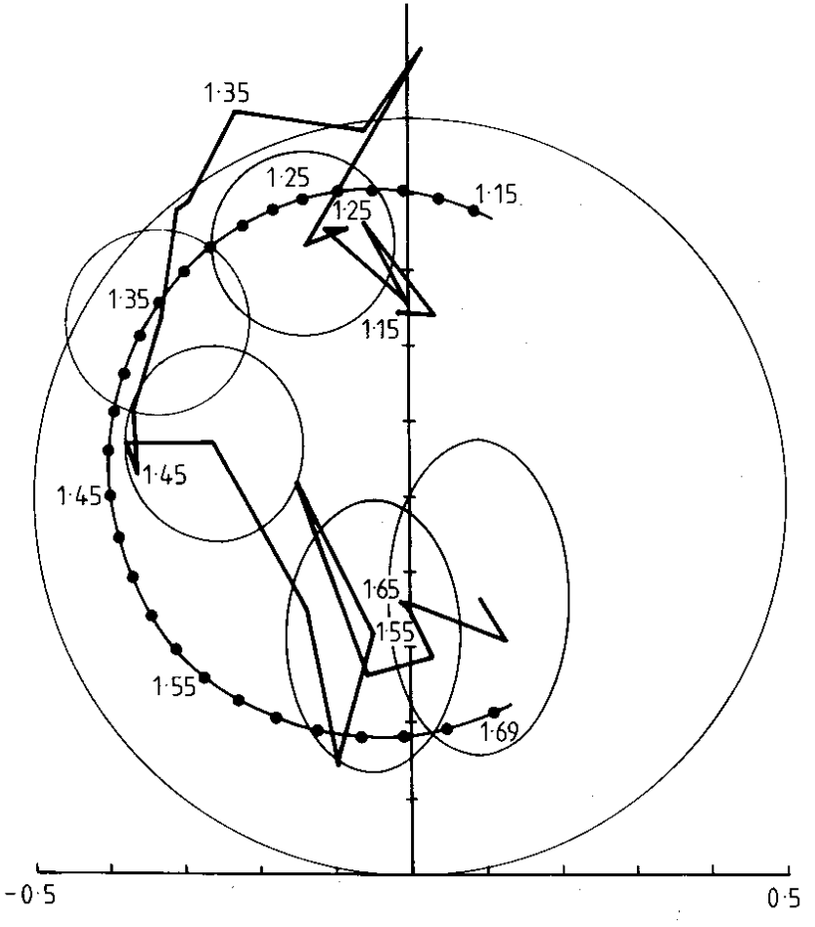
1·35
1·25
1·15
1·25
1·35
1·15
1·45
1·45
1·65
1·55
1·55
1·69
-0·5
0·5

FIG. 5.4

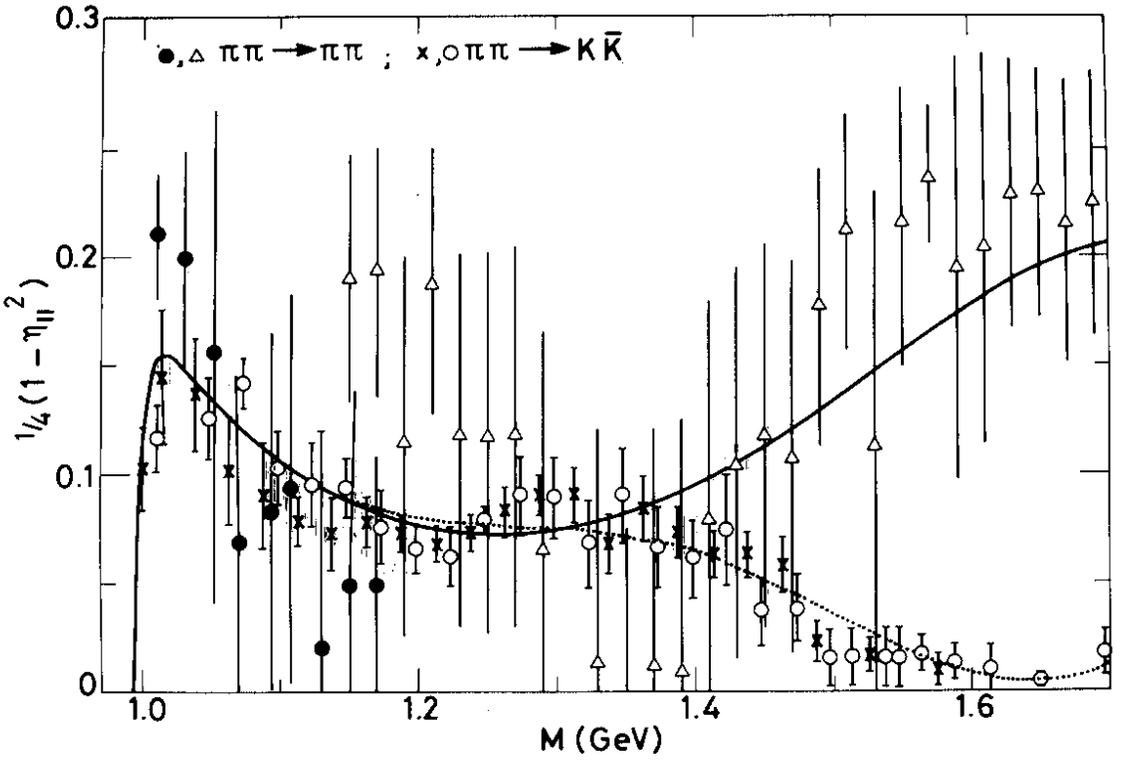
●,△ ππ → ππ ; x,○ ππ → K K̄
0.3
0.2
0.1
0
¼(1 − η₁₁²)
1.0
1.2
1.4
1.6
M (GeV)

FIG. 5.5

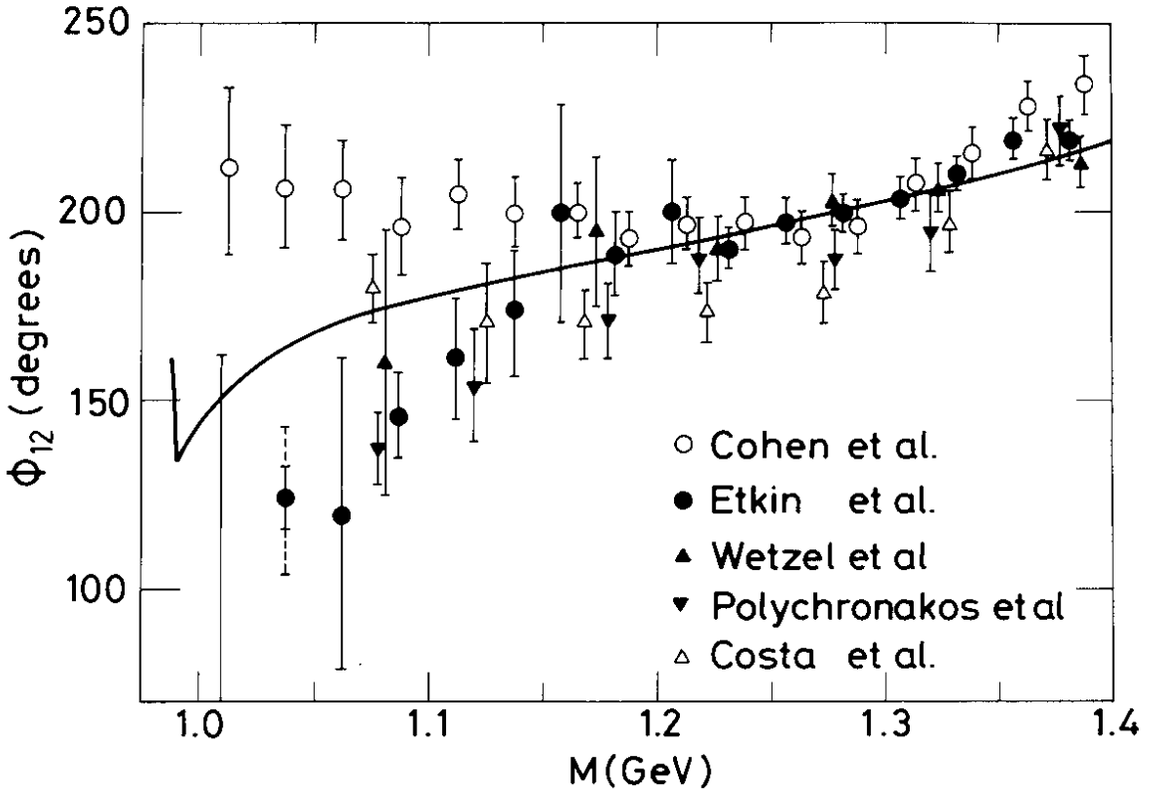
250
200
150
100
Φ12 (degrees)
○ Cohen et al.
● Etkin et al.
▲ Wetzel et al
▼ Polychronakos et al
△ Costa et al.
1.0
1.1
1.2
1.3
1.4
M(GeV)

FIG. 5.6

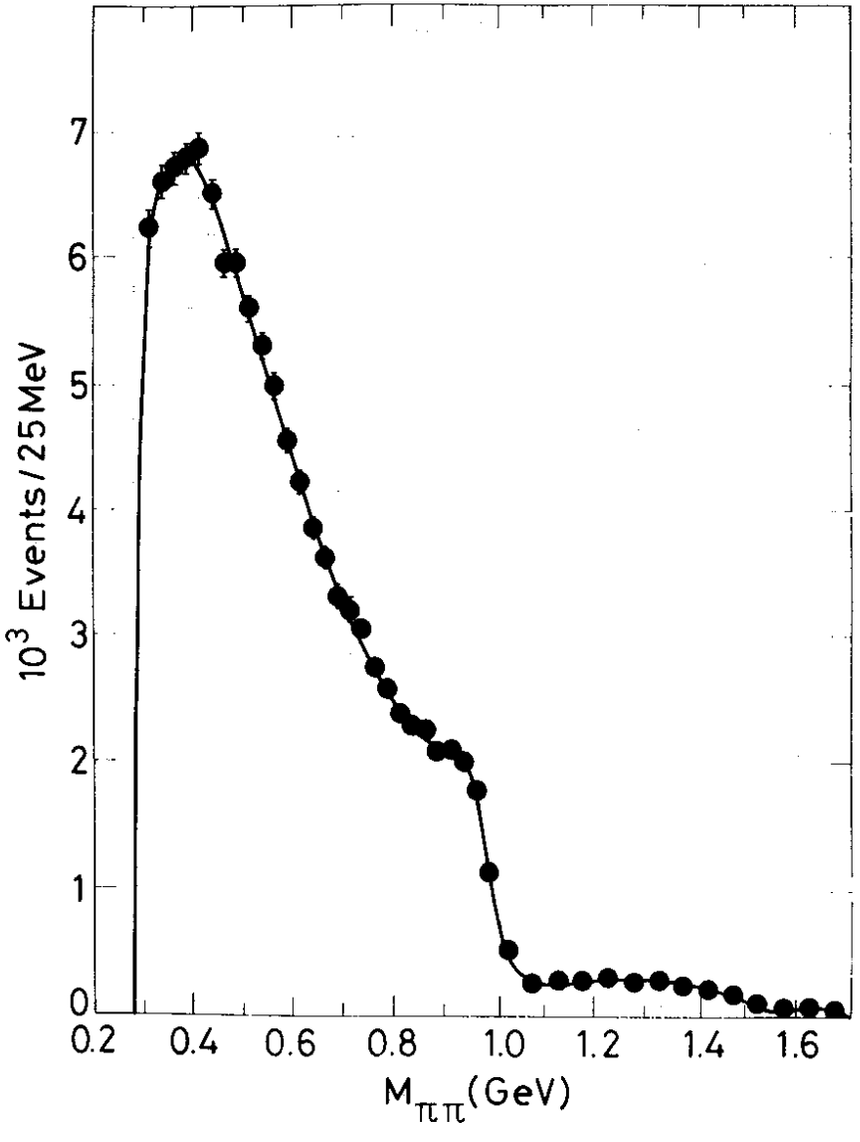
10^3 Events / 25 MeV
0
1
2
3
4
5
6
7
0.2
0.4
0.6
0.8
1.0
1.2
1.4
1.6
$M_{\pi\pi}$ (GeV)

FIG. 5.7

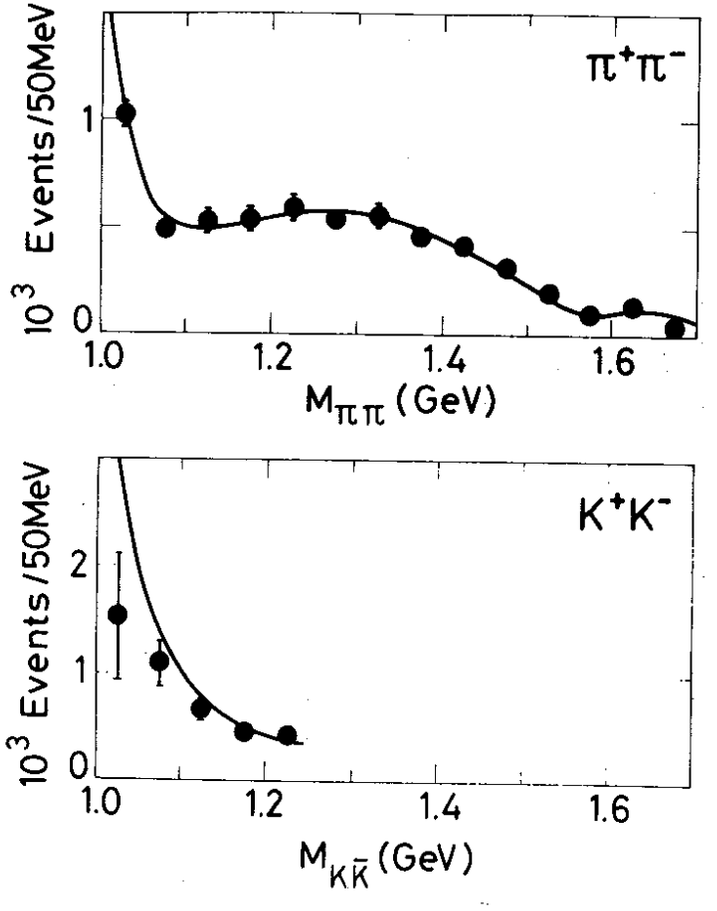
$\pi^+\pi^-$
10^3 Events / 50 MeV
0
1
1.0
1.2
1.4
1.6
$M_{\pi\pi}$ (GeV)
K^+K^-
10^3 Events / 50 MeV
0
1
2
1.0
1.2
1.4
1.6
$M_{K\bar{K}}$ (GeV)

FIG. 5.8

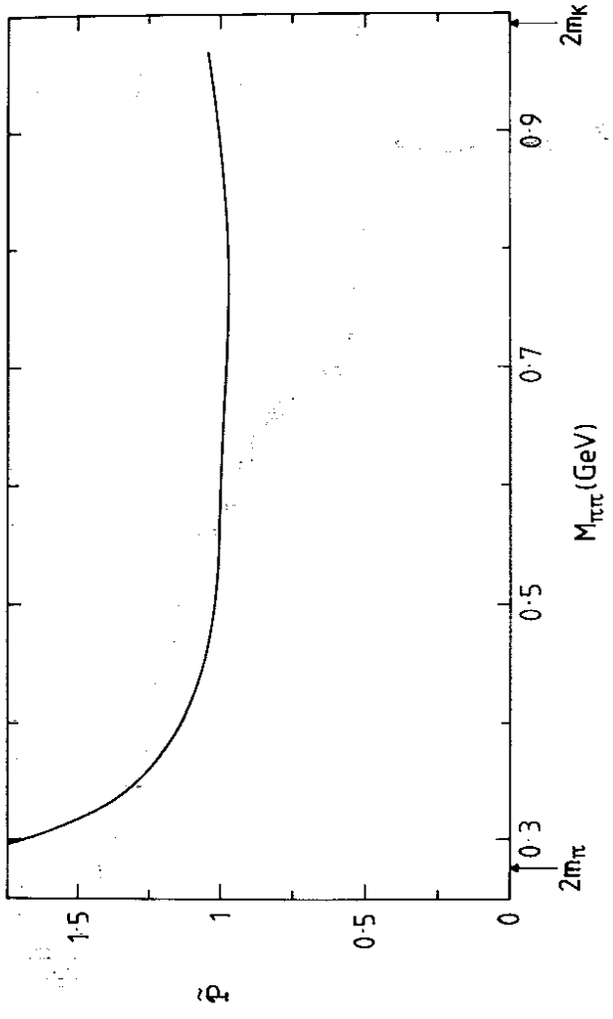

FIG. 5.9

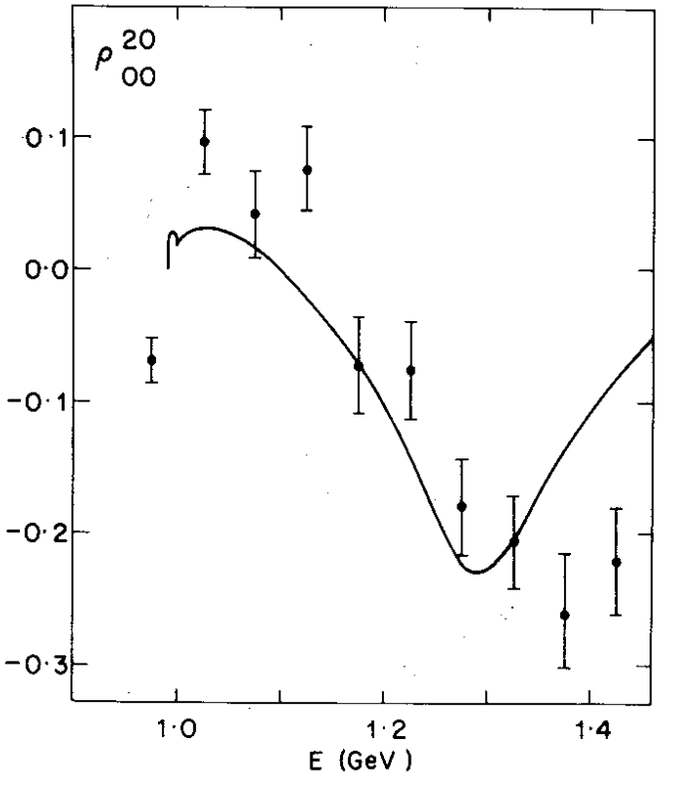

FIG. 5.10

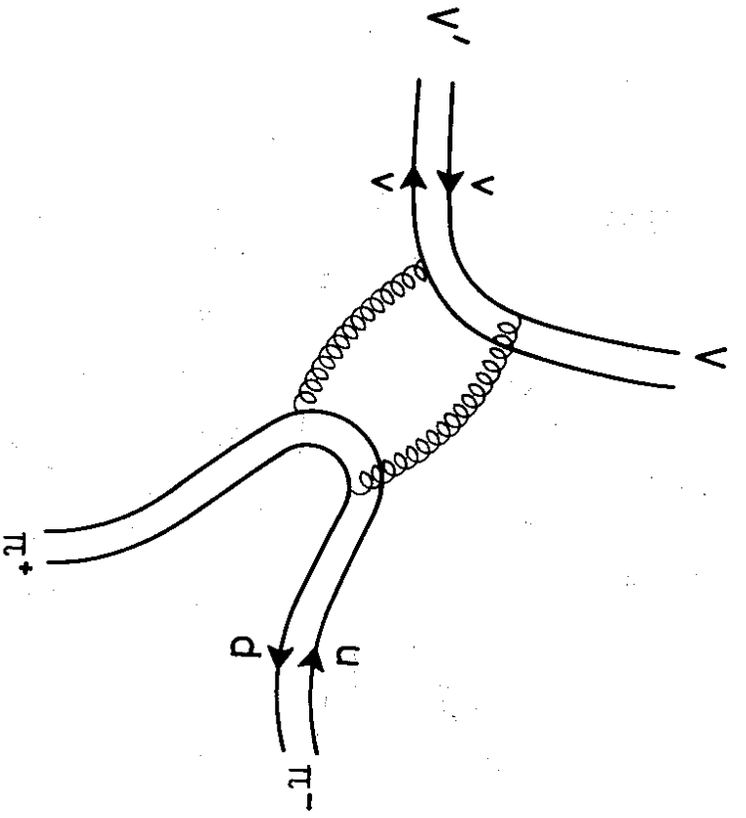
$\bar{c}$
$\bar{c}$
$\bar{c}$
π^+
p
n
π^-

FIG. 6.1

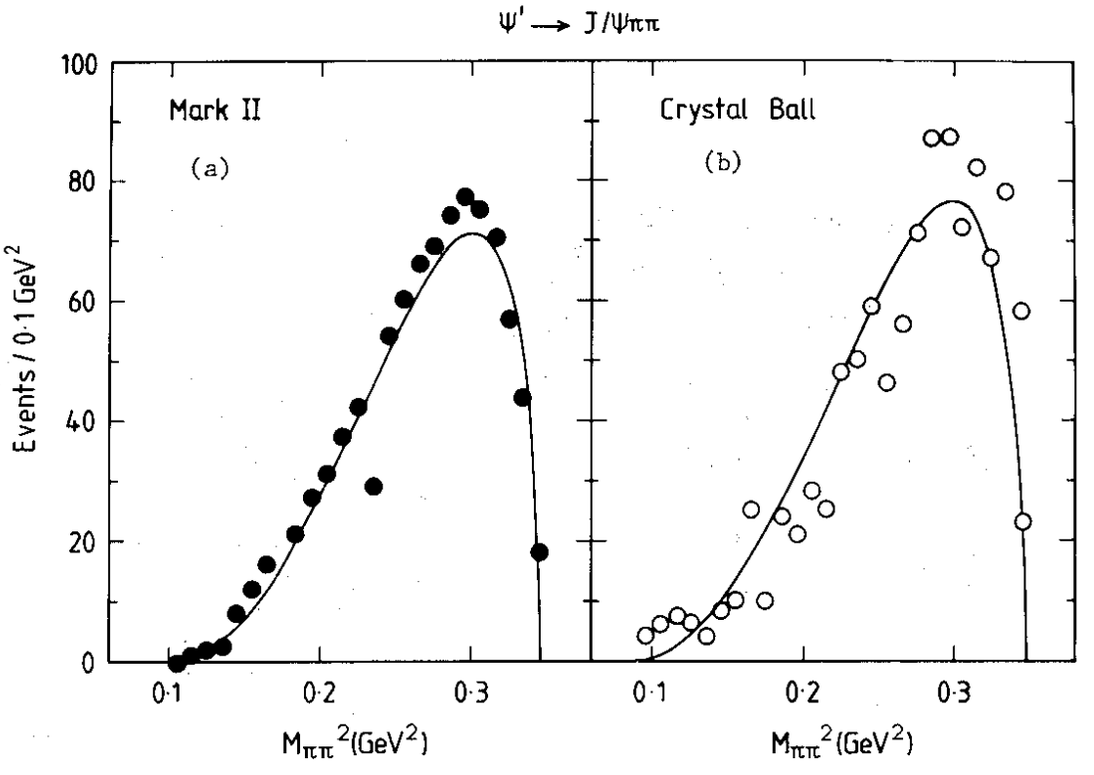
$\psi' \rightarrow J/\psi\pi\pi$
Mark II
(a)
Crystal Ball
(b)
Events / 0·1 GeV^2
100
80
60
40
20
0
0·1
0·2
0·3
$M_{\pi\pi}{}^2$(GeV^2)

FIG. 6.2

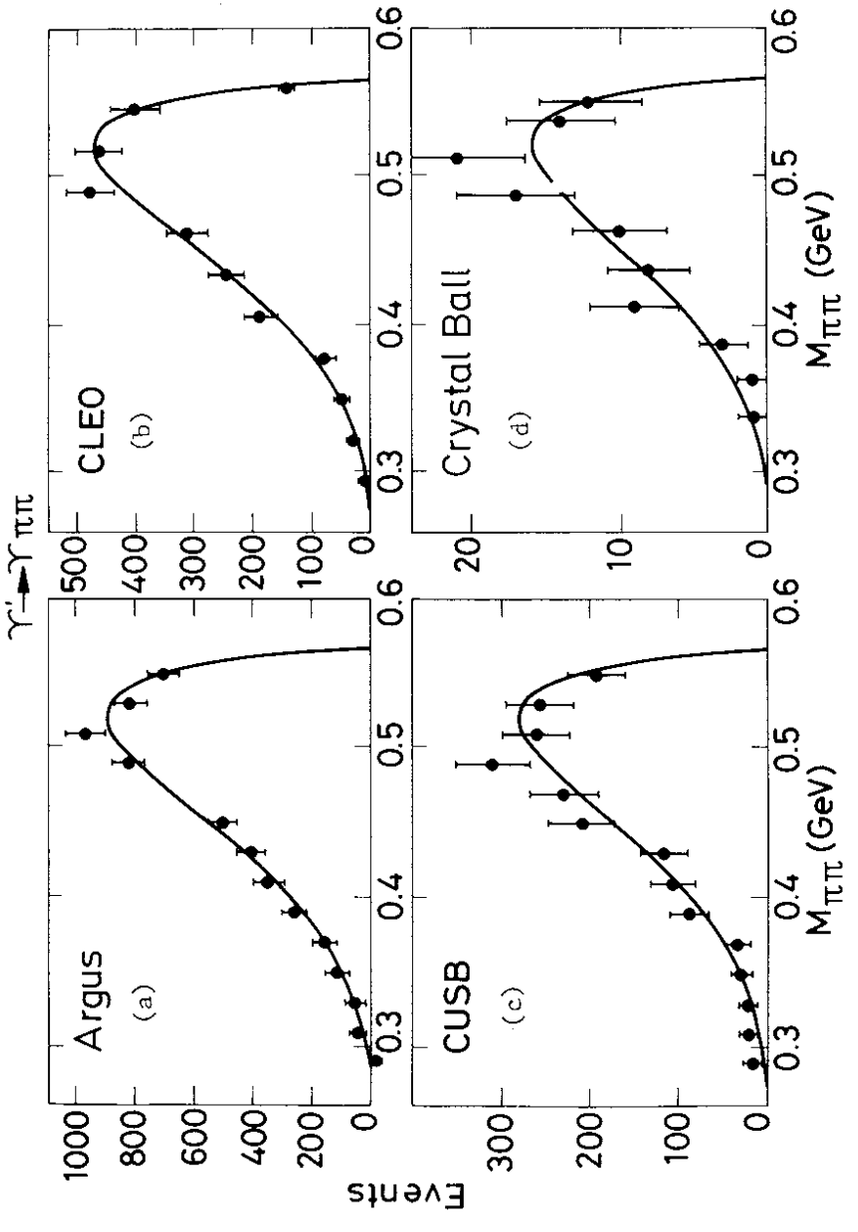
Υ'→Υππ
Argus
(a)
CLEO
(b)
CUSB
(c)
Crystal Ball
(d)
Events
$M_{\pi\pi}$ (GeV)

FIG. 6.3

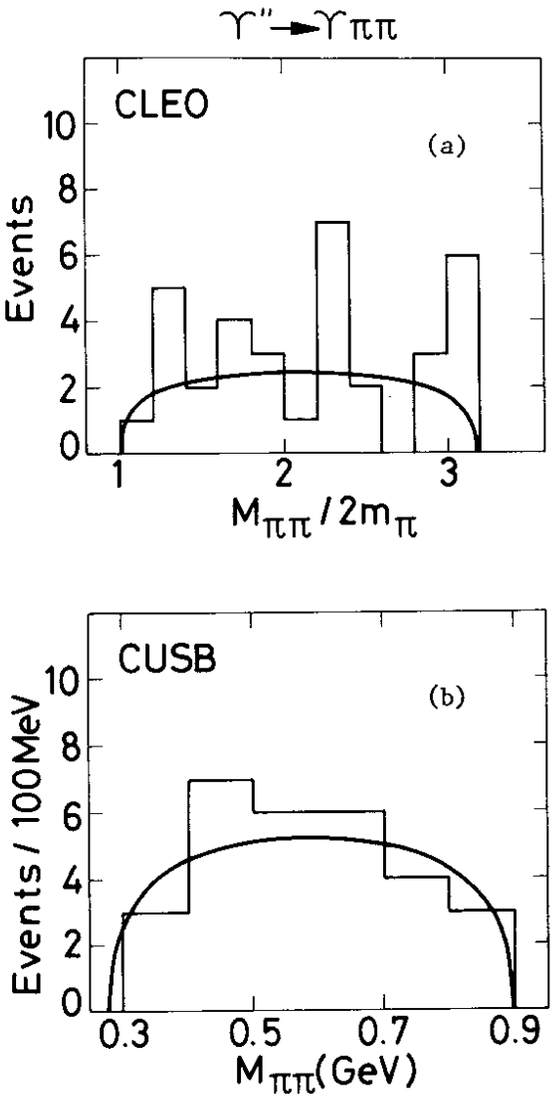
Υ''→Υππ
CLEO
(a)
Events
$M_{\pi\pi}/2m_{\pi}$
CUSB
(b)
Events / 100MeV
$M_{\pi\pi}$(GeV)

FIG. 6.4

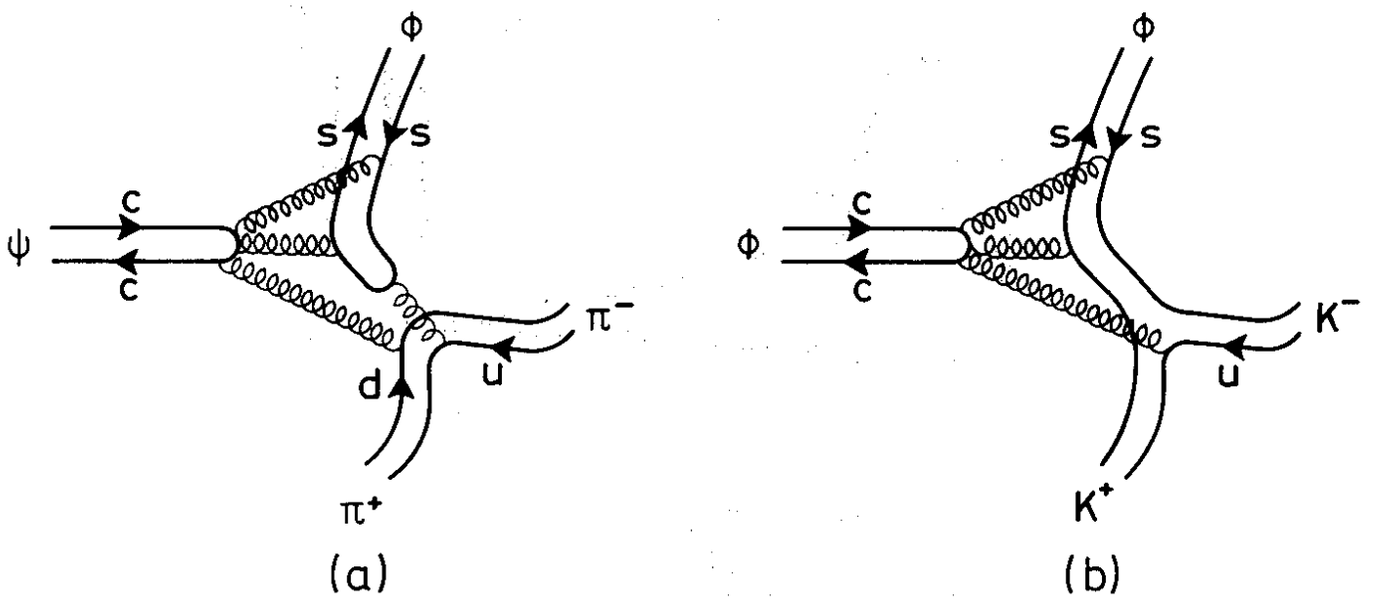
ψ
c
c
s
s
Φ
π⁻
d
u
π⁺
(a)
Φ
c
c
s
s
K⁻
u
K⁺
(b)

FIG. 6.5

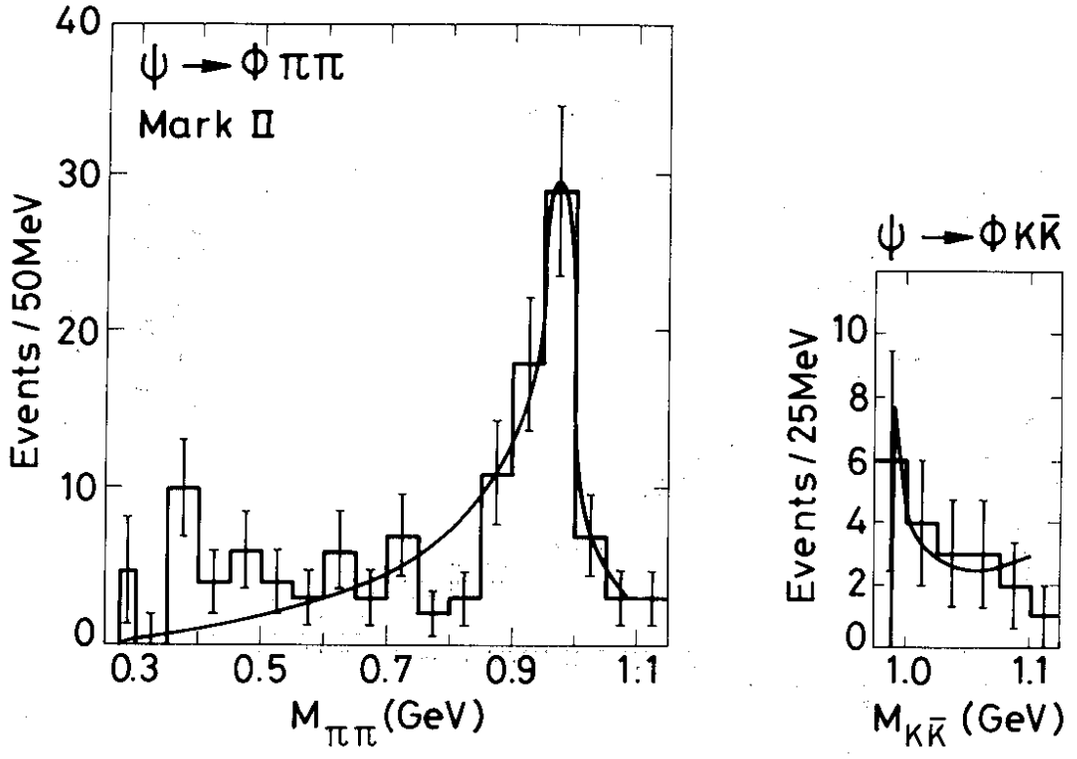
ψ → Φ ππ
Mark II
Events / 50MeV
0
10
20
30
40
0.3
0.5
0.7
0.9
1.1
M ππ (GeV)
ψ → Φ KK̄
Events / 25MeV
0
2
4
6
8
10
1.0
1.1
M KK̄ (GeV)

FIG. 6.6

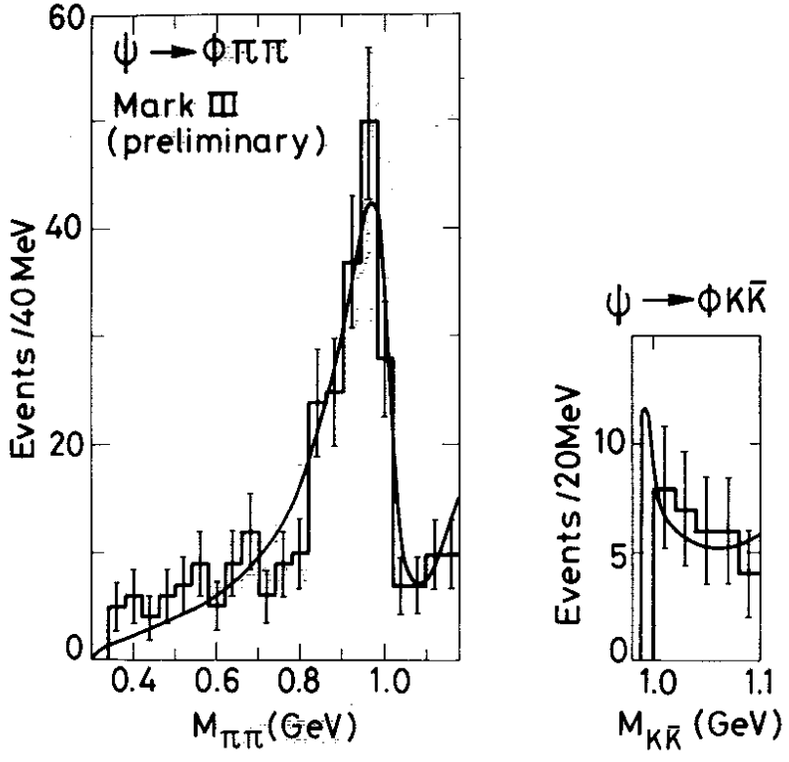
ψ → φππ
Mark III
(preliminary)
Events /40 MeV
60
40
20
0
0.4
0.6
0.8
1.0
Mππ (GeV)
ψ → φKK̄
Events /20 MeV
10
5
0
1.0
1.1
MKK̄ (GeV)

FIG. 6.7

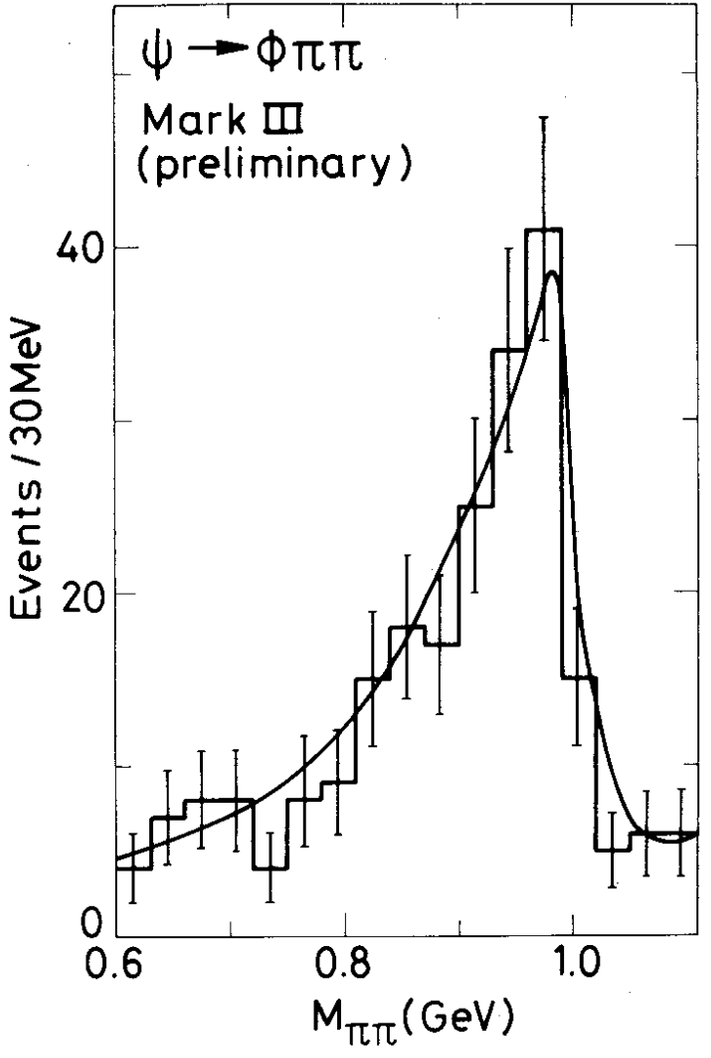
ψ → φππ
Mark III
(preliminary)
Events /30 MeV
40
20
0
0.6
0.8
1.0
Mππ (GeV)

FIG. 6.8

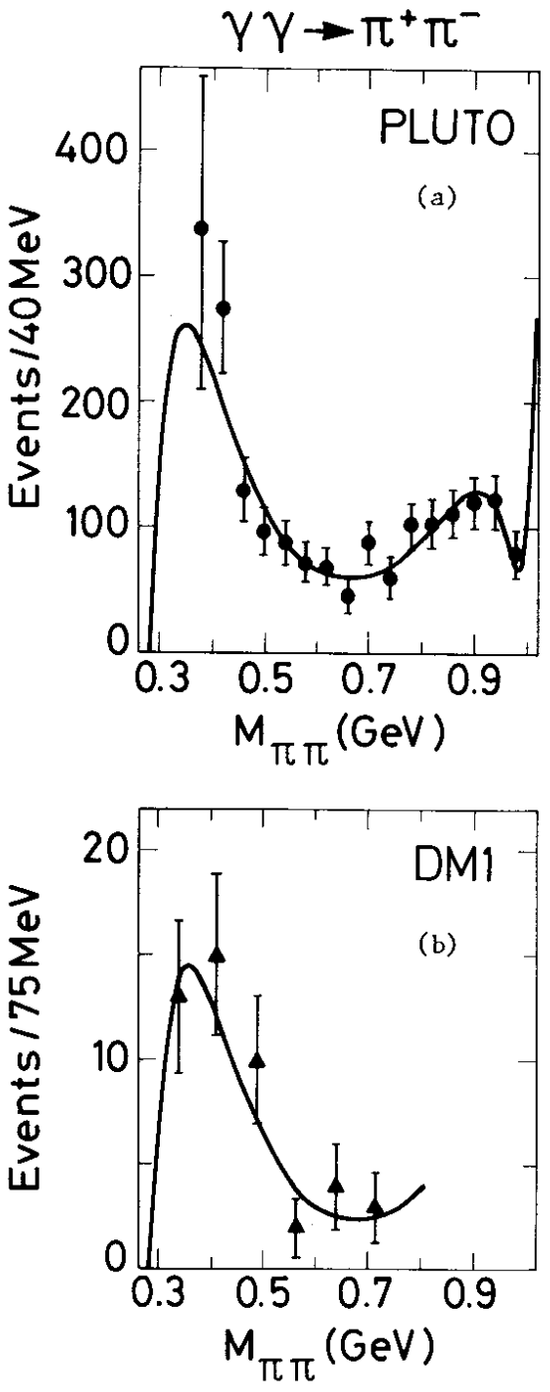

FIG. 6.9

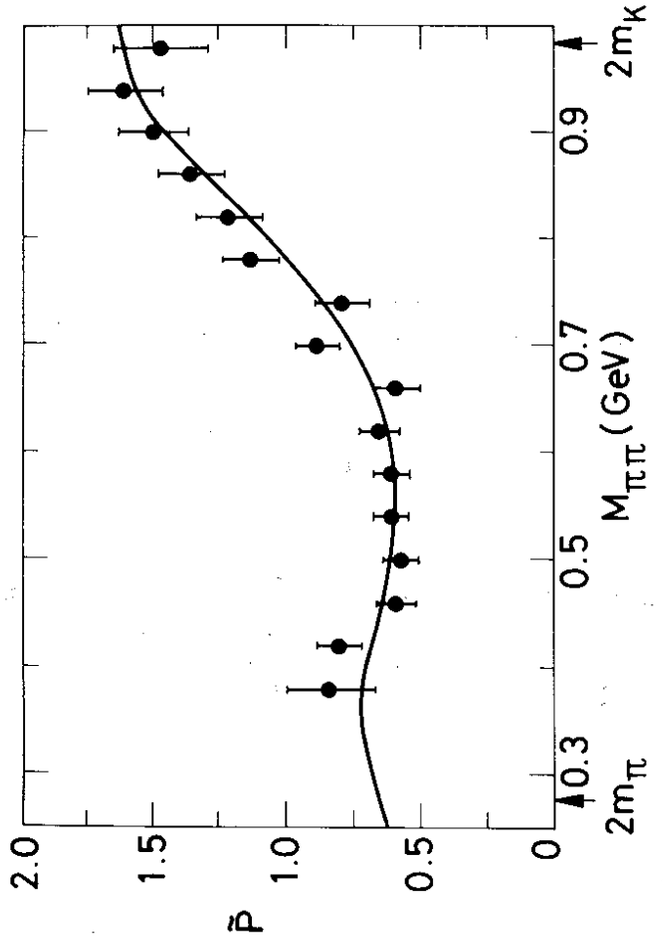

FIG. 6.10

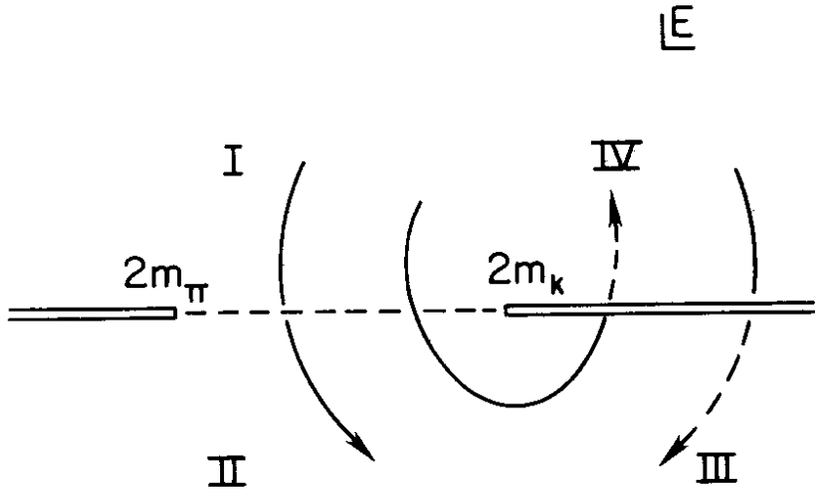

Sheet Structure of the Energy Plane

FIG. 7.1

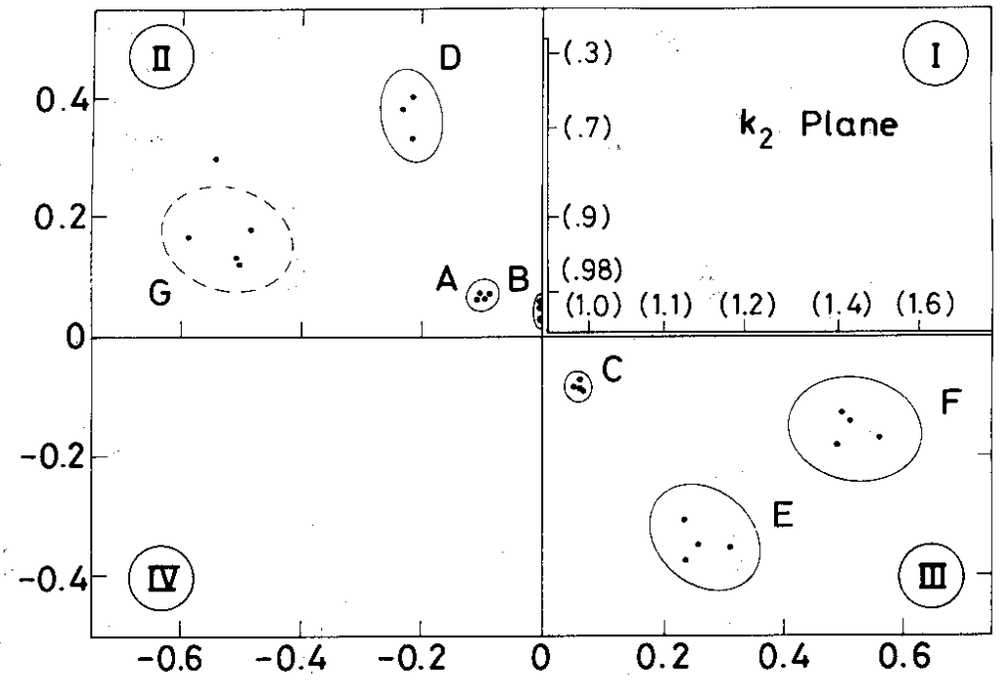

(a)

FIG. 7.2(a)

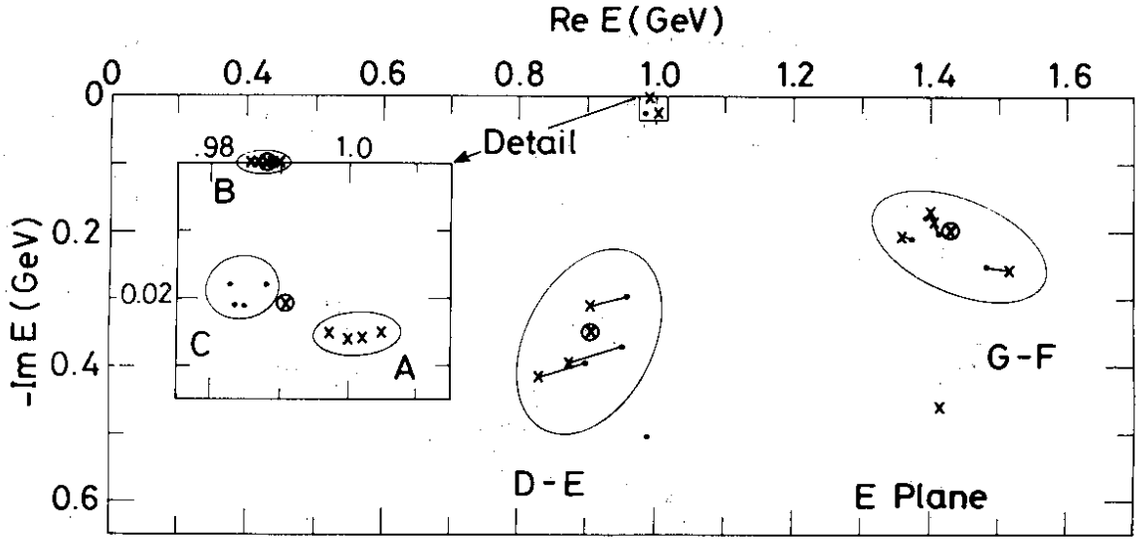

(b)

FIG. 7.2(b)

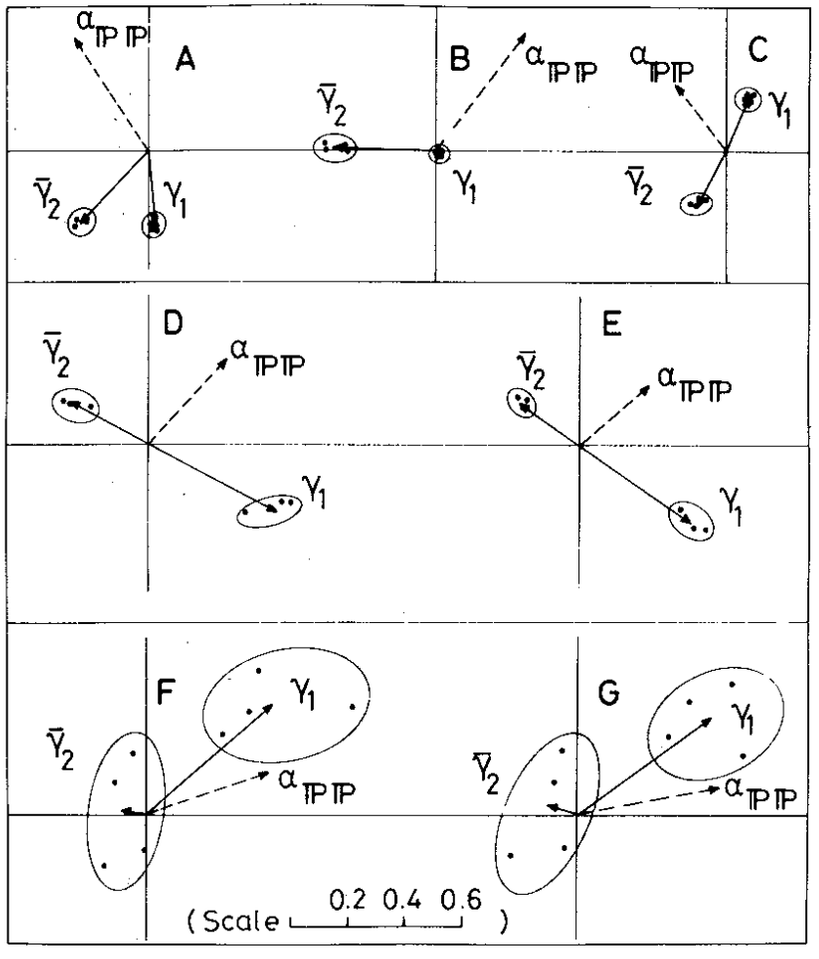
A
B
C
D
E
F
G
$\alpha_{\mathbb{P}\mathbb{P}}$
$\bar{\gamma}_2$
γ_1
(Scale 0.2 0.4 0.6)

FIG. 7.3

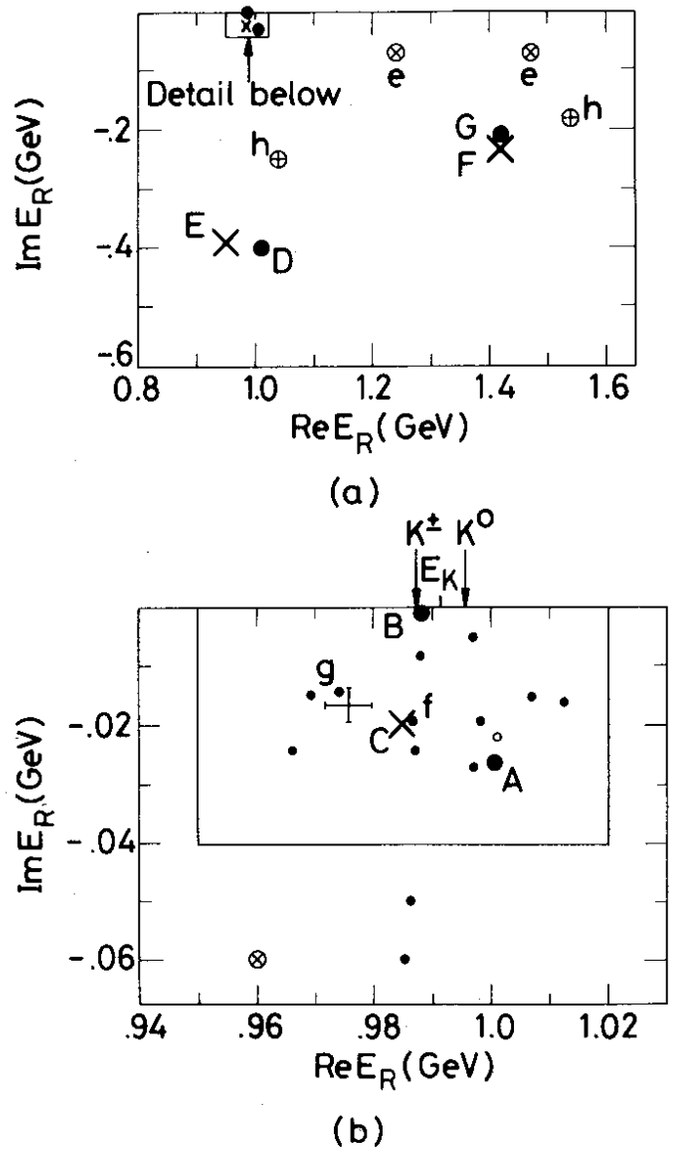
Detail below
e
e
h
G
F
E
D
$\mathrm{Im}E_R$(GeV)
$\mathrm{Re}E_R$(GeV)
(a)
$K^\pm$ K^0
E_K
B
g
f
C
A
$\mathrm{Im}E_R$(GeV)
$\mathrm{Re}E_R$(GeV)
(b)

FIG. 7.4

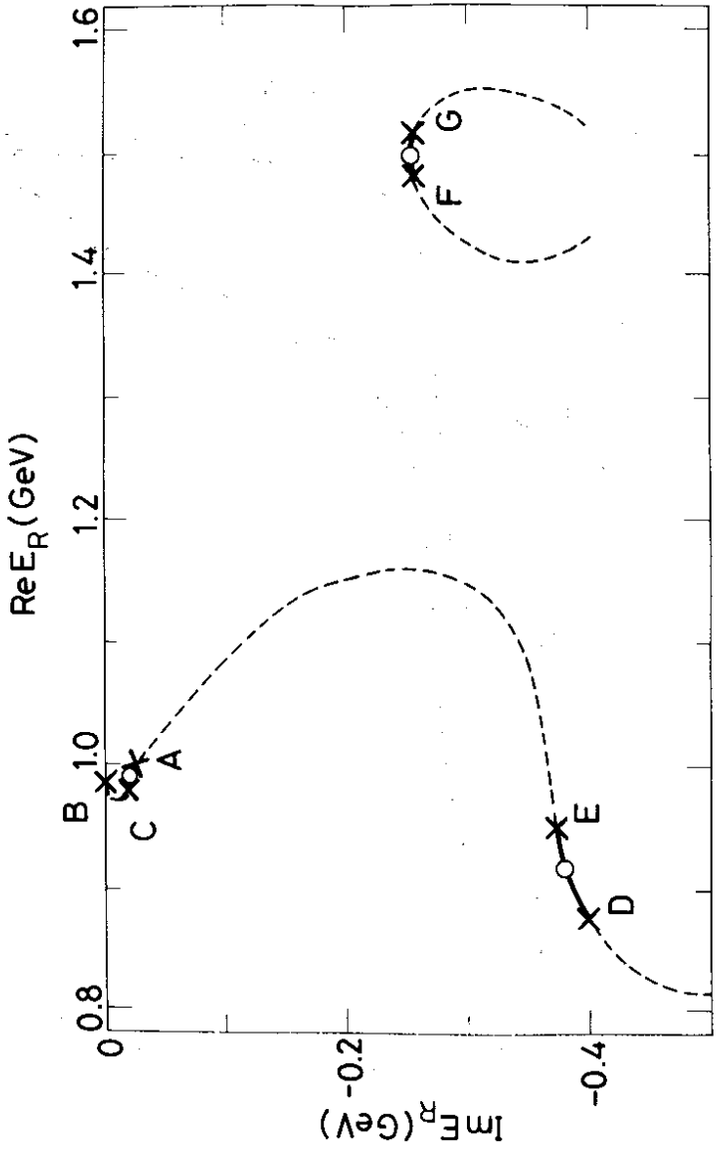
ReE_R(GeV)
1.6
1.4
1.2
1.0
0.8
0
-0.2
-0.4
ImE_R(GeV)
A
B
C
D
E
F
G

FIG. 8.1

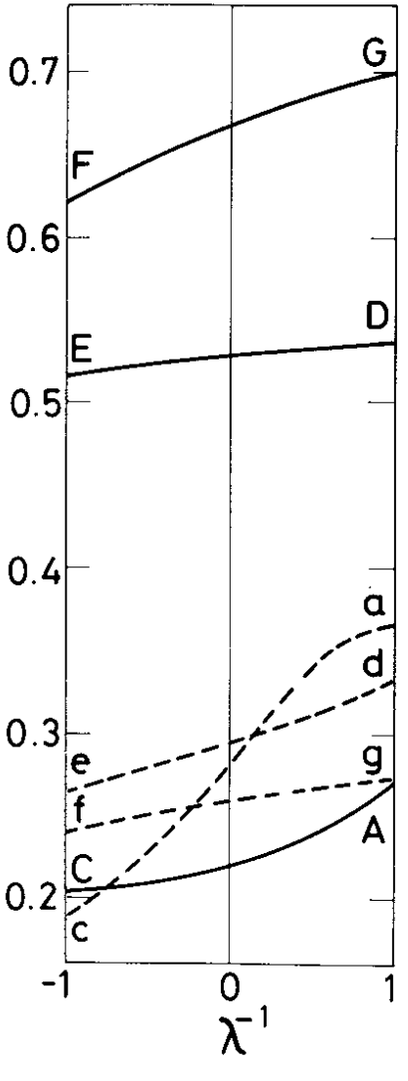
0.7
0.6
0.5
0.4
0.3
0.2
-1
0
1
λ^-1
G
F
E
D
a
d
e
g
f
A
C
c

FIG. 8.2

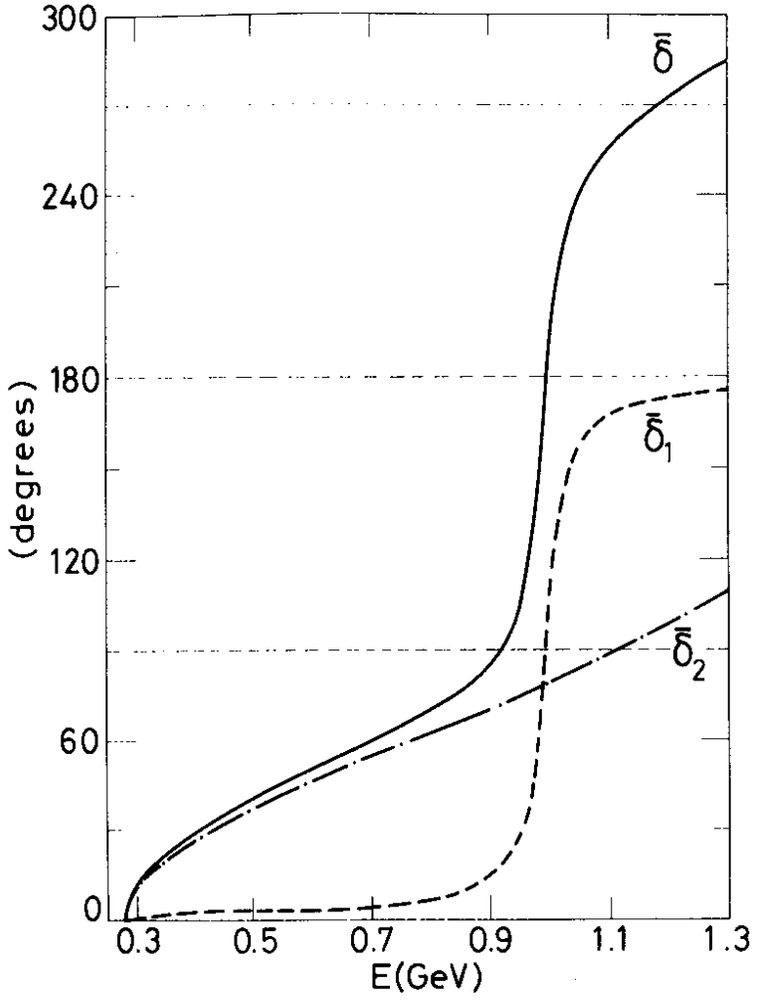
300
240
180
120
60
0
(degrees)
$\bar{\delta}$
$\bar{\delta}_1$
$\bar{\delta}_2$
0.3
0.5
0.7
0.9
1.1
1.3
E(GeV)

FIG. 9.1